

WATER MASER SURVEY TOWARD LOW-MASS YOUNG STELLAR OBJECTS IN THE NORTHERN SKY WITH THE NOBEYAMA 45 METER TELESCOPE AND THE VERY LARGE ARRAY

RAY S. FURUYA

Istituto Nazionale di Astrofisica, Osservatorio Astrofisico di Arcetri, Largo Enrico Fermi 5, I-50125, Firenze, Italy; furuya@arcetri.astro.it

YOSHIMI KITAMURA

Institute of Space and Astronautical Science, Yoshinodai 3-1-1, Sagamihara, Kanagawa 229-8510, Japan; kitamura@pub.isas.ac.jp

ALWYN WOOTTEN

National Radio Astronomy Observatory, 520 Edgemont Road, Charlottesville, VA 22903; awootten@nrao.edu

MARK J. CLAUSSSEN

National Radio Astronomy Observatory, New Mexico Array Operations Center, P.O. Box O, 1003 Lopezville Road, Socorro, NM 87801;
mclaussen@nrao.edu

AND

RYOHEI KAWABE

National Astronomical Observatory, Osawa 2-21-1, Mitaka, Tokyo 181-8588, Japan; kawabe@nro.nao.ac.jp

Received 2002 February 28; accepted 2002 July 9

ABSTRACT

We give a detailed presentation of all the data from a multiepoch 22 GHz H₂O maser survey mainly toward low-mass young stellar objects (YSOs) using the Nobeyama 45 m telescope and the Very Large Array (VLA). Our major results are already published (our Paper I). The Nobeyama survey is the first complete H₂O maser survey toward known Class 0 sources in the northern sky ($\delta > -35^\circ$) and is one of the most sensitive surveys ever performed. The survey was conducted from 1996 May through 1999 March over 32 periods. A total of 606 observations were carried out toward 173 YSOs, including 36 unknown luminosity sources, and toward 31 preprotostellar cores (PPSCs) in the Ophiuchus star-forming region. We detected 149 spectra toward 39 YSOs and zero spectra toward the 31 PPSCs. Subsequent to the Nobeyama survey, we performed a follow-up interferometric survey with the VLA in order to associate 19 maser sources detected by the 45 m telescope with individual YSOs. In this paper we compile properties of 142 YSOs together with their H₂O maser activity. On the basis of this data set, we use properties of water maser emission as a probe of jet phenomena in low-mass stars.

Subject headings: ISM: evolution — ISM: jets and outflows — masers — radio lines: ISM — stars: pre-main-sequence — surveys

1. INTRODUCTION

Deeply embedded protostars invisible even at 60 and 100 μm bands are called “Class 0” in the widely accepted evolutionary scheme based on spectral energy distribution (SED; Lada 1987; André, Ward-Thompson, & Barsony 1993, hereafter AWB93). The bolometric temperature (T_{bol} ; Myers & Ladd 1993), a useful indicator of the evolution of young stellar objects (YSOs), is low ($T_{\text{bol}} < 70 \text{ K}$) for Class 0 sources, while the more evolved Class I and II sources show higher values of $70 \text{ K} \leq T_{\text{bol}} < 650 \text{ K}$ and $650 \text{ K} \leq T_{\text{bol}} < 2800 \text{ K}$, respectively (Chen et al. 1995). At present, 42 Class 0 sources (including four sources more luminous than $1000 L_\odot$) have been identified (André, Ward-Thompson, & Barsony 2000, hereafter AWB00). The “Class 0” phase is also the most powerful CO outflow phase (Bachiller 1996): these outflows are believed to be driven by highly collimated jets and intimately linked to the accretion process. In contrast, CO outflows associated with Class I sources are poorly collimated and much less powerful (Bontemps et al. 1996). Outflows are thought to remove excess angular momentum from the accretion disks and to regulate the stellar rotation so that stars continue to grow without spinning up to breakup speeds (Uchida & Shibata 1985). Meanwhile, outflows dissipate parent cloud cores

that supply material for protostar growth. Outflow phenomena thus represent the fossil record of the accretion process, and the study of outflow phenomena is expected to shed light on the star formation process itself.

In order to understand outflow phenomena, it is essential to investigate the kinematic structure of protostellar jets in the vicinity of the central stars. Very high angular resolution H₂O maser observations using VLBI techniques provide us a unique opportunity for such studies. With present continental-wide VLBI networks such as the Very Long Baseline Array (VLBA), we can attain an angular resolution down to submilliarcseconds (mas), which corresponds to sub-AU scale spatial resolution in the nearby star-forming regions. H₂O maser emission at 22.235077 GHz is frequently seen in low-mass YSOs and is known to be a good tracer of jet activities very close to protostars ($\lesssim 100 \text{ AU}$); some H₂O masers are associated with protostellar disks (Fiebig et al. 1996; Torrelles et al. 1998a). Furthermore, it is well known that H₂O masers are highly time variable on timescales of a day to a month (e.g., Reid & Moran 1981 and references therein; Comoretto et al. 1990; Felli, Palagi, & Tofani 1992, hereafter FPT92; Wilking et al. 1994; Persi, Palagi, & Felli 1994; Claussen et al. 1996). The first systematic multiepoch H₂O maser survey of low-mass YSOs was a monthly 13 epoch survey using the Haystack 37 m telescope (Wilking et

al. 1994). They showed that the correlation between the maser luminosities and far-infrared (FIR) luminosities holds even for low-mass stars less luminous than $120 L_{\odot}$. Another important result was that of Claussen et al. (1996), who found that the maser luminosities correlate well with the luminosities of radio continuum emission from ionized gas, suggesting that H₂O masers trace jet activity closely. In fact, VLA images have shown that the masers in low-mass YSOs appear to be concentrated within several hundred AU of the central stars (Wootten 1989, 1993; Terebey, Vogel, & Myers 1992; Chernin 1995; Meehan et al. 1998; Furuya et al. 1999). Moreover, recent VLBA observations have revealed that in most cases the masers originate behind shocked gas very close to the protostars (Claussen et al. 1998; Patel et al. 2000; Furuya et al. 2000).

We performed a multiepoch H₂O maser survey toward low-mass YSOs using the Nobeyama 45 m telescope and the Very Large Array (VLA). Major results from the survey have been published (Furuya et al. 2001, hereafter Paper I). Purposes of the survey were (1) to establish a general view of H₂O maser phenomena in low-mass YSOs, (2) to investigate jet and outflow phenomena using H₂O masers as a probe, and (3) to prepare for future VLBI observations. Because of the time variable nature of masers, our survey was conducted in several epochs. The Nobeyama survey is the first complete H₂O maser survey toward known Class 0 sources in the northern sky ($\delta > -35^{\circ}$), and we showed that Class 0 sources are favorable sites to harbor water masers. In addition, we found that the H₂O maser luminosities in low-mass stars are more closely related to the luminosities of the 100 AU scale radio jets than to the mechanical luminosities of large-scale CO outflows. In this paper we present all the data from the series of observations (§ 4) and discuss what physical processes are related to maser phenomena (§ 5).

2. SOURCE SELECTION

In order to measure the occurrence of H₂O masers and their properties, we selected sources in the northern sky ($\delta > -35^{\circ}$) as follows: (1) all of the known 38 Class 0 sources less luminous than $100 L_{\odot}$, which are listed by Bachiller (1996) and AWB00; and (2) the sample in Bontemps et al. (1996), which comprises nine Class 0 and 35 Class I sources. Properties of molecular outflows and dense envelopes associated with these sources were well studied in CO $J = 2-1$ lines and 1.3 mm continuum emission, respectively. We note that the evolutionary classification of some sources remains controversial; identification in these three lists thus does not necessarily match. (3) As a lower priority sample, we selected from individual papers Class I and II sources for which T_{bol} was well defined (Chen et al. 1995, 1997) and CO outflow sources reported in Fukui et al. (1993). In addition to the above sources, we selected 31 preprotostellar cores (PPSCs) in the Ophiuchus star-forming region identified by 1.3 mm continuum emission (Motte, André, & Neri 1998; Figs. 1a–1f) in order to investigate maser activity in starless cloud cores. We also selected 25 high- and intermediate-luminosity ($L_{\text{bol}} \gtrsim 100 L_{\odot}$) YSOs as a control sample. The 25 sources include two luminous Class 0 sources, IRAS 20050+2720 ($L_{\text{FIR}} \approx 388 L_{\odot}$; Molinari et al. 1996) and S106 FIR ($L_{\text{bol}} \lesssim 1080 L_{\odot}$; Furuya et al. 2002).

3. OBSERVATIONS

The monitoring survey was done principally using the 45 m telescope at the Nobeyama Radio Observatory.¹ The survey was conducted from 1996 May through 1999 March over 32 periods except the annual shutdown of the telescope (from July to late November). Most of the observing time was allocated irregularly as a backup of higher frequency observations and as a bit of time available at the end of weekly telescope maintenance. Subsequent to the 45 m telescope observations, a follow-up interferometric survey was performed using the VLA of the NRAO² from 1998 October through 1999 February.

In Table 1 we present all of the observing information. In column (1) we give a YSO name, which is thought to be most commonly used, together with a source identification number. In column (2) we give either an alternative YSO name and/or a name of the associated cloud core. Columns (3) and (4) give the source B1950.0 equatorial coordinate with which we observed. Column (5) gives the type of object: the SED class is given in the case of low-mass YSOs. Column (6) gives the observing date. Column (7) provides the names of telescopes used. In the case of the VLA observations, names of the array configuration are also described. For the reader's convenience, we show observed center positions with the 45 m telescope and the field of view (FOV) of the VLA observations for the crowded star-forming regions of ρ Ophiuchus and Serpens: Figures 1a–1f present positions observed with the 45 m telescope plotted on the 1.3 mm continuum emission maps of the ρ Ophiuchus region (Motte et al. 1998); Figure 1g presents points observed with the 45 m telescope and the VLA FOVs in the Serpens cloud (Testi & Sargent 1998). In particular, Figures 1a–1f will help the reader find positions of the PPSCs.

3.1. Nobeyama 45 m Telescope Observations

In the course of the Nobeyama survey, we carried out a total of 606 observations toward 173 YSOs, mainly low-mass sources, including 36 unknown luminosity sources. Furthermore, we observed 31 PPSCs. The telescope beam size (HPBW) was $75''$. We checked the telescope pointing by observing strong H₂O masers: typical pointing accuracies were better than $7''$. The observations were made in position switching mode. We used the cooled HEMT receiver (H22) and employed the standard chopper wheel calibration to derive the intensity scale in antenna temperature (T_A^*). The spectra were obtained using the eight 40 MHz bandwidth acousto-optical spectrometers (AOSSs), each of which has 1024 spectral channels: the total velocity coverage was 2560 km s^{-1} with a velocity resolution of 0.5 km s^{-1} .

The sensitivity in 5 minute integrations with 0.5 km s^{-1} resolution was typically 30 mK in T_A^* from December to March and 100 mK from April to June. This difference in sensitivity is due to the difference of the contribution of the thermal noise from the terrestrial atmosphere. These sensitivities correspond to 37 and 120 mK in main-beam brightness temperature (T_{mb}) for the main-beam efficiency (η_{mb})

¹ Nobeyama Radio Observatory (NRO) is a branch of the National Astronomical Observatory, an interuniversity research institute operated by the Ministry of Education, Science, Culture, and Sports of Japan.

² The National Radio Astronomy Observatory (NRAO) is operated by Associated Universities, Inc., under cooperative agreement with the National Science Foundation.

TABLE 1
LIST OF OBSERVED SOURCES IN THE NOBEYAMA 45 m TELESCOPE AND THE VLA H₂O MASER SURVEY

YSO Name (1)	Alternative Name/Core Name (2)	R.A. (B1950.0) (3)	Decl. (B1950.0) (4)	Source Type (5)	Date (6)	Instruments (7)
(1) IRAS 00338+6312.....	L1287	00 33 53.15	63 12 32.1	Class I	1998 Jan 5 1998 Feb 26 1998 Jun 3	NRO 45 m NRO 45 m NRO 45 m
(2) IRAS 00494+5617.....	NGC 281-A	00 49 29.2	56 17 37		1998 Jun 22	NRO 45 m
(3) L1448-IRS 2	L1448	03 22 17.9	30 34 40	Class 0	1997 Dec 30 1998 Feb 26 1998 Jun 5 1998 Jun 14 1998 Jun 22 1998 Oct 24 1999 Jan 31 1999 Mar 15	NRO 45 m NRO 45 m NRO 45 m NRO 45 m NRO 45 m VLA CnB NRO 45 m NRO 45 m NRO 45 m
(4) L1448-IRS 3	L1448	03 22 31.5	30 34 49	Class 0	1997 Dec 30 1998 Feb 26 1998 Jun 1 1998 Jun 14 1998 Jun 22 1998 Oct 24 1999 Jan 31 1999 Mar 15	NRO 45 m NRO 45 m NRO 45 m NRO 45 m NRO 45 m VLA CnB NRO 45 m NRO 45 m NRO 45 m
(5) L1448C	L1448	03 22 34.3	30 33 35	Class 0	1998 Jan 10 1998 Jun 1 1998 Jun 14 1998 Jun 22 1999 Jan 31 1999 Mar 15	NRO 45 m NRO 45 m NRO 45 m NRO 45 m NRO 45 m NRO 45 m
(6) IRAS 03245+3002.....	RNO 15-FIR L1455	03 24 34.9	30 02 36	Class 0/I	1998 Jan 10 1998 Jun 21 1998 Oct 24 1999 Jan 31 1999 Feb 25 1999 Mar 15	NRO 45 m NRO 45 m VLA CnB NRO 45 m VLA DnC NRO 45 m
(7) HH 338	NGC 1333 IRAS 1	03 25 13.08	31 07 23.8		1998 Jun 1 1999 Jan 31	NRO 45 m NRO 45 m
(8) HH 339	NGC 1333 IRAS 1	03 25 25.52	31 04 24.9		1998 Jun 1 1999 Jan 31	NRO 45 m NRO 45 m
(9) NGC 1333 IRAS 2A	IRAS 03258+3104	03 25 49.9	31 04 16	Class 0	1998 Jan 4 1998 Jan 10 1998 Jun 1 1998 Jun 14 1998 Jun 22 1999 Jan 31 1999 Feb 25 1999 Mar 15	NRO 45 m NRO 45 m NRO 45 m NRO 45 m NRO 45 m NRO 45 m VLA DnC NRO 45 m
(10) NGC 1333 SVS 13A	HH 12	03 25 57.5	31 05 34	Class 0	1998 Jan 4 1998 Jun 1 1998 Jun 14 1998 Jun 22 1999 Jan 31	NRO 45 m NRO 45 m NRO 45 m NRO 45 m NRO 45 m
(11) NGC 1333 IRAS 4A	NGC 1333	03 26 4.78	31 03 13.6	Class 0	1997 Dec 31 1998 Jan 14 1998 Jun 1 1998 Jun 5 1998 Jun 22 1999 Jan 31 1999 Feb 25 1999 Mar 15	NRO 45 m NRO 45 m NRO 45 m NRO 45 m NRO 45 m NRO 45 m VLA DnC NRO 45 m

TABLE 1—Continued

YSO Name (1)	Alternative Name/Core Name (2)	R.A. (B1950.0) (3)	Decl. (B1950.0) (4)	Source Type (5)	Date (6)	Instruments (7)
(12) NGC 1333 IRAS 4B.....	NGC 1333	03 26 06.5	31 02 51.0	Class 0	1997 Dec 31 1998 Jan 14 1998 Jun 1 1998 Jun 5 1998 Jun 22 1999 Jan 31 1999 Feb 25 1999 Mar 15	NRO 45 m NRO 45 m NRO 45 m NRO 45 m NRO 45 m NRO 45 m VLA DnC NRO 45 m
(13) HH 6-VLA.....	NGC 1333 IRAS 7	03 26 05.78	31 08 11.2	Class 0	1998 Jan 14 1998 Feb 26 1998 Jun 1 1999 Jan 31	NRO 45 m NRO 45 m NRO 45 m NRO 45 m
(14) HH 346-SVS 20.....	NGC 1333	03 26 15.97	31 05 10.3		1998 Jan 4 1998 Jan 10 1998 Jun 1 1999 Jan 31	NRO 45 m NRO 45 m NRO 45 m NRO 45 m
(15) IRAS 03282+3035		03 28 15.2	30 35 14	Class 0	1998 Jan 4 1998 Jan 10 1998 Feb 26 1998 Jun 14 1998 Jun 22 1998 Oct 24 1999 Jan 31	NRO 45 m NRO 45 m NRO 45 m NRO 45 m NRO 45 m VLA CnB NRO 45 m
(16) IRAS 03301+3057	B1-IRS	03 30 10.5	30 57 47	Class 0	1998 Jun 1 1998 Jun 5 1998 Jun 14 1998 Jun 22 1999 Jan 31 1999 Feb 25 1999 Mar 15	NRO 45 m NRO 45 m NRO 45 m NRO 45 m NRO 45 m VLA DnC NRO 45 m
(17) HH 211-FIR	IC 348	03 40 48.7	31 51 24	Class 0	1998 Jan 4 1998 Jan 10 1998 Jan 13 1998 Feb 26 1998 Jun 1 1998 Jun 14 1998 Oct 24 1999 Jan 31 1999 Mar 15	NRO 45 m NRO 45 m NRO 45 m NRO 45 m NRO 45 m NRO 45 m VLA CnB NRO 45 m NRO 45 m
(18) IRAS 03445+3234	B5-IRS	03 44 31.8	32 42 34	Class I	1998 Jan 11 1998 Jun 1 1999 Jan 31	NRO 45 m NRO 45 m NRO 45 m
(19) IRAS 04016+2610	L1489-IRS	04 01 40.6	26 10 49	Class I	1998 Feb 26 1998 Jun 1 1998 Oct 24 1999 Jan 31	NRO 45 m NRO 45 m VLA CnB NRO 45 m
(20) L1498.....		04 07 52.5	25 02 13		1998 Jun 1 1999 Jan 31	NRO 45 m NRO 45 m
(21) IRAS 04108+2803	L1495	04 10 48	28 03 49	Class I	1998 Jan 11 1998 Jun 1 1998 Oct 24	NRO 45 m NRO 45 m VLA CnB
(22) IRAS 04113+2758		04 11 20.9	27 58 30	Class I	1998 Jan 11 1998 Feb 26 1998 Jun 1	NRO 45 m NRO 45 m NRO 45 m
(23) IRAS 04158+2805	L1495	04 15 52.2	28 05 10	Class I	1998 Jan 11 1998 Jun 1 1998 Oct 24	NRO 45 m NRO 45 m VLA CnB

TABLE 1—Continued

YSO Name (1)	Alternative Name/Core Name (2)	R.A. (B1950.0) (3)	Decl. (B1950.0) (4)	Source Type (5)	Date (6)	Instruments (7)
(24) IRAS 04166+2706	B213	04 16 37.8	27 06 29	Class 0/I	1998 Jan 10 1998 Feb 26 1998 Jun 22 1998 Oct 24 1999 Jan 31	NRO 45 m NRO 45 m NRO 45 m VLA CnB NRO 45 m
(25) IRAS 04169+2702	B213	04 16 53.8	27 02 54	Class I	1998 Jan 13 1998 Feb 26 1998 Jun 1 1998 Jun 5 1998 Oct 24 1999 Jan 31	NRO 45 m NRO 45 m NRO 45 m NRO 45 m VLA CnB NRO 45 m
(26) IRAS 04181+2655	B213	04 18 06.4	26 55 01	Class I	1998 Jan 10 1998 Jun 14	NRO 45 m NRO 45 m
(27) IRAS 04181+2654	B213	04 18 06.9	26 54 04	Class I	1998 Jan 10 1998 Jun 5	NRO 45 m NRO 45 m
(28) IRAS 04190+1924	T Tau South	04 19 4.2	19 25 05	Class II	1998 Feb 26 1998 Jun 5 1998 Oct 24 1999 Jan 31 1999 Mar 15	NRO 45 m NRO 45 m VLA CnB NRO 45 m NRO 45 m
(29) IRAM 04191+1522.....		04 19 06.4	15 23 45	Class 0	1998 Feb 26 1998 Jun 5	NRO 45 m NRO 45 m
(30) IRAS 04191+1523		04 19 10.6	15 23 16		1998 Feb 26 1998 Jun 5	NRO 45 m NRO 45 m
(31) IRAS 04239+2436	HH 6–10/L1524	04 23 54.5	24 36 54	Class I	1998 Feb 26 1998 Jun 1	NRO 45 m NRO 45 m
(32) IRAS 04240+2559	DG Tau	04 24 01	25 59 36	Class II	1998 Jun 5	NRO 45 m
(33) IRAS 04248+2612	HH 31-IRS/B217	04 24 42.5	26 11 13		1998 Jun 5	NRO 45 m
(34) L1521E	L1521	04 26 17	26 07 47		1998 Jun 1 1998 Jun 5	NRO 45 m NRO 45 m
(35) IRAS 04263+2426	L1524/HH 6–10 GV Tau B	04 26 21.9	24 26 30	Class I	1998 Feb 26 1998 Jun 5 1998 Oct 24	NRO 45 m NRO 45 m VLA CnB
(36) IRAS 04287+1807	HL Tau HH 30-IRS	04 28 44.4	18 07 36	Class I	1998 Jan 11 1998 Feb 26 1998 Jun 5	NRO 45 m NRO 45 m NRO 45 m
(37) IRAS 04289+1802	L1551 NE	04 28 50.5	18 02 10	Class I	1998 Jan 4 1998 Jan 11 1998 Jun 5 1998 Oct 24 1999 Jan 31	NRO 45 m NRO 45 m NRO 45 m VLA CnB NRO 45 m
(38) IRAS 04288+2417	HH 6–13	04 28 49.2	24 17 58	Class I	1998 Feb 26 1998 Jun 5	NRO 45 m NRO 45 m
(39) TMC 2A	IRAS 04292+2422	04 29 13.1	24 43 21	Class I	1998 Feb 26 1998 Jun 5	NRO 45 m NRO 45 m
(40) IRAS 04295+2251	L1536-IRS	04 29 32.2	22 51 11	Class I	1998 Jan 4 1998 Jan 11 1998 Feb 26 1998 Jun 5 1998 Oct 24 1999 Jan 31	NRO 45 m NRO 45 m NRO 45 m NRO 45 m VLA CnB NRO 45 m
(41) IRAS 04296+1725	GG Tau	04 29 37.1	17 25 22	Class II	1998 Jun 5	NRO 45 m

TABLE 1—Continued

YSO Name (1)	Alternative Name/Core Name (2)	R.A. (B1950.0) (3)	Decl. (B1950.0) (4)	Source Type (5)	Date (6)	Instruments (7)
(42) IRAS 04287+1801	L1551-IRS 5	04 31 34.14	18 08 04.9	Class I	1998 Jan 4 1998 Jun 5 1998 Oct 24 1999 Jan 31	NRO 45 m NRO 45 m VLA CnB NRO 45 m
(43) IRAS 04302+2247	L1536	04 30 16.8	22 47 04	Class I	1998 Feb 26 1998 Jan 4 1998 Oct 24	NRO 45 m NRO 45 m VLA CnB
(44) IRAS 043230+1746		04 32 40.4	17 45 34	Class II	1998 Jun 5	NRO 45 m
(45) IRAS 04361+2547	TMR-1	04 36 09.8	25 47 28	Class I	1998 Jan 4 1998 Feb 26 1998 Jun 5 1998 Oct 24	NRO 45 m NRO 45 m NRO 45 m VLA CnB
(46) IRAS 04365+2535	TMC 1A L1534	04 36 31.2	25 35 56	Class I	1998 Feb 26 1998 Jan 4 1998 Oct 24	NRO 45 m NRO 45 m VLA CnB
(47) IRAS 04368+2557	L1527	04 36 49.5	25 57 16	Class 0/I	1998 Jan 4 1998 Jan 11 1998 Feb 12 1998 Oct 24 1999 Jan 31	NRO 45 m NRO 45 m NRO 45 m VLA CnB NRO 45 m
(48) IRAS 04381+2540	TMC 1	04 38 08.5	25 40 53	Class I	1998 Jan 4 1998 Feb 26 1998 Oct 24	NRO 45 m NRO 45 m VLA CnB
(49) IRAS 04385+2550	TMC 1C HH 6–33	04 38 34.6	25 50 44	Class I	1998 Jan 4 1998 Feb 26	NRO 45 m NRO 45 m
(50) IRAS 04489+3032	L1513	04 48 58.1	30 32 49	Class I	1998 Jan 4 1998 Jun 5 1998 Oct 24	NRO 45 m NRO 45 m VLA CnB
(51) L1517B		04 52 07.2	30 33 18		1998 Feb 26	NRO 45 m
(52) L1512		05 00 54.4	32 38 60		1998 Feb 26 1998 Jun 1	NRO 45 m NRO 45 m
(53) L1544		05 01 14	25 07 00		1998 Feb 26 1998 Jun 1	NRO 45 m NRO 45 m
(54) L1523		05 02 60	31 38 20		1998 Jun 1	NRO 45 m
(55) IRAS 05155+0707	HH 114 λ Ori region	05 15 35.1	07 07 54	Class 0	1998 Jan 18 1998 Jan 27 1998 Feb 26 1998 Jun 1	NRO 45 m NRO 45 m NRO 45 m NRO 45 m
(56) IRAS 05173–0555	RNO 40-IRS HH 240	05 17 21.4	−05 55 06.1	Class 0/I	1998 Jan 13 1998 Feb 26 1998 Jun 1	NRO 45 m NRO 45 m NRO 45 m
(57) IRAS 05295+1247	RNO 43-MM HH 243	05 29 30.6	12 47 35	Class 0/I	1997 Dec 30 1998 Jan 10 1998 Feb 26 1998 Jun 1 1998 Jun 5 1999 Mar 15	NRO 45 m NRO 45 m NRO 45 m NRO 45 m NRO 45 m NRO 45 m
(58) IRAS 05302–0537	Orion A West NGC 1976	05 30 14.5	−05 37 52	Class I	1998 Feb 26 1998 Jun 1 1998 Jun 22 1999 Mar 15	NRO 45 m NRO 45 m NRO 45 m NRO 45 m
(59) OMC 3-MMS 6	OMC 3	05 32 55.62	−05 03 24.8	Class 0	1998 Jan 14	NRO 45 m
(60) OMC 3-MMS 9	OMC 3	05 32 58.16	−05 07 36.2		1998 Jan 14	NRO 45 m

TABLE 1—Continued

YSO Name (1)	Alternative Name/Core Name (2)	R.A. (B1950.0) (3)	Decl. (B1950.0) (4)	Source Type (5)	Date (6)	Instruments (7)
(61) OMC 2-FIR 4	OMC 2	05 32 59.25	-05 11 53.8		1998 Jan 14	NRO 45 m
(62) HH 34		05 33 03.7	-06 28 53	Class I?	1998 Jan 13 1998 Feb 26 1998 Jun 22	NRO 45 m NRO 45 m NRO 45 m
(63) IRAS 05339-0647	HH 1-2 HH 11a L1641	05 33 52.35	-06 47 34.4	Class 0/I	1998 Jan 13 1998 Feb 26 1998 Jun 1	NRO 45 m NRO 45 m NRO 45 m
(64) IRAS 05338-0624	L1641 North	05 33 52.4	-06 23 58	Class 0/I	1998 Feb 26 1998 Jun 1	NRO 45 m NRO 45 m
(65) IRAS 05369-0728	HH 4-255	05 36 57.3	-07 28 20	Class I	1998 Feb 26 1998 Jun 1	NRO 45 m NRO 45 m
(66) IRAS 05375-0731	L1641-S3 MMS 1	05 37 31	-07 31 51	Class I	1998 Feb 26 1998 Jun 1 1999 Feb 25 1999 Mar 15	NRO 45 m NRO 45 m VLA DnC NRO 45 m
(67) HH 65	Re 50-IRS	05 38 2.49	-07 28 58.3		1997 Dec 31 1998 Jan 14	NRO 45 m NRO 45 m
(68) NGC 2024 FIR 5.....	Orion B	05 39 13.0	-01 57 08	Class 0	1998 Jan 4 1998 Jan 10 1998 Jun 1 1998 Jun 22 1999 Feb 25 1999 Mar 15	NRO 45 m NRO 45 m NRO 45 m NRO 45 m VLA DnC NRO 45 m
(69) NGC 2024 FIR 6.....	Orion B	05 39 13.7	-01 57 30	Class 0	1998 Jan 4 1998 Jan 10 1998 Jun 1 1998 Jun 22 1999 Feb 25 1999 Mar 15	NRO 45 m NRO 45 m NRO 45 m NRO 45 m VLA DnC NRO 45 m
(70) HH 24-MMS.....	L1630-VLA 5	05 43 34.9	-00 11 49	Class 0	1997 Dec 30 1998 Jan 4 1998 Jan 10 1998 Jun 1 1998 Jun 5 1999 Mar 15	NRO 45 m NRO 45 m NRO 45 m NRO 45 m NRO 45 m NRO 45 m
(71) IRAS 05413-0104	HH 212	05 41 18.84	-01 04 10.8	Class 0/I	1998 Jan 18 1998 Feb 26 1998 Jun 1 1999 Mar 15	NRO 45 m NRO 45 m NRO 45 m NRO 45 m
(72) IRAS 05417+0907	B35A	05 41 45.3	09 07 40	Class I	1998 Feb 26 1998 Jun 1	NRO 45 m NRO 45 m
(73) IRAS 05435-0011	L1630-SSV 63E L1630	05 43 34.6	-00 11 2	Class I	1997 Dec 27 1998 Jun 5	NRO 45 m NRO 45 m
(74) HH 25-MMS.....	IRAS 05435-0014 L1630	05 43 33.82	-00 14 36.4	Class 0/I	1998 Jan 4 1998 Jan 13 1998 Jun 5	NRO 45 m NRO 45 m NRO 45 m
(75) IRAS 05435-0015	HH 26-IR L1630	05 43 30	00 15 56	Class I	1998 Jan 13 1998 Jun 5	NRO 45 m NRO 45 m
(76) IRAS 05445+0020	NGC 2071 IRS	05 44 30.3	00 20 42	B?	1998 Jun 1 1998 Jun 5 1998 Jun 22 1999 Mar 15	NRO 45 m NRO 45 m NRO 45 m NRO 45 m

TABLE 1—Continued

YSO Name (1)	Alternative Name/Core Name (2)	R.A. (B1950.0) (3)	Decl. (B1950.0) (4)	Source Type (5)	Date (6)	Instruments (7)
(77) IRAS 05451+0037	NGC 2071 North	05 45 7.8	00 37 41	Class I	1998 Jan 13 1998 Jun 1 1999 Mar 15	NRO 45 m NRO 45 m NRO 45 m
(78) IRAS 05491+0247	HH 111-VLA L1617	05 49 9.41	02 47 48.6	Class 0	1998 Jan 11 1998 Feb 26 1998 Jun 1	NRO 45 m NRO 45 m NRO 45 m
(79) IRAS 06308+0402	RNO 73-MM	06 30 52.7	-04 02 27		1998 Jan 10 1998 Feb 26 1998 Jun 1	NRO 45 m NRO 45 m NRO 45 m
(80) IRAS 06384+0958	NGC 2264G	06 38 25.67	09 58 55.1	Class 0	1997 Dec 30 1998 Jan 4 1998 Jan 10 1998 Feb 26 1998 Jun 1 1999 Mar 15	NRO 45 m NRO 45 m NRO 45 m NRO 45 m NRO 45 m NRO 45 m
(81) IRAS 06453-0209	S287 North	06 45 19.2	-02 09 32		1998 Jun 1	NRO 45 m
(82) IRAS 06567-0350	BFS 56	06 56 45.1	-03 50 41		1998 Feb 27 1998 Jun 1	NRO 45 m NRO 45 m
(83) IRAS 06567-0355	BIP 14	06 56 46.5	-03 55 28		1998 Feb 27 1998 Jun 1	NRO 45 m NRO 45 m
(84) IRAS 06751-0441	S287B	06 57 06.4	-04 41 48	Ae/Be	1998 Jun 1	NRO 45 m
(85) IRAS 06571-0436	S287C	06 57 08.2	-04 36 10		1998 Jun 1	NRO 45 m
(86) IRAS 06572-0742	L1654	06 57 16.8	-07 42 16	B2-B3 ZAMS	1998 Jan 18 1998 Feb 26 1998 Jun 1	NRO 45 m NRO 45 m NRO 45 m
(87) IRAS 06579-0432	S287A	06 57 54.5	-04 32 22		1998 Jun 1	NRO 45 m
(88) IRAS 07180-2356	L1660	07 18 00.9	-23 56 42		1998 Feb 26 1998 Jun 1	NRO 45 m NRO 45 m
(89) IRAS 08076-3556	HH 120	08 07 40.3	-35 56 06	Class 0/I	1998 Jan 11 1998 Jun 1 1998 Mar 15	NRO 45 m NRO 45 m NRO 45 m
(90) L134A.....		15 50 58.1	-04 26 36		1998 Feb 12 1998 Jun 1	NRO 45 m NRO 45 m
(91) L183.....		15 51 35.7	-02 40 54		1997 Dec 31 1998 Jun 1	NRO 45 m NRO 45 m
(92) IRAS 16191-1936	L1719B	16 19 09	-19 36 25	Class I	1997 Dec 30 1998 Jan 18 1998 Jun 1	NRO 45 m NRO 45 m NRO 45 m
(93) ROX 6	EL 13/SR 4	16 22 54.87	-24 14 01.5	Class II	1998 Jan 14	NRO 45 m
(94) A3-MM 1.....	Oph A	16 23 08.3	-24 16 21	PPSC	1998 Jan 14	NRO 45 m
(95) A2-MM 1.....	Oph A	16 23 09.9	-24 17 55	PPSC	1998 Jan 14	NRO 45 m
(96) GSS 30-IRS.....	Oph A EL 21	16 23 20	-24 16 06	Class I	1997 Dec 31 1998 Jan 18 1998 Jun 1 1998 Jun 2 1998 Jun 13 1999 Feb 12	NRO 45 m NRO 45 m NRO 45 m NRO 45 m NRO 45 m VLA DnC
(97) A-N	Oph A	16 23 20.2	-24 12 56	PPSC	1998 Jun 2	NRO 45 m
(98) A-MM 2.....	Oph A	16 23 21.6	-24 17 16	PPSC	1998 Jun 2	NRO 45 m

TABLE 1—Continued

YSO Name (1)	Alternative Name/Core Name (2)	R.A. (B1950.0) (3)	Decl. (B1950.0) (4)	Source Type (5)	Date (6)	Instruments (7)
(99) ROX 10B	Oph A	16 23 21.9	−24 14 13	Class II/III	1998 Jan 14 1998 Jun 2	NRO 45 m NRO 45 m
(100) GSS 31	Oph A	16 23 22.04	−24 14 14.3		1998 Jan 14 1998 Jun 2	NRO 45 m NRO 45 m
(101) VLA 1623.....	Oph A	16 23 25	−24 17 47	Class 0	1997 Dec 27 1997 Dec 31 1998 Jan 5 1998 Jan 11 1998 Jan 14 1998 Jun 1 1998 Jun 2 1998 Jun 13 1999 Feb 12	NRO 45 m NRO 45 m VLA DnC
(102) SM 1	Oph A	16 23 26	−24 17 14	PPSC	1997 Dec 27 1998 Dec 30 1998 Jun 1	NRO 45 m NRO 45 m NRO 45 m
(103) SM 2	Oph A	16 23 27.6	−24 17 40	PPSC	1998 Jan 3 1998 Jun 1	NRO 45 m NRO 45 m
(104) A-S.....	Oph A	16 23 41.6	−24 18 35.4	PPSC	1998 Jun 2	NRO 45 m
(105) C-W	Oph C	16 23 48.3	−24 26 07	PPSC	1998 Jun 3	NRO 45 m
(106) C-N.....	Oph C	16 23 55.6	−24 24 57	PPSC	1998 Jun 3	NRO 45 m
(107) E-MM 1	Oph E	16 23 55.9	−24 30 14	PPSC	1998 Jun 3	NRO 45 m
(108) SR 24	Oph/HH 224 WSB 47	16 23 56.4	−24 38 48	Class I	1998 Jun 3	NRO 45 m
(109) GRBR 51	Oph E	16 23 56.6	−24 30 58		1998 Jun 3	NRO 45 m
(110) IRAS 16243−2422	Oph C WL 12	16 23 42.5	−24 28 04	Class I	1997 Dec 27 1998 Jan 3 1998 Jan 18 1998 Jun 1	NRO 45 m NRO 45 m NRO 45 m NRO 45 m
(111) MM 7.....	Oph C	16 24 01.6	−24 27 40	PPSC	1998 Jun 3	NRO 45 m
(112) MM 3.....	Oph E	16 24 04.1	−24 30 28	PPSC	1998 Jun 3	NRO 45 m
(113) B1-MM 1	Oph B1	16 24 07.1	−24 21 09	PPSC	1998 Jun 2	NRO 45 m
(114) GY 213.....	Oph E	16 24 07.5	−24 33 42	Class I	1998 Jun 3	NRO 45 m
(115) EL 29	Oph E	16 24 07.7	−24 30 37.2	Class I	1998 Jun 3 1998 Jun 13	NRO 45 m NRO 45 m
(116) E-MM 4	Oph E	16 24 08.8	−24 32 49	PPSC	1998 Jun 3	NRO 45 m
(117) B1-MM 2	Oph B1	16 24 09.7	−24 22 37	PPSC	1998 Jun 2	NRO 45 m
(118) E-MM 5	Oph E	16 24 10	−24 31 16	PPSC	1998 Jun 3	NRO 45 m
(119) B1-MM 3	Oph B1	16 24 10.8	−24 23 17	PPSC	1998 Jun 2	NRO 45 m
(120) GY 236.....	Oph B2	16 24 13	−24 20 04	Class I	1998 Jun 2	NRO 45 m
(121) B1-MM 4	Oph B1	16 24 14.1	−24 24 01	PPSC	1998 Jun 2	NRO 45 m
(122) WL 6	Oph B YLW 14	16 24 19.8	−24 23 8	Class I	1997 Dec 27 1998 Jan 18	NRO 45 m NRO 45 m
(123) IRS 43	L1681B Oph F	16 24 25.1	−24 34 10	Class I	1997 Dec 27 1998 Jan 18 1998 Jun 13	NRO 45 m NRO 45 m NRO 45 m

TABLE 1—Continued

YSO Name (1)	Alternative Name/Core Name (2)	R.A. (B1950.0) (3)	Decl. (B1950.0) (4)	Source Type (5)	Date (6)	Instruments (7)
(124) IRAS 16244–2432	Oph F YLW 16A IRS 44	16 24 26.17	−24 32 53	Class I	1997 Dec 27 1998 Jan 11 1998 Jun 13	NRO 45 m NRO 45 m NRO 45 m
(125) IRS 46	L1681B Oph F	16 24 27.4	−24 32 36	Class I	1998 Jan 3 1998 Jan 18 1998 Jun 1	NRO 45 m NRO 45 m NRO 45 m
(126) GY 284.....	Oph B2	16 24 29.4	−24 18 15	Class I	1998 Jun 3	NRO 45 m
(127) B2-MM 17	Oph B2	16 24 33.6	−24 19 42	PPSC	1998 Jun 3	NRO 45 m
(128) IRS 48	ρ Oph	16 24 35.5	−24 23 55	Class I	1998 Jan 3 1998 Jan 18 1998 Jun 1	NRO 45 m NRO 45 m NRO 45 m
(129) IRAS 16246–2436	L1681B2 IRS 51 YLW 45	16 24 37.6	−24 36 35	Class I	1998 Jan 3 1998 Jan 18 1998 Jun 13	NRO 45 m NRO 45 m NRO 45 m
(130) ROX 30C		16 24 37.9	−23 51 37.0	Class II/III	1998 Jan 14	NRO 45 m
(131) IRS 55/ROX 31	Oph F	16 24 50.3	−24 34 10	Class I	1998 Jan 18	NRO 45 m
(132) D-MM 2.....	Oph D	16 25 27.6	−24 12 28	PPSC	1998 Jun 3	NRO 45 m
(133) L1696A		16 25 30	−24 11 32		1998 Feb 27 1998 Jun 3	NRO 45 m NRO 45 m
(134) D-MM 5.....	Oph D	16 25 35.4	−24 11 50	PPSC	1998 Jun 3	NRO 45 m
(135) ROX 34.....	SR 13	16 25 43.67	−24 21 42.2	Class II	1998 Jan 13	NRO 45 m
(136) ROX 44.....	DoAr 44	16 28 31.74	−24 21 10.0	Class II	1998 Jan 13 1998 Jun 2	NRO 45 m NRO 45 m
(137) IRAS 16285–2355	IRS 63 L1709B	16 28 34.6	−23 55 05	Class I	1998 Jan 3 1998 Jan 18 1998 Jun 2	NRO 45 m NRO 45 m NRO 45 m
(138) IRS 67	L1689S	16 28 58.3	−24 50 20	Class I	1998 Jan 3 1998 Jan 18 1998 Jun 2	NRO 45 m NRO 45 m NRO 45 m
(139) IRAS 16293–2422	L1689N	16 29 21	−24 22 16	Class 0	1997 Dec 27 1998 Jan 3 1998 Jan 5 1998 Jan 11 1998 Jan 14 1998 Jan 18 1998 Jun 1 1998 Jun 2 1998 Jun 13	NRO 45 m NRO 45 m
(140) IRAS 16316–1540	L43-RNO 91	16 31 38	−15 40 50	Class I/II	1997 Dec 31 1998 Jun 3 1998 Jun 13	NRO 45 m NRO 45 m NRO 45 m
(141) IRAS 16442–0929	L260	16 44 13.9	−09 29 59	Class I	1997 Dec 31 1998 Jan 18	NRO 45 m NRO 45 m
(142) L234E		16 45 18.5	−10 51 43		1998 Jun 3	NRO 45 m
(143) IRAS 16451–1045	L234A	16 45 21	−10 46 33		1998 Jun 3	NRO 45 m
(144) L63.....		16 47 21	−18 01 00		1998 Feb 12	NRO 45 m
(145) IRAS 16544–1604	L146	16 54 27.2	−16 04 48		1998 Jan 3 1998 Feb 26 1998 Jun 2	NRO 45 m NRO 45 m NRO 45 m

TABLE 1—Continued

YSO Name (1)	Alternative Name/Core Name (2)	R.A. (B1950.0) (3)	Decl. (B1950.0) (4)	Source Type (5)	Date (6)	Instruments (7)
(146) IRAS 17130–2053	L100 B362	17 13 03.9	−20 53 39		1997 Dec 31 1998 Jun 2	NRO 45 m NRO 45 m
(147) IRAS 18148–0440	L483 FIR	18 14 50.6	−04 40 49	Class 0/I	1998 Jan 3 1998 Jan 5 1998 Jan 18 1998 Feb 12 1998 Jun 2 1998 Jun 3 1998 Jun 14 1998 Jun 21 1999 Jan 27 1999 Feb 12	NRO 45 m NRO 45 m VLA DnC
(148) IRAS 18162–2048	HH 80–81	18 16 13	−20 48 48.27		1997 Dec 31 1998 Jan 5 1998 Jan 18 1998 Jun 2	NRO 45 m NRO 45 m NRO 45 m NRO 45 m
(149) IRAS 18265–1517	L379-IRS 1	18 26 32.9	−15 17 51	B0–5 ZAMS?	1997 Dec 31 1998 Jun 2	NRO 45 m NRO 45 m
(150) IRAS 18269+0116	HH 106–107 ESO H α 279	18 26 59.69	01 16 42.7		1998 Jan 18 1998 Jan 27	NRO 45 m NRO 45 m
(151) S68N	Serpens SMM 9	18 27 15.8	−01 14 50	Class 0	1998 Jan 5 1998 Jan 11 1998 Jan 19 1998 Jun 2 1998 Jun 14 1998 Dec 14 1999 Jan 27 1999 Feb 12	NRO 45 m NRO 45 m NRO 45 m NRO 45 m NRO 45 m NRO 45 m NRO 45 m VLA DnC
(152) FU Orionis.....		18 27 16.8	01 14 15		1997 Dec 31 1998 Jan 5 1998 Jun 2 1999 Feb 12	NRO 45 m NRO 45 m NRO 45 m VLA DnC
(153) Serpens FIRS 1	Serpens SMM 1	18 27 17.5	01 13 15	Class 0	1997 Dec 15 1998 Jan 5 1998 Jan 18 1998 Jun 2 1998 Jun 3 1998 Jun 14 1998 Jun 21 1998 Dec 14 1999 Jan 27	NRO 45 m NRO 45 m
(154) Serpens SMM 5	IRS 53	18 27 18.9	01 14 36		1998 Jan 5 1998 Jan 18 1998 Jun 2 1999 Jan 27 1999 Feb 12	NRO 45 m NRO 45 m NRO 45 m NRO 45 m VLA DnC
(155) Serpens SVS 2		18 27 24.5	01 12 41	Class I?	1998 Jan 18 1998 Jun 2	NRO 45 m NRO 45 m
(156) Serpens SMM 4		18 27 24.7	01 11 10	Class 0	1998 Jan 5 1998 Jan 18 1998 Jun 2 1999 Jan 27 1999 Feb 12	NRO 45 m NRO 45 m NRO 45 m NRO 45 m VLA DnC
(157) Serpens SMM 6	SVS 20	18 27 25.4	01 12 02		1998 Jan 5 1998 Jan 18 1998 Jun 2 1999 Jan 27 1999 Feb 12	NRO 45 m NRO 45 m NRO 45 m NRO 45 m VLA DnC

TABLE 1—Continued

YSO Name (1)	Alternative Name/Core Name (2)	R.A. (B1950.0) (3)	Decl. (B1950.0) (4)	Source Type (5)	Date (6)	Instruments (7)
(158) Serpens SVS 4.....		18 27 26	01 10 50		1998 Jun 2 1999 Feb 12	NRO 45 m VLA DnC
(159) Serpens SMM 3.....		18 27 27.3	01 11 55	Class 0	1998 Jan 5 1998 Jan 18 1998 Jun 2 1998 Jun 14 1999 Jan 27 1999 Feb 12	NRO 45 m NRO 45 m NRO 45 m NRO 45 m NRO 45 m VLA DnC
(160) Serpens SMM 2.....		18 27 28	01 10 45	Class 0	1998 Jan 5 1998 Jan 11 1998 Jun 2 1999 Jan 27 1999 Feb 12	NRO 45 m NRO 45 m NRO 45 m NRO 45 m VLA DnC
(161) IRAS 18277–1516	L379-IRS 2	18 27 43.4	−15 16 45	Ae/Be	1997 Dec 31 1998 Jun 2	NRO 45 m NRO 45 m
(162) IRAS 18331–0035	HH 108-IR L588	18 33 07.76	−00 35 48.4		1998 Jan 18 1998 Jan 27 1998 Jun 2	NRO 45 m NRO 45 m NRO 45 m
(163) HH 108-MMS.....		18 33 12.11	−00 35 21.7	Class 0	1998 Jan 11 1998 Jan 14 1998 Jun 2	NRO 45 m NRO 45 m NRO 45 m
(164) HH 100-IR.....		18 58 28.7	−37 02 03		1997 Dec 31	NRO 45 m
(165) IRAS 18585–3701	R CrA	18 58 31.27	−37 01 28.8		1997 Dec 31	NRO 45 m
(166) IRAS 19156+1906	L723 FIR	19 15 42	19 06 55	Class 0	1996 May 5 1996 Oct 15 1997 Dec 30 1998 Jan 5 1998 Jan 18 1998 Jan 27 1998 Feb 12 1998 Jun 2 1998 Jun 14 1998 Jun 21 1998 Dec 14 1999 Jan 27 1999 Feb 12	NRO 45 m VLA A NRO 45 m NRO 45 m VLA DnC
(167) IRAS 19180+1116	L673 RNO 109	19 18 01.30	11 16 26.9		1997 Dec 31 1998 Jun 3	NRO 45 m NRO 45 m
(168) IRAS 19180+1114	L673	19 18 04.60	11 14 12.0		1997 Dec 31 1998 Jun 3	NRO 45 m NRO 45 m
(169) IRAS 19244+2352	L778	19 24 26.4	23 52 37		1998 Feb 12 1998 Jun 3	NRO 45 m NRO 45 m
(170) B335-IRS	HH 119	19 34 35.1	07 27 24	Class 0	1997 Dec 15 1998 Jan 5 1998 Jan 18 1998 Jan 27 1998 Feb 12 1998 Jun 2 1998 Jun 14 1998 Jun 21 1998 Dec 14 1999 Jan 27 1999 Jan 31 1999 Mar 15	NRO 45 m NRO 45 m

TABLE 1—Continued

YSO Name (1)	Alternative Name/Core Name (2)	R.A. (B1950.0) (3)	Decl. (B1950.0) (4)	Source Type (5)	Date (6)	Instruments (7)
(171) HH 165	L1548 I548C27	19 40 47.18	23 17 02.9		1998 Jan 4 1998 Jan 10 1998 Feb 26 1998 Jun 2	NRO 45 m NRO 45 m NRO 45 m NRO 45 m
(172) IRAS 19433+2743	L810	19 43 21.7	27 43 37		1998 Jun 3	NRO 45 m
(173) IRAS 20050+2720	20050+2720 MMS 1	20 05 02.5	27 20 09	Class 0/I	1997 Dec 27 1998 Jan 5 1998 Jan 11 1998 Jan 18 1998 Feb 3 1998 Feb 12 1998 Jun 2 1998 Jun 21 1998 Dec 8 1998 Dec 14 1999 Jan 27 1999 Feb 12	NRO 45 m NRO 45 m VLA DnC
(174) S106 FIR		20 25 32.53	37 12 50.8	Class 0	1997 Oct 8 1997 Oct 18 1997 Dec 23 1997 Dec 30 1998 Jan 5 1998 Jan 11 1998 Jan 18 1998 Feb 3 1998 Feb 12 1998 Jun 2 1998 Jun 21 1999 Jan 27 1999 Feb 12	NRO 45 m NRO 45 m VLA DnC
(175) IRAS 20353+6742	L1152	20 35 19.4	67 42 30	Class 0/I	1997 Dec 30 1998 Jan 18 1998 Feb 12 1998 Jun 2 1998 Jun 14 1998 Jun 21 1999 Jan 27 1999 Feb 12	NRO 45 m NRO 45 m NRO 45 m NRO 45 m NRO 45 m NRO 45 m NRO 45 m VLA DnC
(176) IRAS 20386+6751	L1157-MM	20 38 39.3	67 51 36	Class 0	1997 Dec 30 1998 Jan 5 1998 Jan 11 1998 Jan 18 1998 Feb 12 1998 Jun 2 1998 Jun 14 1998 Jun 21 1999 Jan 27 1999 Feb 12	NRO 45 m NRO 45 m VLA DnC
(177) IRAS 20503+6006	L1082C	20 50 19.5	60 06 40	Class I	1998 Jan 3 1998 Feb 12 1998 Jun 2 1998 Jun 21	NRO 45 m NRO 45 m NRO 45 m NRO 45 m
(178) GF 9-2	L1082	20 50 22.05	60 07 19	Class 0	2000 Apr 8	NRO 45 m
(179) IRAS 20520+6003	L1082A	20 52 04.5	60 03 18	Class I	1997 Dec 31 1998 Jan 3 1998 Jun 2 1998 Jun 13 1998 Jun 21	NRO 45 m NRO 45 m NRO 45 m NRO 45 m NRO 45 m

TABLE 1—Continued

YSO Name (1)	Alternative Name/Core Name (2)	R.A. (B1950.0) (3)	Decl. (B1950.0) (4)	Source Type (5)	Date (6)	Instruments (7)
(180) IRAS 20526+5958	L1082B	20 52 41	59 58 19	Class I	1998 Jan 3 1998 Jan 18 1998 Feb 12 1998 Jun 2 1998 Jun 14 1998 Jun 21	NRO 45 m NRO 45 m NRO 45 m NRO 45 m NRO 45 m NRO 45 m
(181) IRAS 20582+7724	HH 199 L1228	20 58 14.5	77 24 05		1998 Jan 5 1998 Jun 2	NRO 45 m NRO 45 m
(182) IRAS 20597+6800	L1174	20 59 42.1	68 00 12	Class I	1998 Jan 5 1998 Jan 18 1998 Jun 21 1999 Jan 27	NRO 45 m NRO 45 m NRO 45 m NRO 45 m
(183) IRAS 21007+4951	L988A	21 00 44.9	49 51 13		1998 Jun 3	NRO 45 m
(184) IRAS 21017+6742	L1172-D	21 01 44.2	67 42 24	Class I	1998 Feb 12 1998 Jun 2	NRO 45 m NRO 45 m
(185) IRAS 21023+5002	L988E	21 02 19.6	50 02 40		1998 Jun 3	NRO 45 m
(186) IRAS 21024+4955	L988F	21 02 24.5	49 55 50		1998 Jun 3	NRO 45 m
(187) IRAS 21106+4712	B361	21 10 40.9	47 12 01	Class I	1998 Jan 5 1998 Jan 18 1998 Feb 12	NRO 45 m NRO 45 m NRO 45 m
(188) IRAS 21246+5743	IC 1396W	21 24 38.7	57 43 14		1998 Jan 11	NRO 45 m
(189) IRAS 21391+5802	IC 1396N	21 39 10.3	58 02 29		1996 May 5 1998 Jan 11 1998 Jun 22	NRO 45 m NRO 45 m NRO 45 m
(190) IRAS 21418+6552	LkH α 234	21 41 53.2	65 52 42		1996 May 5 1998 Jan 11 1998 Jun 3 1998 Jun 22	NRO 45 m NRO 45 m NRO 45 m NRO 45 m
(191) IRAS 21445+5712	IC 1396E	21 44 30.8	57 12 29		1998 Jan 11 1998 Jun 3 1998 Jun 22	NRO 45 m NRO 45 m NRO 45 m
(192) IRAS 22176+6303	S140-IRS	22 17 41.2	63 03 43		1998 Jun 22	NRO 45 m
(193) IRAS 22198+6336	L1204A	22 19 50.7	63 36 33		1998 Jun 2 1998 Jun 14 1998 Jun 21	NRO 45 m NRO 45 m NRO 45 m
(194) IRAS 22199+6322	L1204B	22 19 55.7	63 22 12		1998 Jun 2 1998 Jun 21	NRO 45 m NRO 45 m
(195) IRAS 22266+6845	L1221	22 26 37.2	68 45 52		1998 Jan 5 1998 Jun 2	NRO 45 m NRO 45 m
(196) IRAS 22267+6244	L1203	22 26 46.7	62 44 22		1998 Feb 12 1998 Jun 2	NRO 45 m NRO 45 m
(197) IRAS 22272+6358	L1206	22 27 12.2	63 58 21		1998 Jun 2	NRO 45 m
(198) IRAS 22343+7501	L1251A	22 34 22	75 01 32	Class I/II	1998 Jan 5 1998 Jun 2 1999 Jan 27	NRO 45 m NRO 45 m NRO 45 m
(199) IRAS 22376+7455	L1251B	22 37 40.8	74 55 50	Class I	1998 Jan 5 1998 Jun 2 1999 Jan 27	NRO 45 m NRO 45 m NRO 45 m
(200) IRAS 22543+6145	Cepheus A	22 54 20.2	61 45 55	B0.5 ZAMS	1998 Jan 11 1998 Jan 18	NRO 45 m NRO 45 m

TABLE 1—Continued

YSO Name (1)	Alternative Name/Core Name (2)	R.A. (B1950.0) (3)	Decl. (B1950.0) (4)	Source Type (5)	Date (6)	Instruments (7)
					1998 Feb 12 1998 Jun 22	NRO 45 m NRO 45 m
(201) IRAS 23011+6126	Cepheus E	23 01 10.1	61 26 16	Class 0	1997 Dec 30 1998 Jan 5 1998 Jan 11 1998 Jan 18 1998 Feb 12 1998 Feb 26 1998 Jun 2 1998 Jun 14 1998 Jun 21 1999 Jan 27 1999 Feb 12	NRO 45 m NRO 45 m VLA DnC
(202) IRAS 23037+6123	Cepheus C	23 03 45.6	62 13 49		1998 Jan 11 1998 Jun 2	NRO 45 m NRO 45 m
(203) IRAS 23238+7401	L1262	23 23 48.7	74 01 08	Class I	1998 Jan 5 1998 Feb 12 1998 Jun 2 1999 Jan 27	NRO 45 m NRO 45 m NRO 45 m NRO 45 m

NOTE.—Units of right ascension are hours, minutes, and seconds, and units of declination are degrees, arcminutes, and arcseconds.

of 0.82 and correspond to 80 and 270 mJy in flux density (S_ν) for the aperture efficiency (η_a) of 0.64. These telescope efficiencies were stable within 2% from 1996 to 2000. For the reader's convenience, conversion from T_A^* in K to flux density in Jy is given by $S_\nu = 2kT_A^*/\eta_a A_p = 2.7 \text{ Jy}(T_A^*/1 \text{ K})(\eta_a/0.64)$, where A_p is the physical aperture of the telescope. We stress that this is one of the most sensitive H₂O maser surveys ever conducted: the sensitivity attained reached down to the order of $10^{-13} L_\odot$ in isotropic H₂O maser luminosity ($L_{\text{H}_2\text{O}}$) for a nearby molecular cloud such as Taurus and Ophiuchus.

3.2. VLA Observations

Follow-up interferometric observations were performed using the VLA of the NRAO in three epochs between 1998 October and 1999 February in its CnB and DnC configurations. The primary purpose of the observations was to associate the masers detected by the 45 m telescope with specific YSOs: toward NGC 1333, NGC 2024, and Serpens more than one source exists within the beam of the 45 m telescope. The FOV, primary beam size of the VLA antenna was 2.0'. Resulting synthesized beam sizes were typically 0''.8 and 3'' at the CnB and DnC configurations, respectively. We employed the single intermediate-frequency (IF) mode using 128 channels with a total bandwidth of 3.125 MHz; the velocity coverage was 42.1 km s⁻¹ with a resolution of 0.33 km s⁻¹. For the sources that have high-velocity components, we employed different frequency setups as follows. We observed the masers in the IRAS 20050+2720 region twice by setting the center velocities at $V_{\text{LSR}} = -91$ and -1 km s⁻¹. Moreover, we employed a frequency setup of a total bandwidth of 6.25 MHz with 64 channels for the Cep E-MM masers: this gave the velocity coverage of 84.3 km s⁻¹ with a resolution of 0.66 km s⁻¹. On-source integration time was 3 minutes for the CnB array observations on 1998

October and 15–30 minutes for the DnC array observations on 1999 February. We integrated in 60 minutes for only one field in the Serpens cloud, which covers Serpens SMM 2, SMM 3, SMM 4, and SMM 6 (Fig. 1g). Data reduction was done by standard procedures using the AIPS package. Resulting sensitivities ranged from 0.5 to 15 Jy beam⁻¹ per channel. For NGC 2024 FIR and S106 FIR, we subtracted continuum emission. We employed a self-calibration procedure for some sources using only the phase of the strongest maser spot in order to improve the signal-to-noise ratio of the spectra.

4. RESULTS

4.1. Nobeyama 45 m Telescope Results

In Figures 2–41 we present H₂O maser spectra obtained by the Nobeyama 45 m telescope for 39 sources that exhibited the emission at least once. For 15 sources, the spectra were presented on two different scales in order to show both overall shape and weak maser emission at low level. In these spectra, one can recognize characteristics of the masers common in low-mass stars. Observed maser emission (1) is principally weak and tends to show relatively simple spectral profiles compared with those of high-mass objects and (2) is highly time variable as seen in high-mass objects. In addition to the characteristics known so far, we discovered extremely high velocity (EHV) components toward Cep E-MM and IRAS 20050+2720, which are relatively luminous Class 0 sources. Notes on individual sources are given in § 4.3.

Table 2 presents properties of all the detected H₂O maser spectra for the two sources. Column (1) gives the representative YSO name, which is the same as column (1) of Table 1. Column (2) gives the observing date. Columns (3), (4), and (5) give a peak LSR velocity of the detected emission, a peak

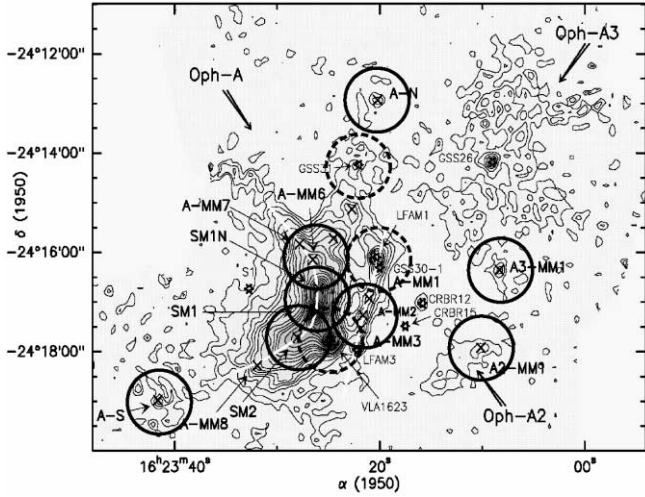


FIG. 1a

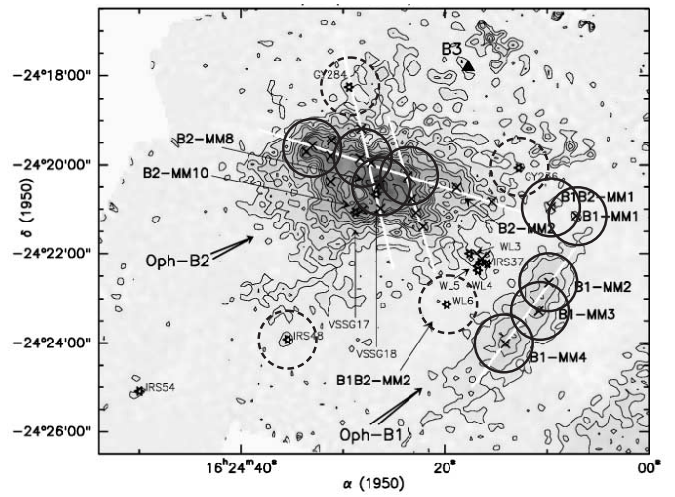


FIG. 1b

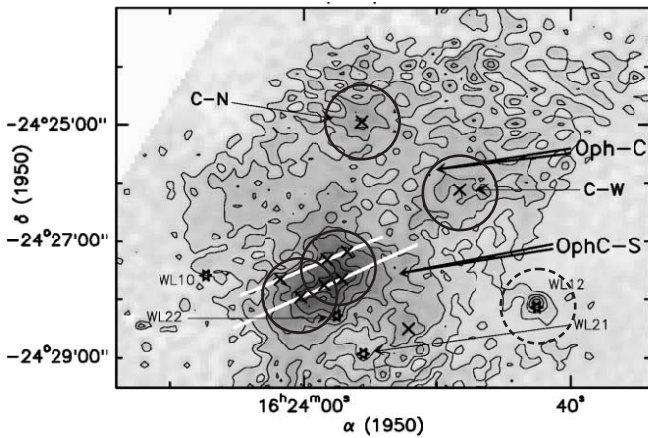


FIG. 1c

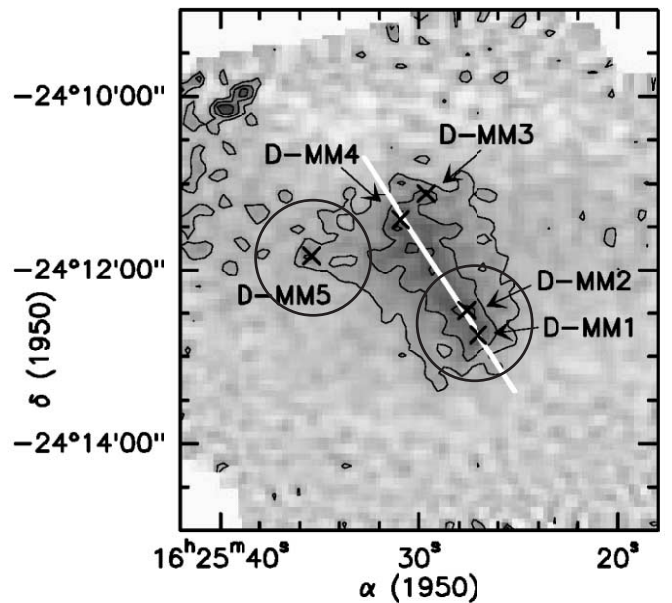


FIG. 1d

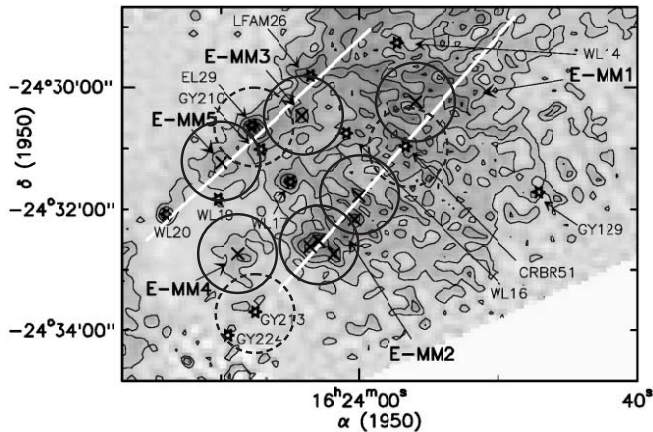


FIG. 1e

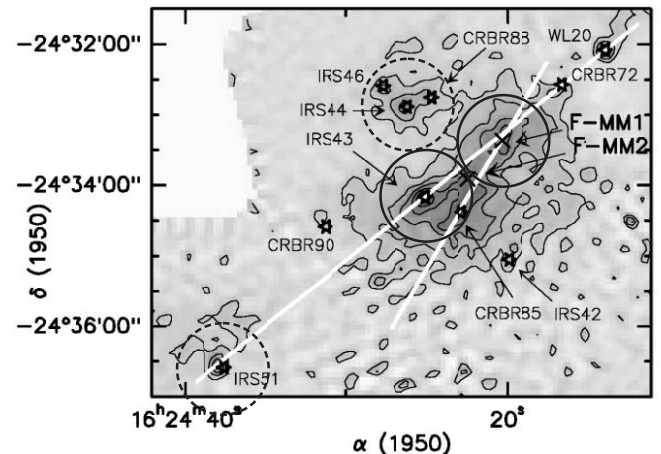


FIG. 1f

FIG. 1.—Observed positions by the H₂O maser survey using the Nobeyama 45 m telescope toward the regions of (a) Ophiuchus A, (b) Ophiuchus B1/B2, (c) Ophiuchus C, (d) Ophiuchus D, (e) Ophiuchus E, and (f) Ophiuchus F indicated on the 1.3 mm continuum emission maps by the MPIfR bolometer array at the IRAM 30 m telescope (Motte et al. 1998). The circles and dashed circles indicate the PPSCs and YSOs, respectively. (g) Observed positions by the Nobeyama 45 m telescope and the FOVs of the VLA observations in the Serpens star-forming region indicated on the 1.3 mm continuum emission image obtained by the Owens Valley Radio Observatory array (Testi & Sargent 1998). Thick and short-dashed circles present the beam of the Nobeyama 45 m telescope and the VLA FOVs, respectively.

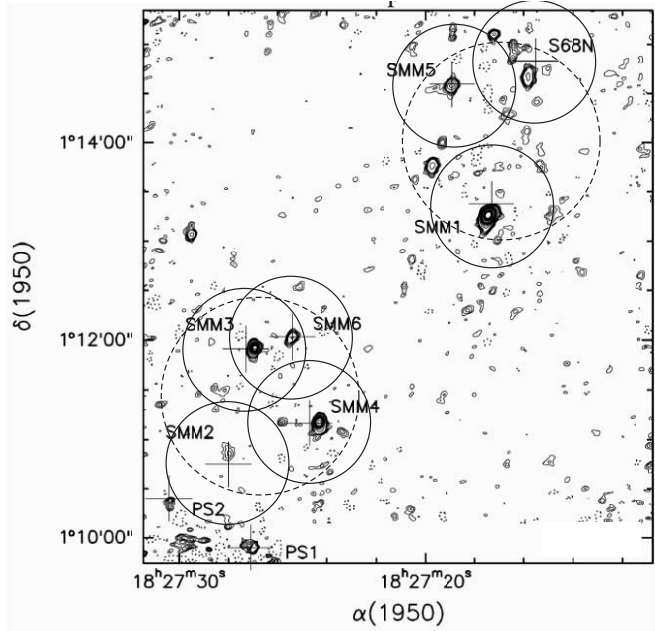


FIG. 1g

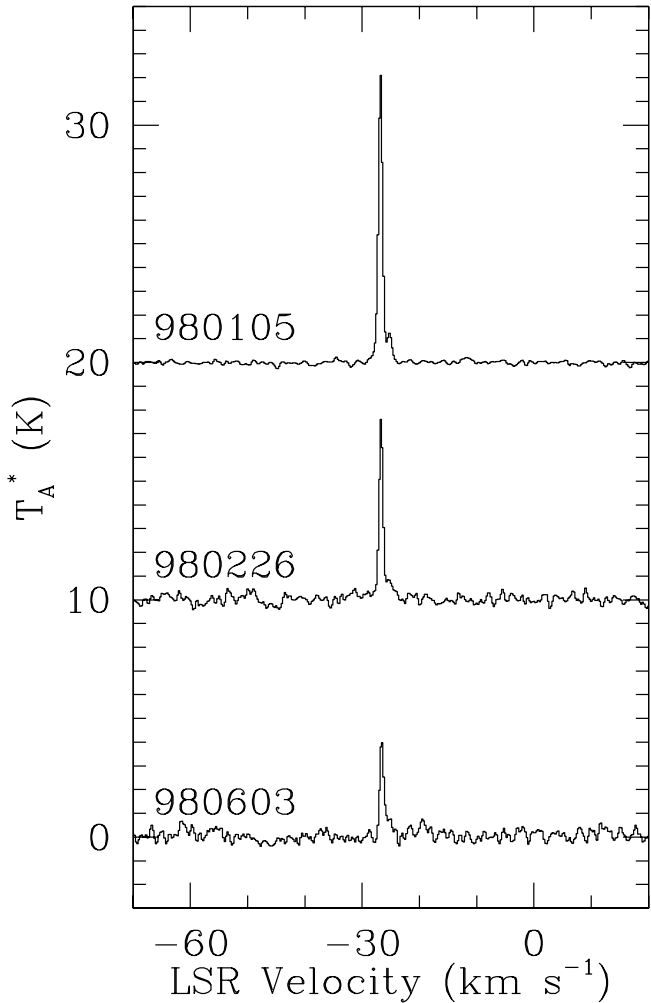


FIG. 2.— H_2O maser spectra for the source IRAS 00338+6312 (L1287) from the Nobeyama 45 m telescope survey. The ambient cloud velocity estimated from the CS $J = 2-1$ line is $V_{\text{LSR}} = -18 \text{ km s}^{-1}$ (Yang, Ohashi, & Fukui 1995).

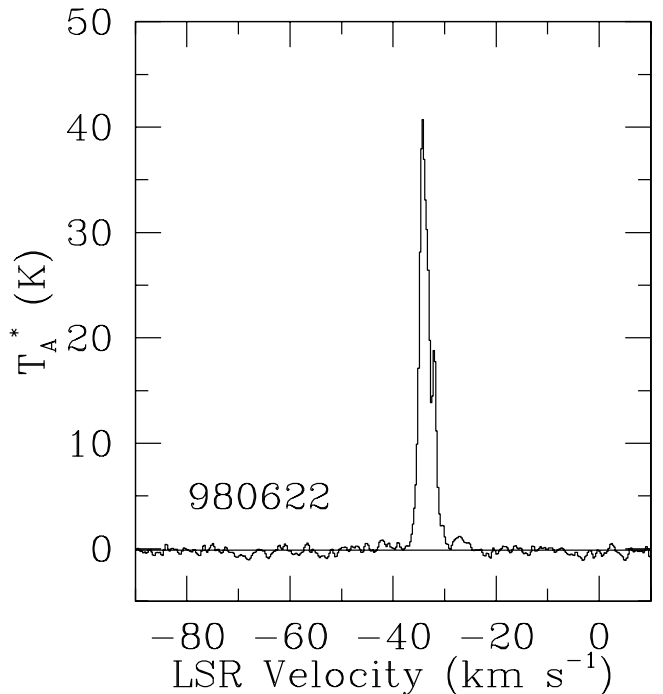


FIG. 3.— H_2O maser spectrum for the source IRAS 00494+5617 (NGC 281A) from the Nobeyama 45 m telescope survey. The ambient cloud velocity estimated from the NH_3 line is $V_{\text{LSR}} \sim -30 \text{ km s}^{-1}$ (Wouterloot, Walmsley, & Henkel 1988; Harju, Walmsley, & Wouterloot 1993; Henning et al. 1994).

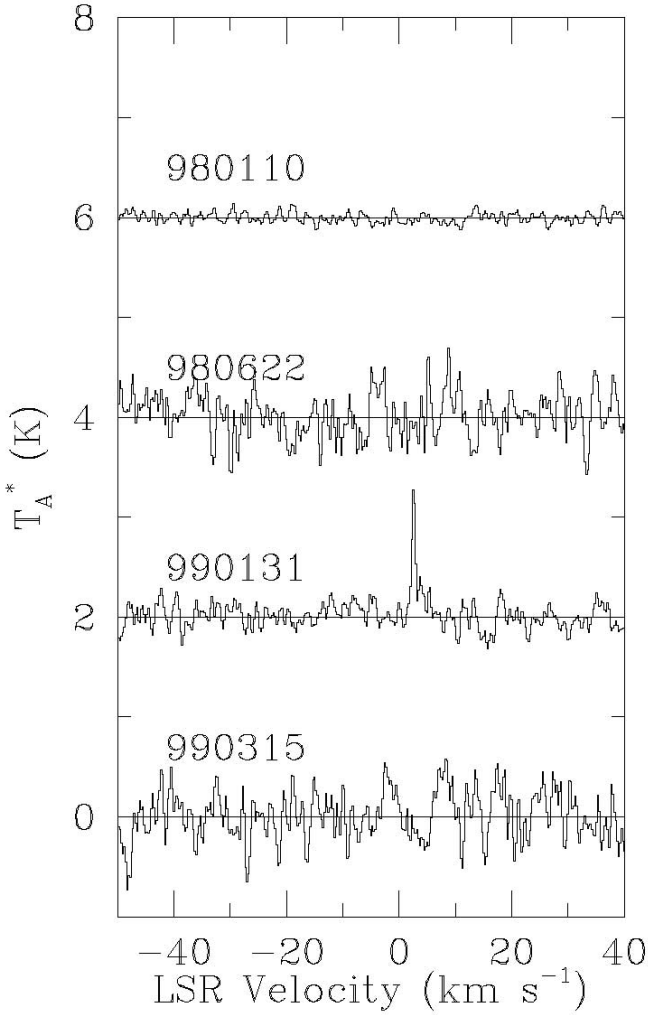


FIG. 4a

FIG. 4.— H_2O maser spectra for the source RNO 15-FIR (IRAS 03245+3002) from (a) the Nobeyama 45 m telescope survey and (b) VLA CnB array observations. The ambient cloud velocity estimated from the CO $J = 2-1$ line is $V_{\text{sys}} = 4.7 \text{ km s}^{-1}$ (Davis et al. 1997).

intensity in T_A^* scale, and a half-width of the spectrum derived from Gaussian fitting, respectively. Column (6) gives an integrated intensity ($\int T_A^* dv$) of each velocity component in units of K km s^{-1} . Column (7) gives a total isotropic luminosity ($L_{\text{H}_2\text{O}}$) of the H_2O masers on each observing day, which is a sum of that of each velocity component calculated by

$$\begin{aligned} L_{\text{H}_2\text{O}} &= 4\pi d^2 \frac{2k}{\eta_a A_p c} \nu \int T_A^* dv \\ &= 1.59 \times 10^{-12} L_\odot \left(\frac{d}{160 \text{ pc}} \right)^2 \left(\frac{\int T_A^* dv}{1 \text{ K km s}^{-1}} \right) \left(\frac{\eta_a}{0.65} \right), \end{aligned} \quad (1)$$

where d is the distance to the source and ν is the rest frequency of the maser line.

During the course of the Nobeyama survey, only eight Class 0 sources (NGC 1333 IRAS 4A, NGC 1333 IRAS 4B, NGC 1333 SVS 13A, NGC 2024 FIR 5, IRAS 16293–2422, L483 FIR, IRAS 20050+2720, and S106 FIR) continued to show maser emission at all epochs: some spectral components persisted for up to a year. On the

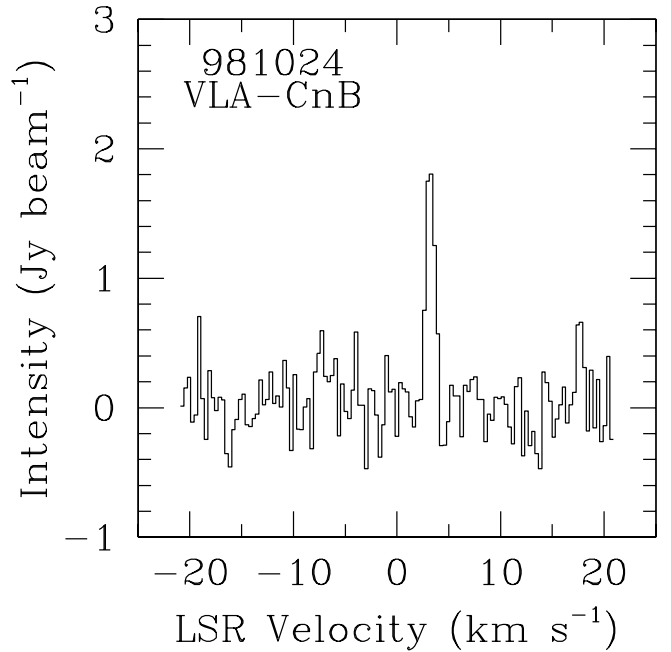


FIG. 4b

other hand, weak maser features typically appeared and disappeared on timescales less than a couple of months. In order to investigate short duration time variation, we present a time variation contour map, which is a diagram of the observing time versus LSR velocity of maser emission. Here we present the maps for seven Class 0 sources observed by the 45 m telescope more than 5 times with intervals less than 2 weeks: they are VLA 1623 with the data from 1997 December 27 to 1998 February 12 (Fig. 18c), IRAS 16293–2422 for the data from 1997 December 27 to 1998 January 18 (Fig. 20c), Serpens FIRS 1 for the data from 1998 June 2 to 21 (Fig. 26b), IRAS 20050+2720 for the data from 1997 December 27 to 1998 February 12 (Figs. 29c and 29d), S106 FIR for the data from 1997 October 18 to 1998 February 12 (Figs. 30b and 30c), and Cep E-MM for the data from 1997 December 27 to 1998 June 2 (Fig. 41d). In order to plot them, we linearly interpolated the spectra along the time axes after resampling each spectrum by a 0.5 km s^{-1} bin, which is the velocity resolution of the Nobeyama observations. Comments on these individual maps are given in § 4.3, and the duration of the maser emission for Class 0 and Class I sources is discussed in § 5.1.

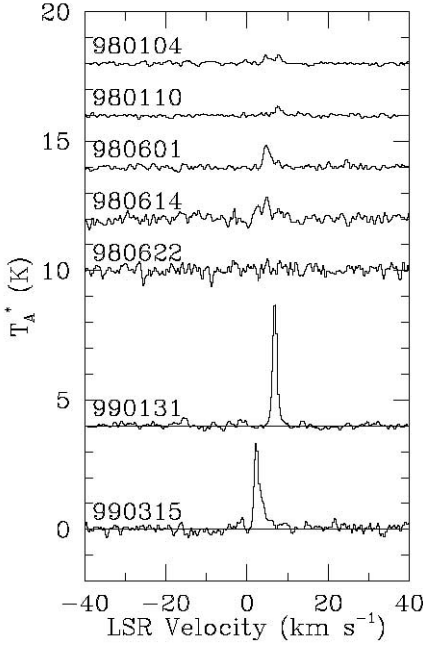


FIG. 5a

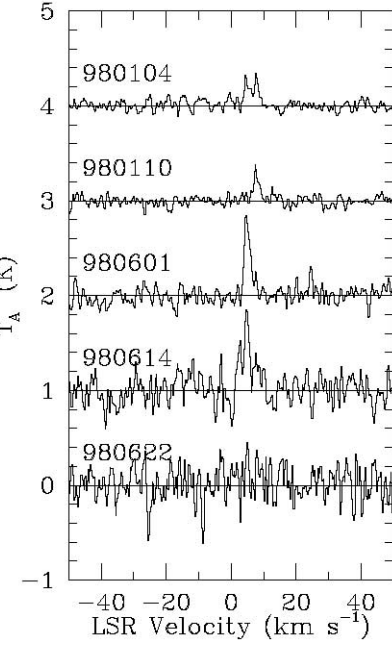


FIG. 5b

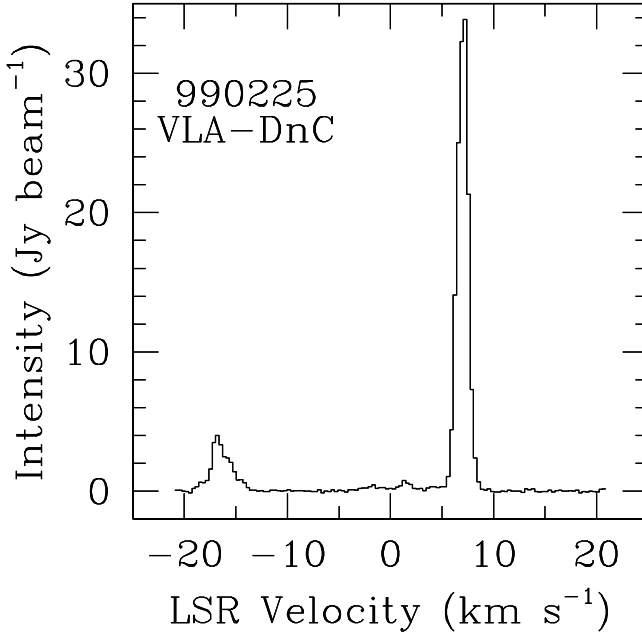
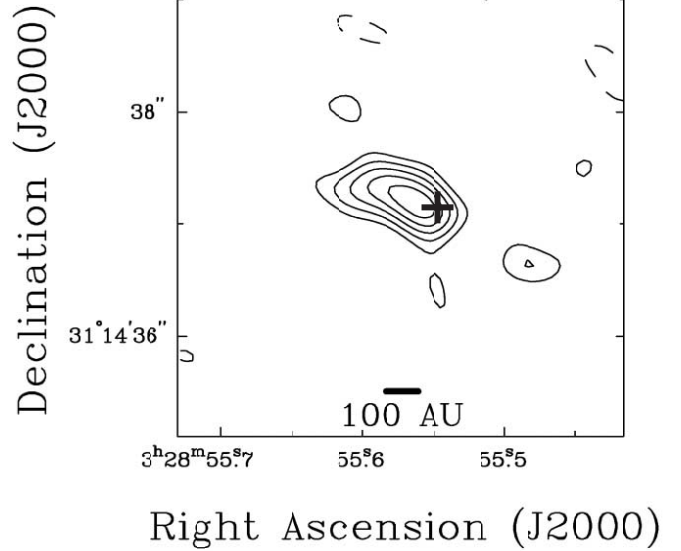


FIG. 5c



Right Ascension (J2000)

FIG. 5d

FIG. 5.— H_2O maser spectra for the source NGC 1333 IRAS 2A from (a) and (b) the Nobeyama 45 m telescope survey and (c) the VLA DnC array observations. The ambient cloud velocity estimated from the $\text{C}^{18}\text{O } J = 2-1$ line is 7.3 km s^{-1} (Sandell et al. 1994) and from the $\text{H}^{13}\text{CO}^+ J = 4-3$ line is 7.6 km s^{-1} (Ward-Thompson et al. 1996). (d) Position of the masers from the VLA observations (cross) indicated on the $\lambda = 2.7 \text{ mm}$ continuum emission image from the BIMA array (Looney et al. 2000).

4.2. VLA Results

In Figures 4–41 we present three H_2O maser spectra obtained by the VLA survey. We generated these spectra by integrating data cubes using the task ISPEC in the AIPS package. For five Class 0 sources, we present the positions of the maser emission on the maps of continuum emission at $\lambda = 2.7 \text{ mm}$ taken with the BIMA array (Looney, Mundy, & Welch 2000); these are NGC 1333 IRAS 2A (Fig. 5d), NGC 1333 SVS 13A (Fig. 6d), NGC 1333 IRAS 4A (Fig.

7e), NGC 1333 IRAS 4B (Fig. 7f), and VLA 1623 (Fig. 18e). Furthermore, we present the positions of the maser emission in L723 on the map of $\lambda = 3.6 \text{ cm}$ free-free emission (Anglada, Rodríguez, & Torrelles 1996; Fig. 28d). In Table 3 we list the parameters of the observations and the detected H_2O maser emission shown in Figures 4–41. Column (1) gives the representative YSO name, which is the same as column (1) in Table 1. Columns (2) and (3) give the size of the synthesized beam and the position angle, respectively. Columns (4) and (5) give the peak LSR velocity of the

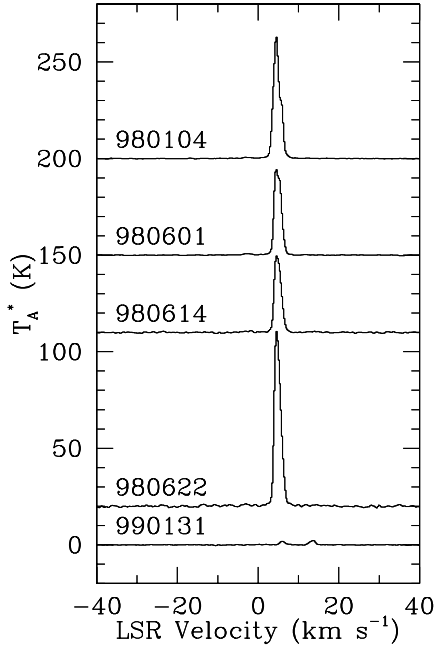


FIG. 6a

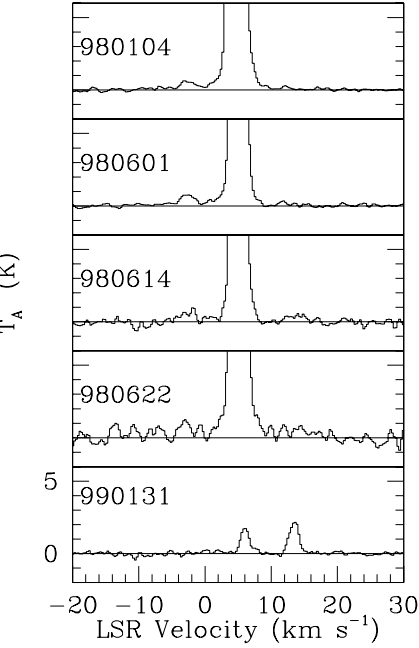


FIG. 6b

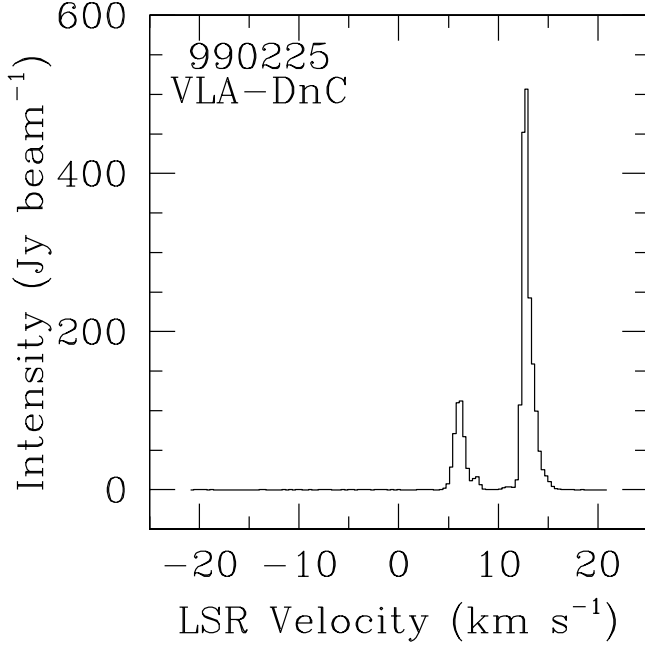


FIG. 6c

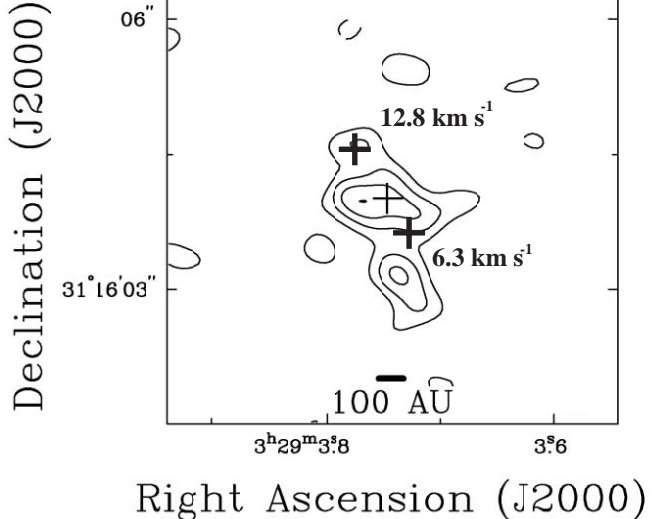


FIG. 6d

FIG. 6.— H_2O maser spectra for the source NGC 1333 SVS 13A from (a) and (b) the Nobeyama 45 m telescope survey and (c) the VLA DnC array observations. The ambient cloud velocity estimated from NH_3 lines (Ho & Barrett 1980) and from the CS $J = 5-4$ line (Lefloch et al. 1998) is $V_{\text{LSR}} \sim 7.0 \text{ km s}^{-1}$. (d) Positions of the masers from the VLA observations (thick crosses with the LSR velocities) indicated on the $\lambda = 2.7 \text{ mm}$ continuum emission image from the BIMA array (Looney et al. 2000). The thin cross indicates the position of $\lambda = 3.6 \text{ cm}$ continuum emission from Rodríguez et al. (1997).

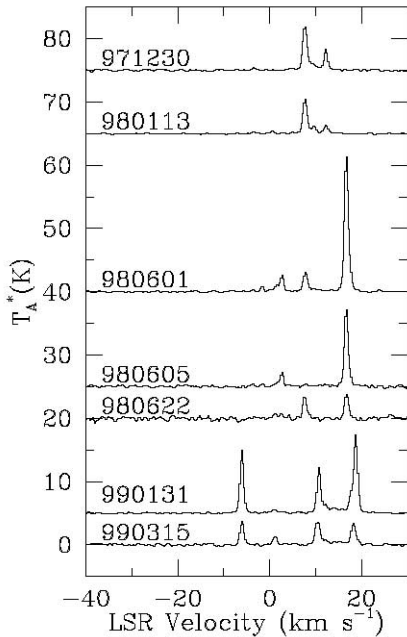


FIG. 7a

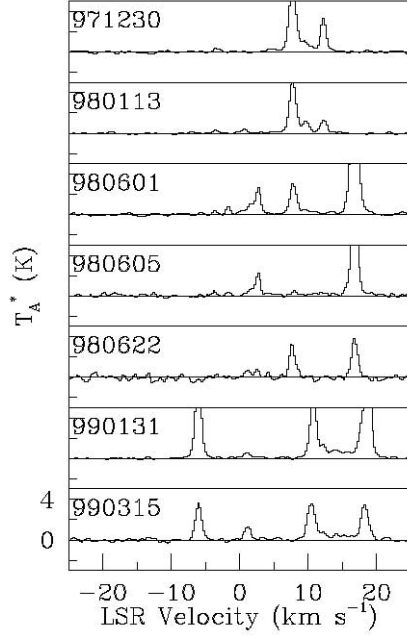


FIG. 7b

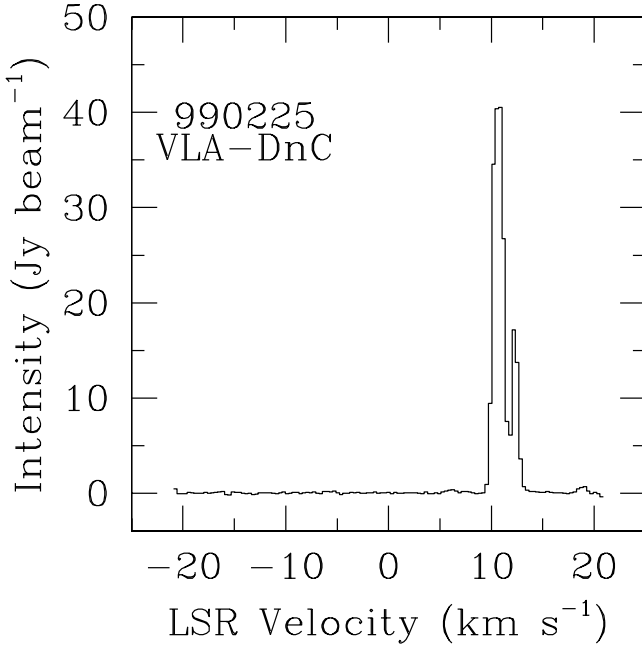


FIG. 7c

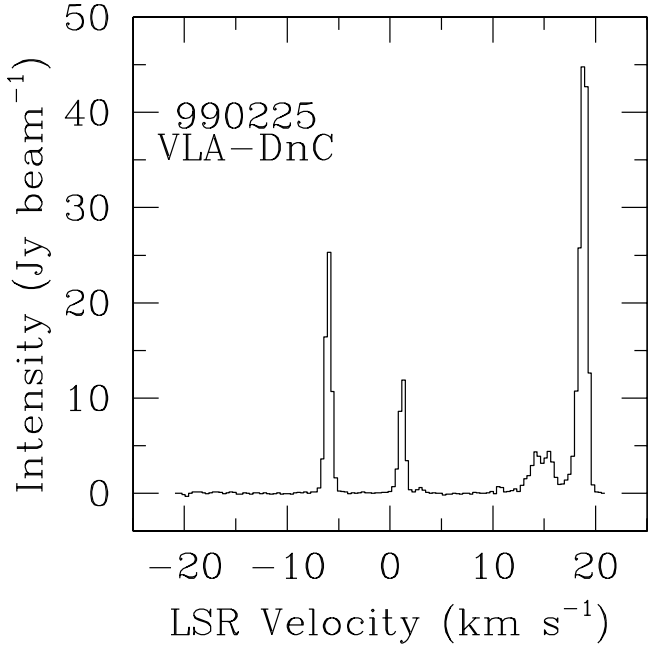


FIG. 7d

Fig. 7.—(a) and (b) H₂O maser spectra for the NGC 1333 IRAS 4A/4B region from the Nobeyama 45 m telescope survey. Both IRAS 4A and 4B exist within the beam of the 45 m telescope ($\theta_{HPBW} \simeq 75''$). The ambient cloud velocity estimated from NH₃ lines (Ho & Barrett 1980) and from the CS $J = 5-4$ line (Lefloch et al. 1998) is $V_{LSR} \sim 7.0$ km s⁻¹. (c) and (d) H₂O maser spectra associated with NGC 1333 IRAS 4A and IRAS 4B, respectively, through the VLA DnC array observations (see text). Thick crosses in panels (e) and (f) show the positions of the masers in IRAS 4A and IRAS 4B, respectively, indicated on the $\lambda = 2.7$ mm continuum emission image obtained with the BIMA array (Looney et al. 2000). Thin crosses are the peak position of $\lambda = 1.3$ cm continuum emission from Mundy et al. (1993). In panel (e), a thin cross at a mark of VLA 25 indicates the position of $\lambda = 3.6$ cm continuum emission (B. Reipurth et al. 2002, private communication).

maser emission and its peak flux density, respectively. Column (6) gives the image noise level of each velocity channel with a resolution of 0.33 km s⁻¹. Columns (7) and (8) give the absolute position of the detected maser spot in B1950.0 equatorial coordinates.

One of the most important results from these VLA observations is that all of the detected maser emission is located

within several hundred AU from the central protostars. Comparisons between the VLA and 45 m telescope data are given in the following subsection.

4.3. Notes on Some Individual Sources

In this subsection we give notes and suggest implications for 22 low-mass YSOs that satisfy at least one of the follow-

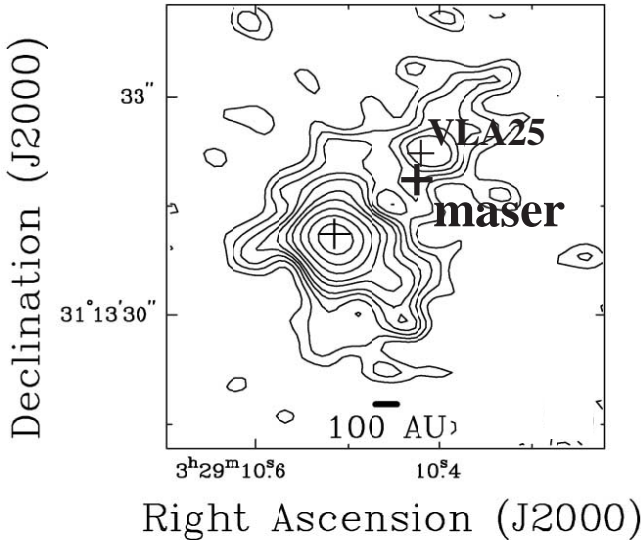


FIG. 7e

ing criteria: (1) H_2O masers were newly detected, (2) they have complex features, (3) H_2O masers were frequently observed, or (4) H_2O masers were resolved into multiple components by the VLA.

4.3.1. NGC 1333 Region

The star-forming region of NGC 1333 and the associated dark cloud L1450 have been assumed to be part of the Perseus OB2 association (Strom, Vrba, & Strom 1976; Sargent 1979); therefore, the distance was determined to be 350 pc (Herbig & Jones 1983). The distance was remeasured to be 220 pc by Cernis (1990). In this paper we adopt the distance of 220 pc. The NGC 1333 region is the site of highly active low-mass star formation as demonstrated by the detection of several groups of HH objects (e.g., Herbig 1974; Bally, Devine, & Reipurth 1996), nine compact *IRAS* sources (Jennings et al. 1987), and some Class 0 sources (Sandell et al. 1991, 1994). At present, 33 submillimeter sources are identified in this region (Lefloch et al. 1998; Sandell & Knee 2001), and very few of them have optical or near-IR counterparts. Ten molecular outflows are identified from CO line observations (Liseau & Sandell 1986; Knee & Sandell 2000): roughly half of the outflows possess highly collimated jetlike flows driven by known or candidate Class 0 sources.

NGC 1333 IRAS 2A.—NGC 1333 IRAS 2 is located at the edge of the large cavity in the NGC 1333 region (Langer, Castets, & Lefloch 1996). The SED of this source was identified as Class 0, showing weak emission at the 12 and 25 μm bands (Jennings et al. 1987) but strong emission at submillimeter wavelengths (Sandell et al. 1994). Recent millimeter interferometric observations show that there are two continuum sources that are likely to be associated with two outflows found by Liseau & Sandell (1986). The northern source, IRAS 2A, is a Class 0 object (Sandell et al. 1994; Ward-Thompson et al. 1996) driving a bipolar jet. The other fainter source, IRAS 2B, which is located $\sim 30''$ southeast of the source IRAS 2A, is likely to drive a jetlike bipolar outflow (Knee & Sandell 2000) and is suggested to be a possible Class 0 source.

The beam of the 45 m telescope encompasses the two sources. The sources in the IRAS 2 region showed weak

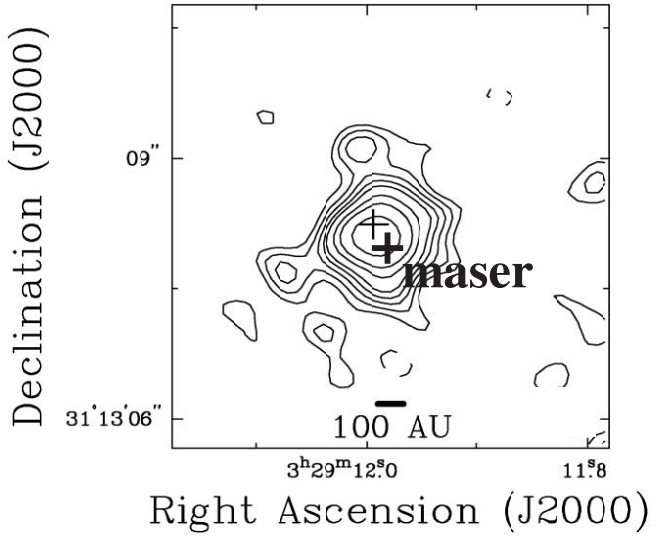


FIG. 7f

maser emission in the period from 1998 January to June and showed strong emission in the period from 1999 January to March (Figs. 5a and 5b). The emission was principally seen around $V_{\text{LSR}} = 4.5$ and 7.0 km s^{-1} . In addition to the 7.0 km s^{-1} component, we detected emission at $V_{\text{LSR}} = -16.8$ km s^{-1} in the VLA DnC array observations on 1999 February (Fig. 5c). One of the aims in this subsection is to associate velocity components of the masers recognized by the 45 m telescope with individual sources using velocity information from the VLA observations. In the case that a velocity difference between the Nobeyama detections and those of the VLA is smaller than a typical value of a maser line width,³ we regarded the two detections to be identical. Our VLA observations toward NGC 1333 IRAS 2 revealed that the maser emission was associated with the northern source of IRAS 2A within 0''.25 (250 AU; Fig. 5d). On the basis of this result, we associated all of the maser emission detected by the 45 m telescope with IRAS 2A.

NGC 1333 SVS 13A.—This source is associated with the NGC 1333 IRAS 3 region (Jennings et al. 1987) and is located at a dense gas ridge (Ho & Barrett 1980). The source NGC 1333 SVS 13 is also referred to as SSV 13 in Herbig & Jones (1983). In spite of so many detailed studies, the region is so rich in YSOs that outflow driving sources cannot be easily identified. For 20 years the infrared source SVS 13 (Strom et al. 1976) was believed to be the driving source of the most prominent HH objects HH 7–11. Recent VLA observations (Rodríguez, Anglada, & Curiel 1997, 1999; Rodríguez et al. 2002) have revealed that a newly found binary radio continuum source close to SVS 13 harbors the driving source. Subsequent to total power continuum emission observations (Chini et al. 1997a, 1997b; Bachiller et al. 1998), the higher resolution $\lambda = 2.7$ mm image taken by the BIMA array clearly showed that SVS 13 is made up of at least three millimeter sources: A, B, and C (Looney et al. 2000); the source located near the position of the infrared source is called source A (Bachiller et al. 1998; also referred

³ From the Nobeyama data for 167 velocity components associated with nearby ($d < 220$ pc) low-mass ($L_{\text{bol}} < 100 L_{\odot}$) sources, we derived a mean value of maser line width to be $1.4 \pm 0.8 \text{ km s}^{-1}$.

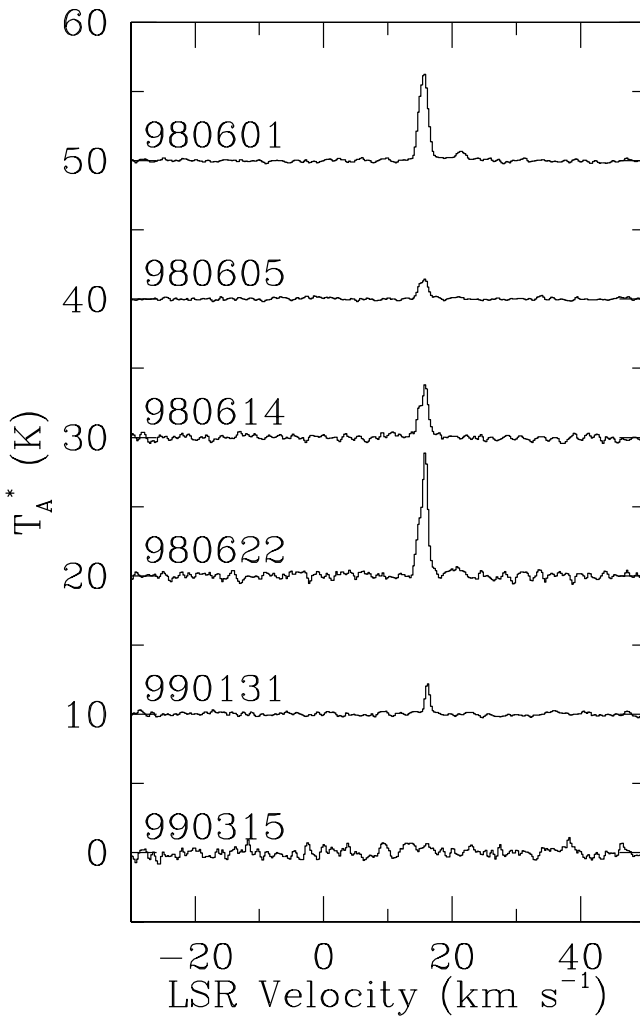


FIG. 8a

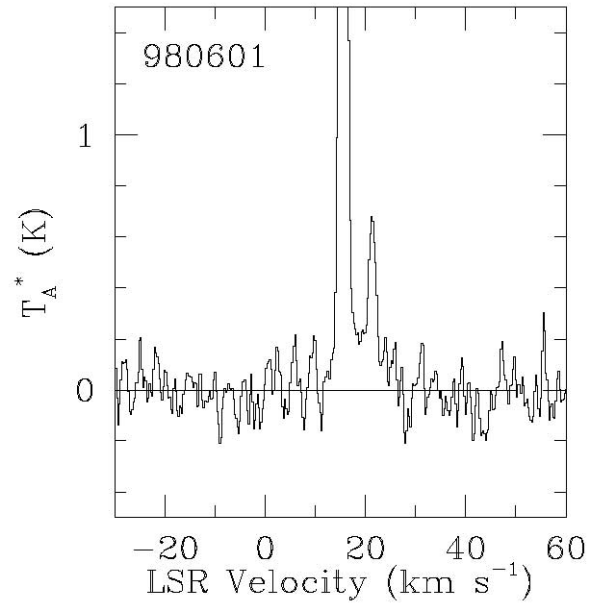


FIG. 8b

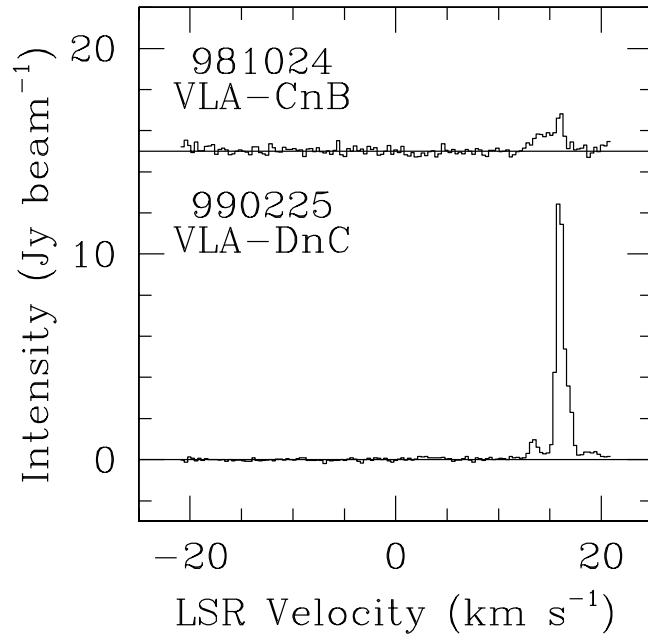


FIG. 8c

FIG. 8.— H_2O maser spectra for the source B1-IRS (IRAS 03301+3057) from (a) and (b) the Nobeyama 45 m telescope survey and (c) VLA observations. The ambient cloud velocity estimated from the CO $J = 1-0$ line is $V_{\text{LSR}} = 6.3 \text{ km s}^{-1}$ (Hirano et al. 1997).

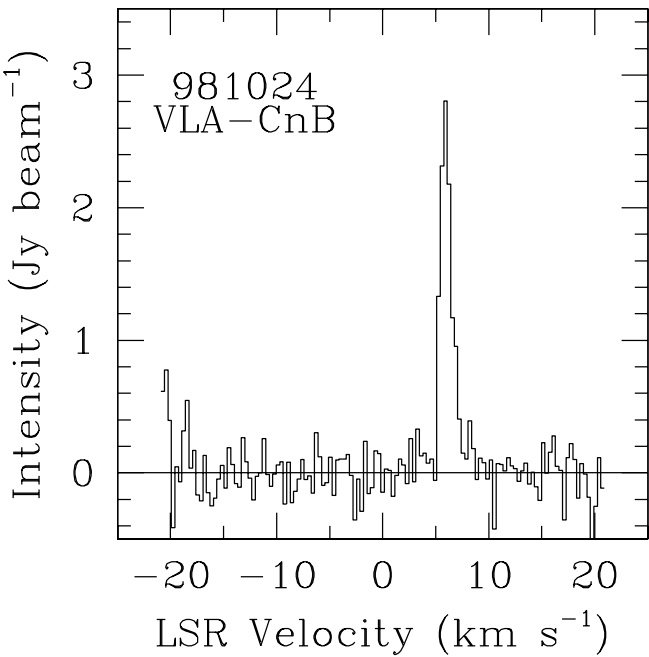


FIG. 9.— H_2O maser spectrum for the source T Tau South (IRAS 04190+1924) observed with the VLA CnB array. The ambient cloud velocity estimated from the $^{13}\text{CO } J = 1-0$ line is 8.2 km s^{-1} (Momose et al. 1996).

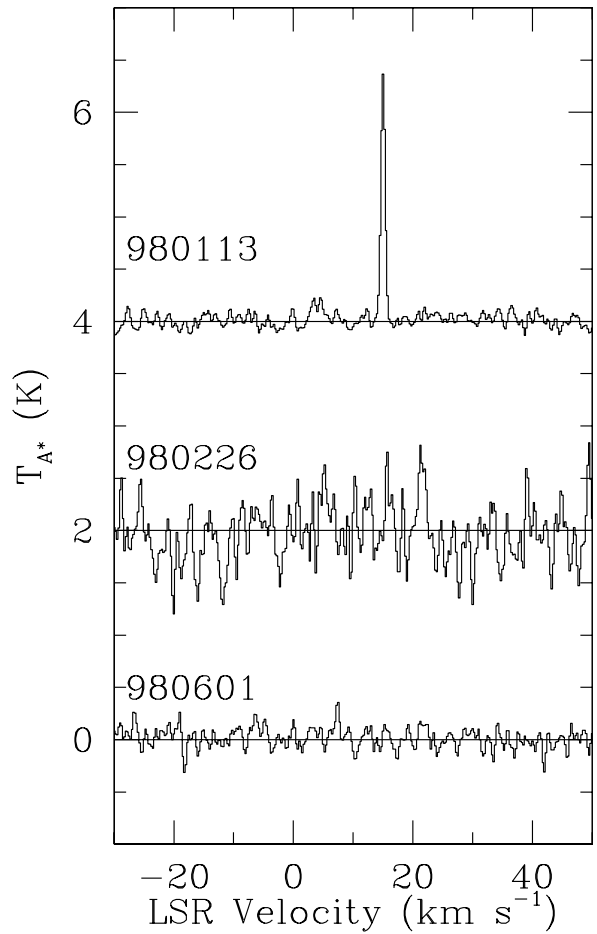


FIG. 11.— H_2O maser spectra for the source HH 1-2 (IRAS 05339-0647) from the Nobeyama 45 m telescope survey. The ambient cloud velocity estimated from the $^{13}\text{CO } J = 1-0$ line is $V_{\text{LSR}} \simeq 9.5 \text{ km s}^{-1}$ (Moro-Martin et al. 1999).

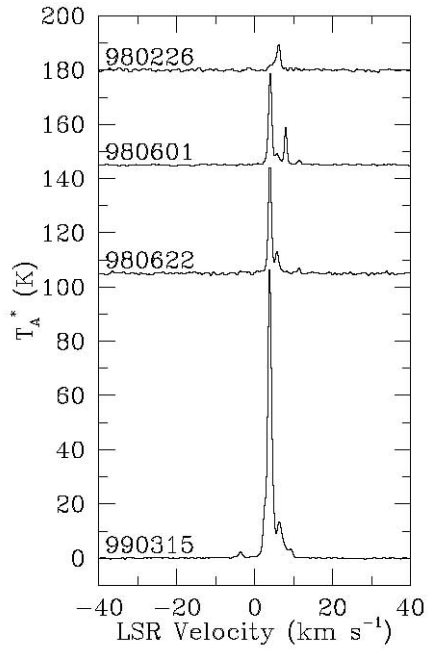


FIG. 10a

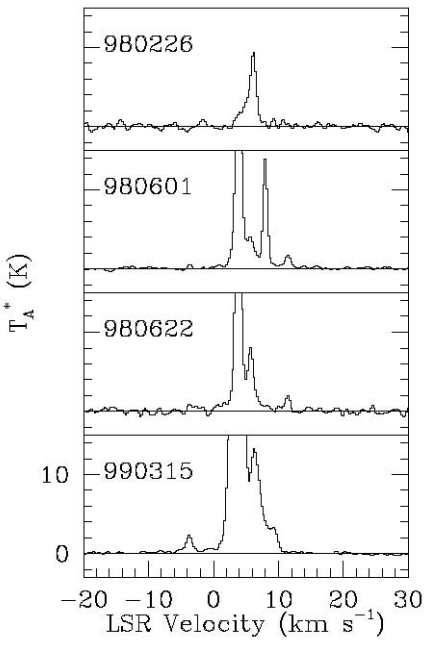


FIG. 10b

FIG. 10.—(a) and (b) H_2O maser spectra for the source Orion A West (IRAS 05302-0537) from the Nobeyama 45 m telescope survey. The ambient cloud velocity estimated from the $^{13}\text{CO } J = 3-2$ line is $V_{\text{LSR}} \sim 10 \text{ km s}^{-1}$ (Yu et al. 2000).

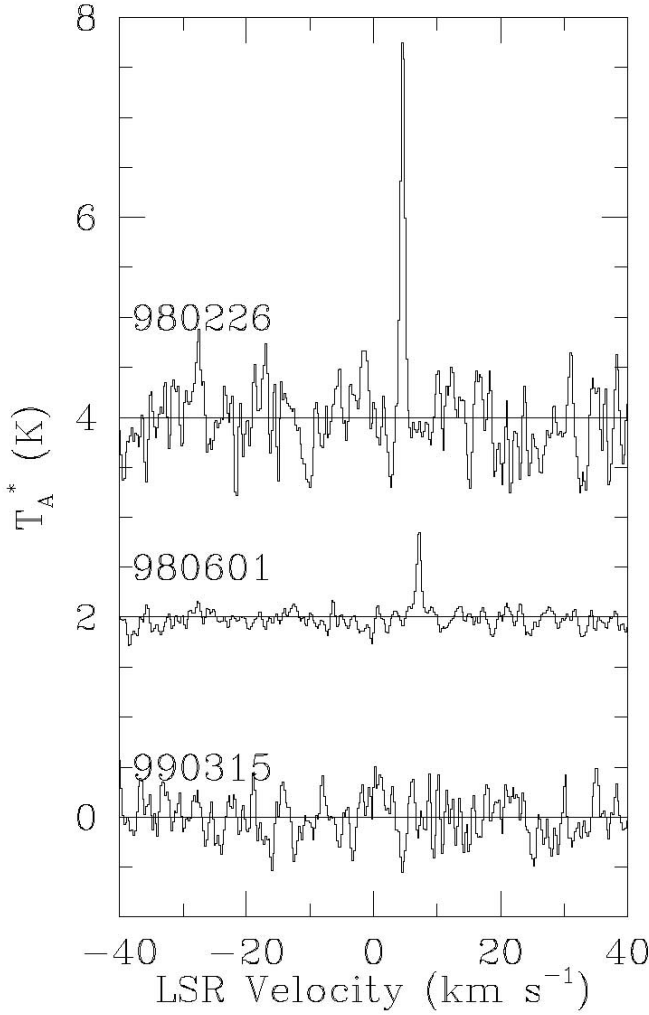


FIG. 12a

FIG. 12.— H_2O maser spectra for the source IRAS 05375–0731 (L1641-S3 MMS 1) from (a) the Nobeyama 45 m telescope survey and (b) VLA DnC observations. The ambient cloud velocity estimated from the $^{13}\text{CO } J = 1-0$ line is $V_{\text{LSR}} = 4.6 \text{ km s}^{-1}$ (Wouterloot, Henkel, & Walmsley 1989).

to as A2 in Looney et al. 2000). Although Rodríguez et al. (1997, 1999) proposed that the source VLA 3 is the better candidate for the driving source of HH 7–11 outflow, Looney et al. (2000) argued that this source is unlikely to be the outflow driving source because of its lack of compact structure. More recently, Rodríguez et al. (2002) have shown that SVS 13 coincides with radio source VLA 4A and a collection of water masers. Proper motion studies (Wootton et al. 2002) secure the identification, showing that the masers move southeast from SVS 13/VLA 4A at a space velocity of about 14 km s^{-1} .

The strong maser emission at $V_{\text{LSR}} = 4.6 \text{ km s}^{-1}$ was observed with the 45 m telescope at least in 1998 January and June (Figs. 6a and 6b). The emission is blueshifted with respect to the ambient cloud velocity of $V_{\text{LSR}} = 7.0 \text{ km s}^{-1}$ (Fig. 6c). Our VLA DnC array observations revealed that the maser emissions at $V_{\text{LSR}} = 6.3$ and 12.8 km s^{-1} were associated with SVS 13A. Figure 6d represents positions of the two maser spots indicated on the BIMA map of 2.7 mm dust continuum emission. This result further supports SVS 13A as the driving source of HH 7–11. The redshifted emission at 12.8 km s^{-1} is located $0.^{\circ}15$ northeast of the peak position of the 3.6 cm free-free emission (Rodríguez et al.

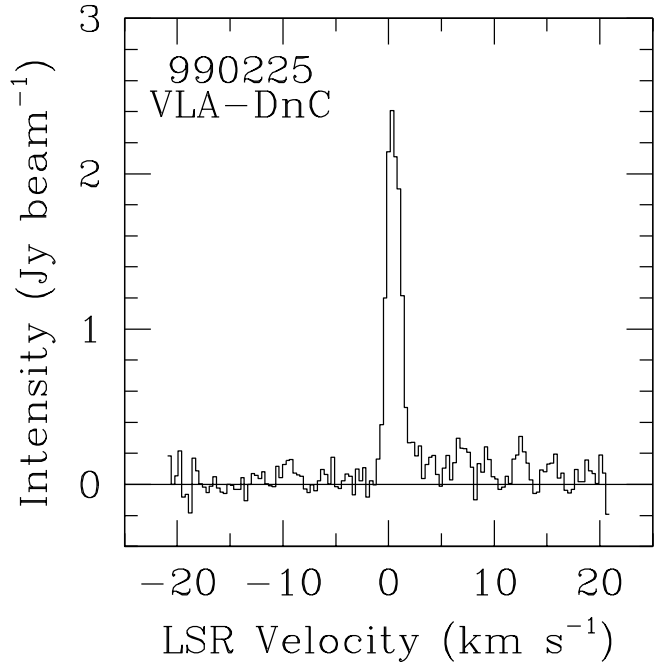


FIG. 12b

1997), while the blueshifted emission at 6.3 km s^{-1} is located at $0.^{\circ}28$ southwest of the 3.6 cm emission. It should be noted that these two maser spots and the 3.6 cm source lie along a line. VLBA observations later in 1998 interpreted these spots as lying on opposite sides of a cone of opening angle about 10° , presumably encompassing the jet from SVS 13A. Comparison of the 45 m telescope spectrum of 1999 January with the VLA spectrum of 1999 February suggests that the velocities of these two components may have decelerated toward the ambient cloud velocity.

NGC 1333 IRAS 4A/4B region.—The source IRAS 4, located southwest of SVS 13, is one of the first recognized Class 0 sources. Sandell et al. (1991) first showed that IRAS 4 consists of two bright protostellar objects, IRAS 4A and IRAS 4B, separated by $31''$. Further interferometric observations (Lay, Carlstrom, & Hills 1995; Looney et al. 2000) revealed that 4A and 4B themselves are multiple protostellar systems. From the SCUBA images at 450 and $850 \mu\text{m}$, Sandell & Knee (2001) showed that the close binary 4A is only slightly extended. They resolved IRAS 4B into a double system separated by $\sim 10''$. The western component (4BW) is a Class 0 object driving a compact bipolar outflow and is associated with free-free emission (Mundy et al. 1993;

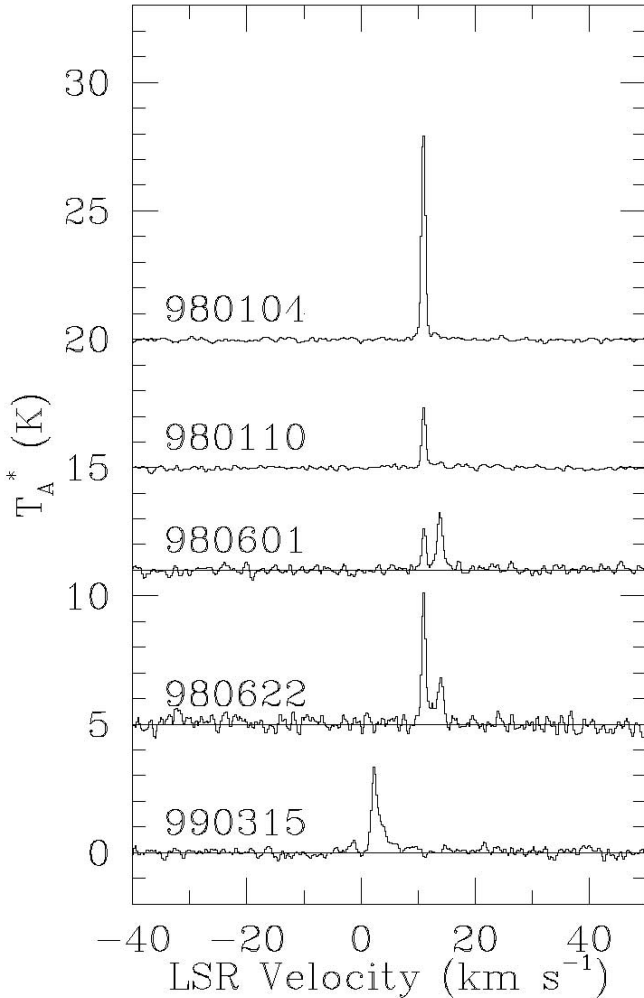


FIG. 13a

FIG. 13.—(a) H_2O maser spectra for the NGC 2024 FIR 5/FIR 6 region from the Nobeyama 45 m telescope survey. Both FIR 5 and FIR 6 exist within the beam of the 45 m telescope. (b) H_2O maser spectrum from the source NGC 2024 FIR 5 obtained with the VLA DnC observations: we associated the maser emission with FIR 5 through the VLA observations (see text). The ambient cloud velocity estimated from nine H_2CO lines is $V_{\text{LSR}} = 10.6 \text{ km s}^{-1}$ (Mangum et al. 1999).

Blake et al. 1995; Rodríguez et al. 1999). The eastern component (4BE) is not detected at centimeter wavelengths nor does it drive a known outflow.

All of these sources in the IRAS 4 region lie within the beam of the 45 m telescope. Published VLA results (Rogers & Gottschalk 1993) located all masers near IRAS 4BW (J. Gottschalk 2001, private communication) but refer to a previous epoch. Thus, we were unable to associate the Nobeyama data taken in 1997 December, 1998 January, and 1998 June with individual YSOs. The spectral profiles obtained show complex features with extreme time variability (Figs. 7a and 7b). For instance, we detected a strong emission at $V_{\text{LSR}} = 16.8 \text{ km s}^{-1}$ on June 1, although no emission was found around that velocity in 1998 January. The peak intensity of the 16.8 km s^{-1} component decreased about one-sixth within 3 weeks: 58 Jy on June 1, 32 Jy on June 5, and 10 Jy on June 22.

We were able to assign velocity components detected in 1999 January and March using the results from the VLA DnC array observations in 1999 February. The VLA observations revealed that the emission at $V_{\text{LSR}} = 10.9$ and 12.2 km s^{-1} was associated with the source IRAS 4A, while the

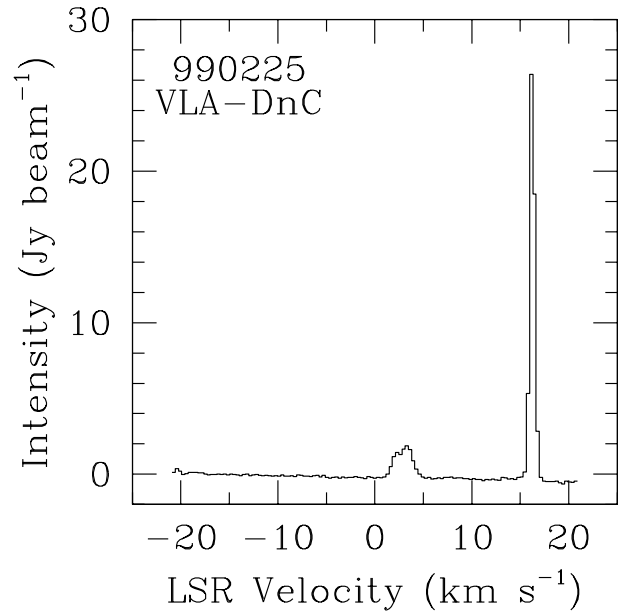


FIG. 13b

emission at -5.9 , 1.1 , ~ 15 , and 18.8 km s^{-1} was associated with the Class 0 source 4BW. The position of the 4A maser lies within 50 AU of the peak of the IRAS 4A2 $\lambda = 2.7 \text{ mm}$ continuum emission and the 3.6 cm radio continuum source VLA 25 (B. Reipurth et al. 2002, private communication; Fig. 7e). During previous observations in 1995 and 1998 (A. Wootten et al. 1995, 1998, unpublished data), the maser was associated with this easternmost source in the binary. The 4BW maser is located exactly at the peak position of the 2.7 mm source. For calculation of maser detection rates in Paper I, we assumed that both 4A and 4BW were showing maser activity in the period from 1997 December to 1998 June. We calculated the ranges of $L_{\text{H}_2\text{O}}$ for 4A and 4B in Table 4 and figures in § 5 using only the data taken in 1999.

4.3.2. B1-IRS

The source B1-IRS is proposed as a Class 0 source and is suggested to be one of the youngest CO outflow sources (Hirano et al. 1997). Bachiller, del Rio Alvarez, & Menten (1990) investigated the core, imaging emission from several molecules, including a compact CO flow centered on IRAS 03301+3057 displaying strong blueshifted emission. Hirano

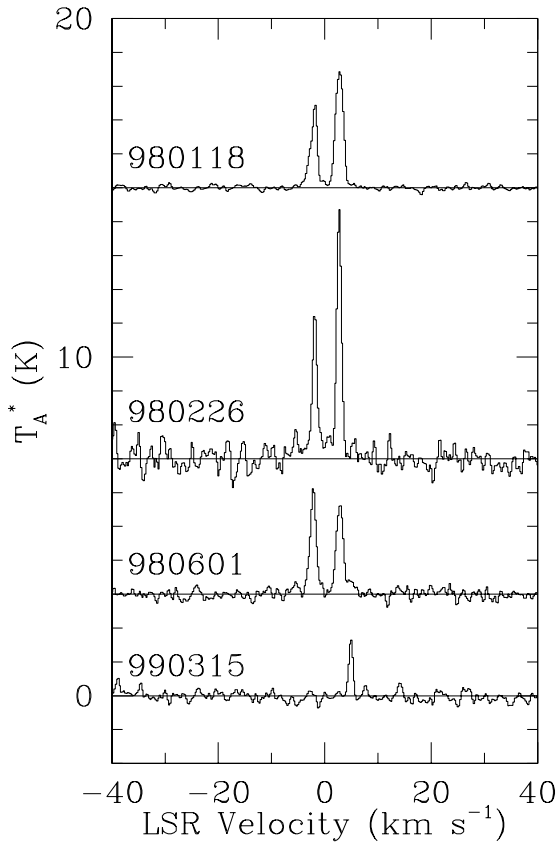


FIG. 14.— H_2O maser spectra for the source IRAS 05413–0104 (HH 212) from the Nobeyama 45 m telescope survey. The ambient cloud velocity estimated from the $^{13}\text{CO } J = 1-0$ line is $V_{\text{LSR}} = 1.6 \text{ km s}^{-1}$ (Wouterloot et al. 1989).

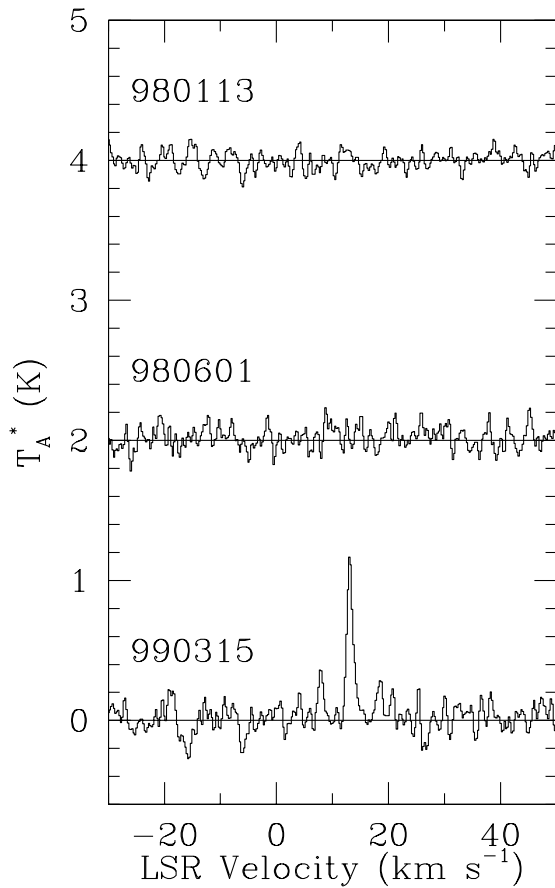


FIG. 16.— H_2O maser spectra for the source NGC 2071 North (IRAS 05451+0037) from the Nobeyama 45 m telescope survey. The ambient cloud velocity estimated from the $\text{C}^{18}\text{O } J = 1-0$ line is 9.0 km s^{-1} (Iwata et al. 1988).

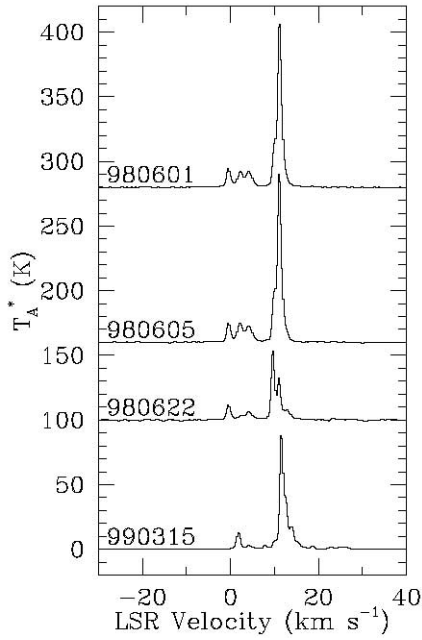


FIG. 15a

FIG. 15.—(a) and (b) H_2O maser spectra for the source NGC 2071 IRS (IRAS 05445+0020) from the Nobeyama 45 m telescope survey. The ambient cloud velocity estimated from the NH_3 line is $V_{\text{LSR}} = 10 \text{ km s}^{-1}$ (Torrelles et al. 1983).

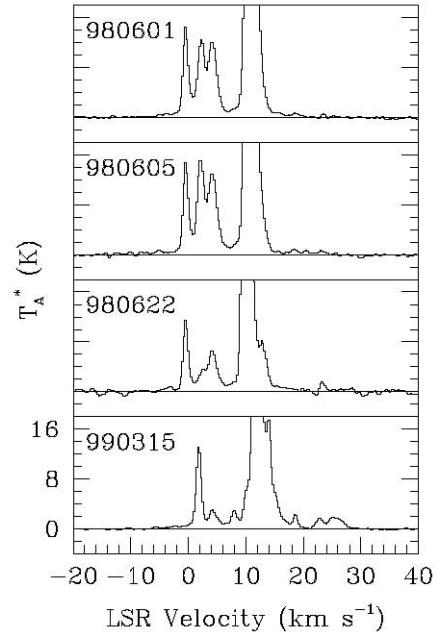


FIG. 15b

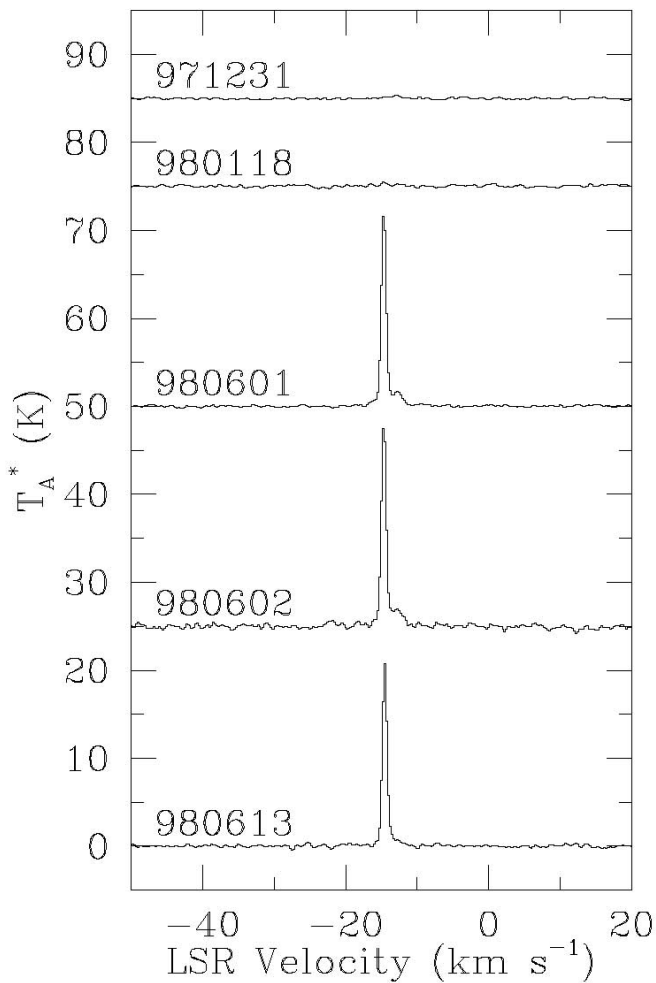


FIG. 17a

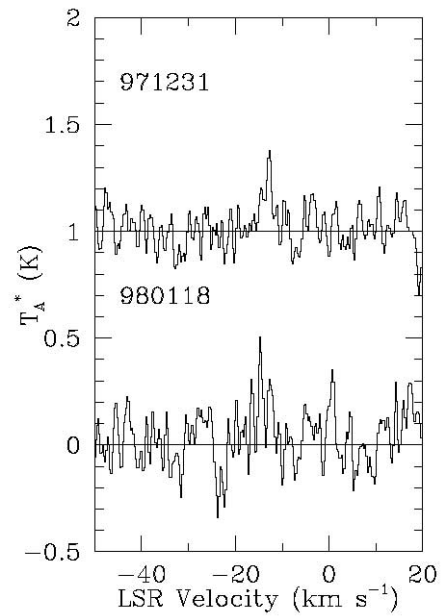


FIG. 17b

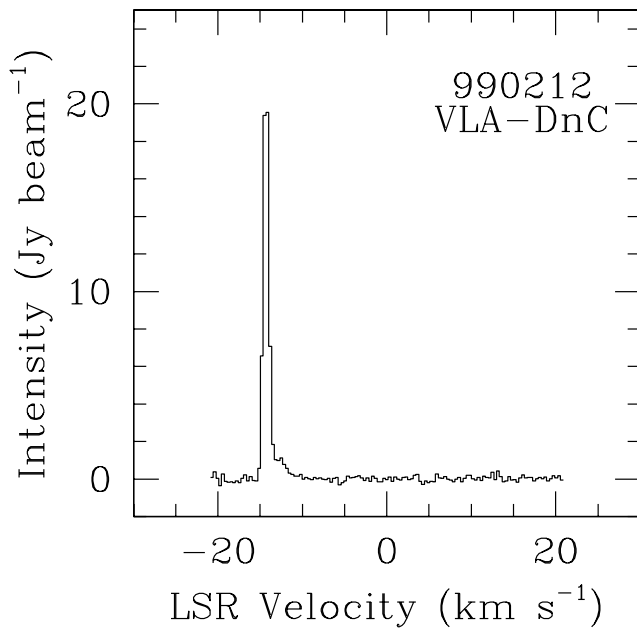


FIG. 17c

FIG. 17.— H_2O maser spectra for the source GSS 30-IRS from (a) and (b) the Nobeyama 45 m telescope survey and (c) VLA DnC array observations. The ambient cloud velocity estimated from the CO $J = 1-0$ line is $V_{\text{LSR}} = 3.5 \text{ km s}^{-1}$ (Tamura et al. 1990).

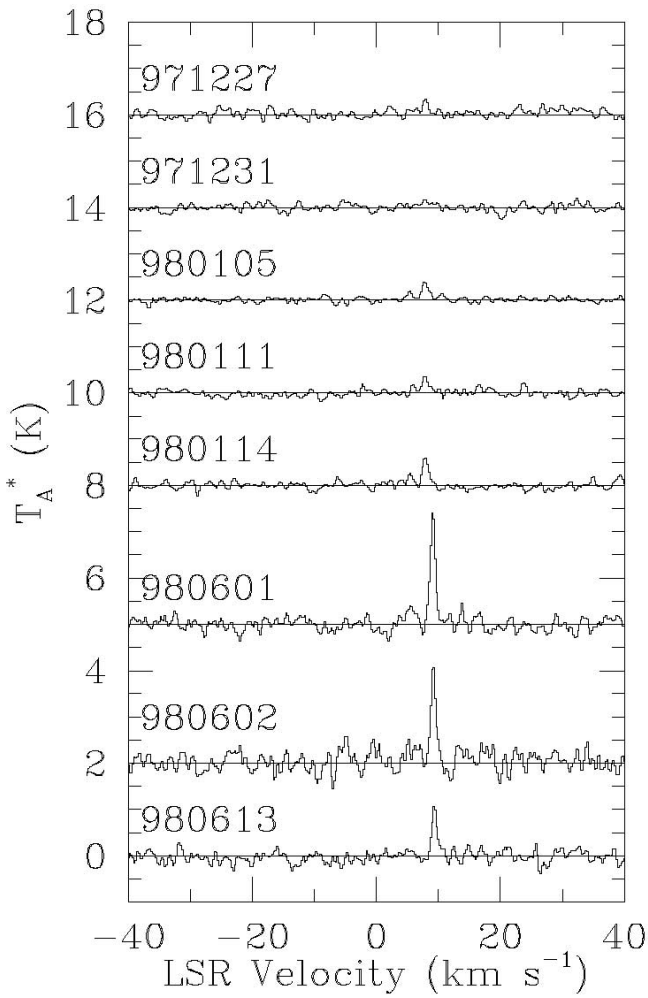


FIG. 18a

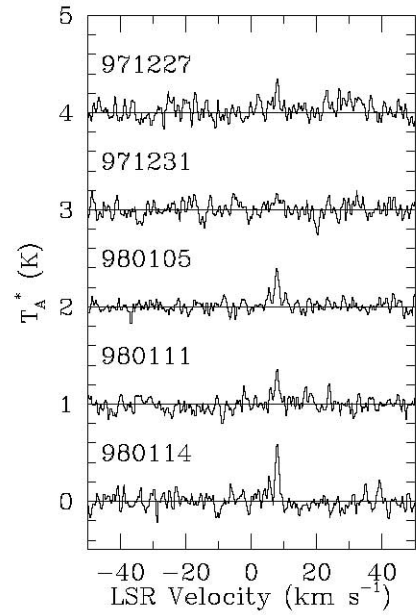


FIG. 18b

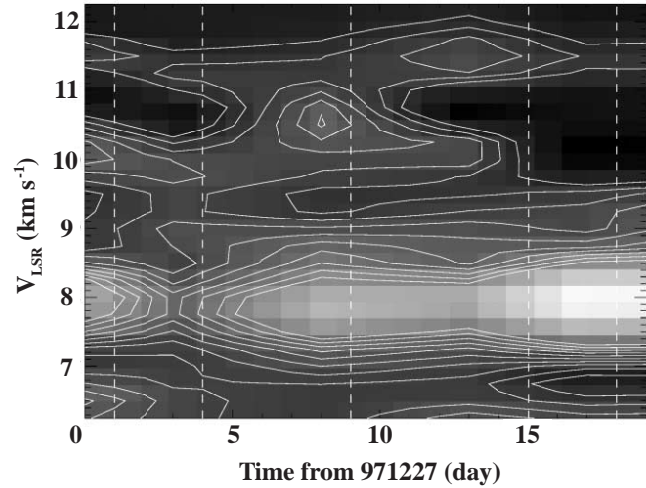


FIG. 18c

FIG. 18.—(a) and (b) H₂O maser spectra for the source VLA 1623 from the Nobeyama 45 m telescope survey. The ambient cloud velocities estimated from the H₂CO 2₁₂–1₁₁ and the N₂H⁺ 101–012 lines are $V_{\text{LSR}} = 3.3$ and 3.7 km s^{-1} , respectively (Mardones et al. 1997). (c) Time variation contour map of the maser emission in the period from 1997 December 27 through 1998 January 15. The vertical dashed lines indicate the dates of observations. Sensitivity of the observations was typically 40 mK in T_A^* : the contour intervals are 5% of the peak intensity. (d) H₂O maser spectrum from the VLA A array observations. (e) Position of the masers from the VLA observations (thick cross at B) indicated on the $\lambda = 2.7 \text{ mm}$ continuum emission image (Looney et al. 2000). The position of the masers is coincident with that of $\lambda = 3.6 \text{ cm}$ continuum emission (Bontemps & André 1997). The thin cross at the source A indicates the position of the 3.6 cm continuum source.

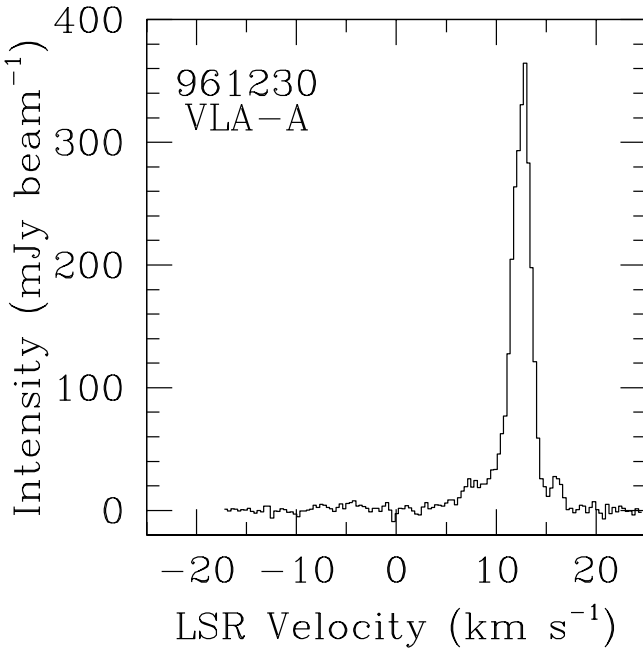


FIG. 18d

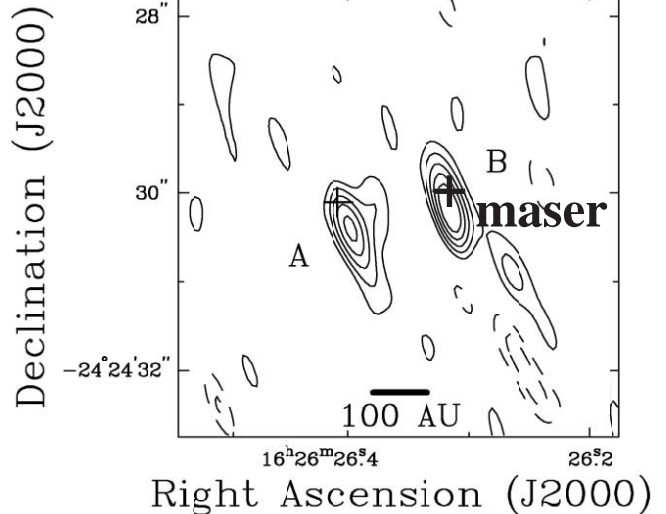


FIG. 18e

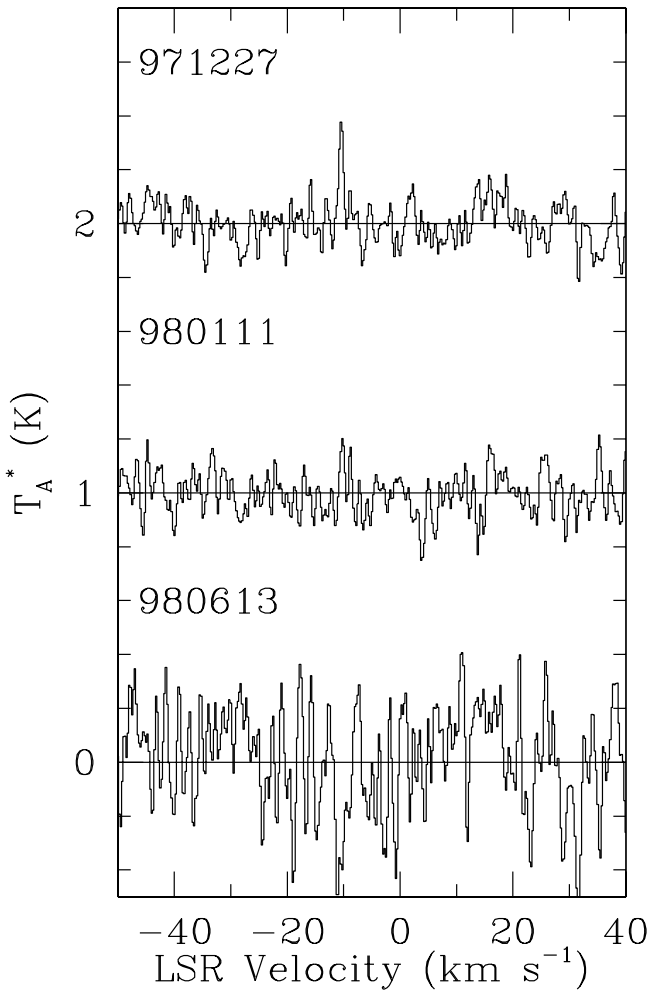


FIG. 19.—H₂O maser spectra for the source IRAS 16244–2432 (YLW 16A) from the Nobeyama 45 m telescope survey. The ambient cloud velocity estimated from the CO $J = 1-0$ line is 5.4 km s⁻¹ (Terebey et al. 1989).

et al. (1997) imaged the compact CO outflow using interferometric CO $J = 1-0$ observations: they detected strong blueshifted emission, while no significant redshifted emission was found. Their CO $J = 1-0$ image revealed the presence of a blueshifted ring structure having a size of 8700 AU \times 5000 AU. The estimated dynamical timescale of the outflow is less than 10³ yr.

We detected H₂O maser emission for the first time in B1-IRS (Figs. 8a and 8b). The velocities of the masers ($V_{\text{LSR}} = 15.7$ and 21.2 km s⁻¹) are always redshifted with respect to the ambient cloud velocity and within the redshifted lobe measured by Bachiller et al. (1990). Subsequently, we succeeded in determining the position of the masers with the VLA in 1998 October and 1999 February (Fig. 8c). During the latter session, when the masers were strongest, the (redshifted) maser features were located 5''.5 southwest of the *IRAS* source, at the center of the blueshifted ring structure. In 1999 March, carried out only 18 days after the VLA observations, we found that the maser emission had vanished (Fig. 8a).

4.3.3. T Tau

The source T Tau is the prototypical T Tauri star, although this is a very rare example of a visible T Tauri star with a bipolar molecular outflow (Edwards & Snell 1982). T Tau turned out to be a triplet system, consisting of the main star T Tau North and an IR companion T Tau South with a projected separation of 0''.6 (Dyck, Simon, & Zuckerman 1982). The presence of a third star between them was claimed on the basis of speckle observations (Niesenson et al. 1985; Maihara & Kataza 1991) and was resolved by high-resolution 6 cm radio continuum emission observations with MERLIN (Ray et al. 1997).

H₂O maser emission from the T Tau system has been controversial: Knapp & Morris (1976) detected maser emission at $V_{\text{LSR}} = 1.4$ km s⁻¹ using the 40 m telescope at the Owens Valley Radio Observatory. They reported that the maser source is displaced by ~ 0.9 from the position of T Tauri,

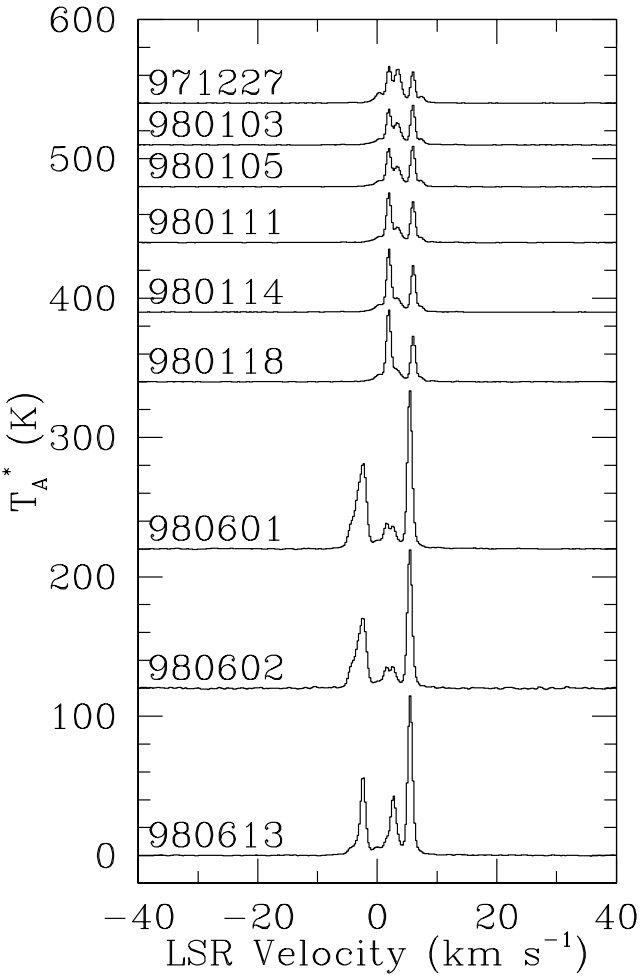


FIG. 20a

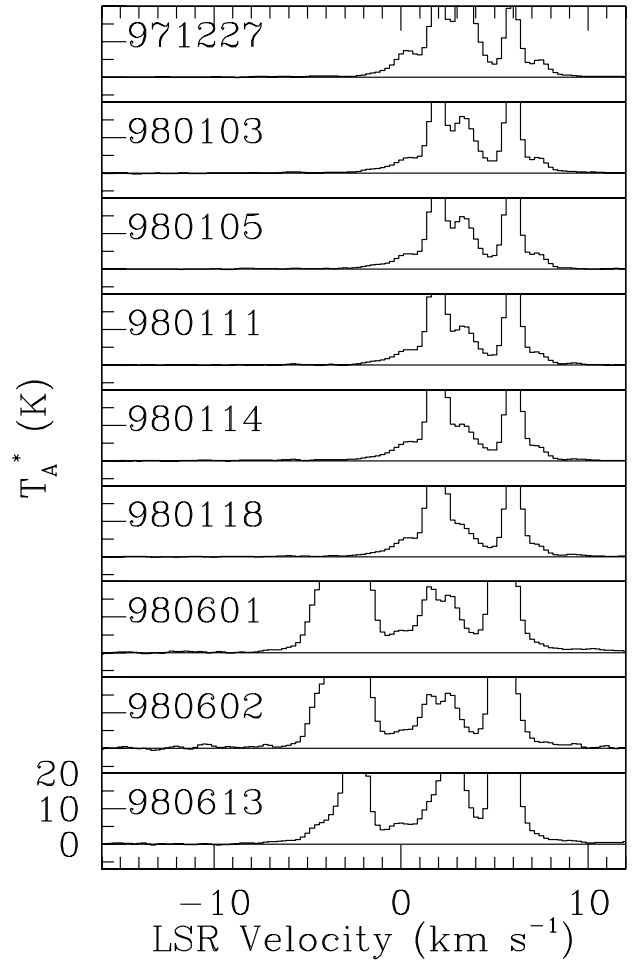


FIG. 20b

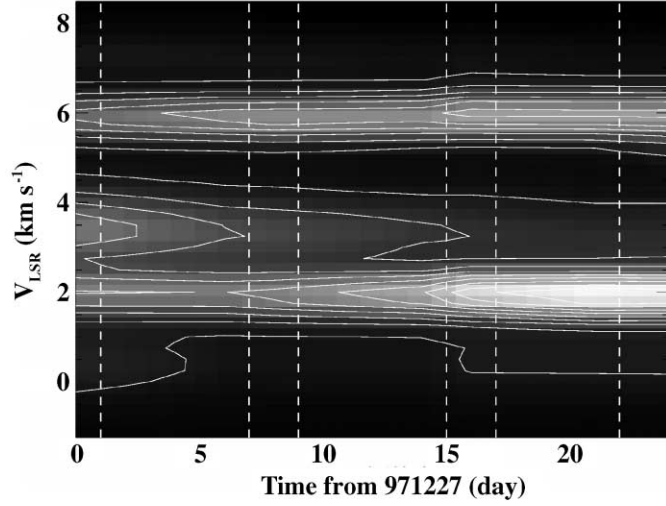


FIG. 20c

FIG. 20.—(a) and (b) H_2O maser spectra for the source IRAS 16293–2422 in L1689N from the Nobeyama 45 m telescope survey. The ambient cloud velocity estimated from the N_2H^+ 101–012 line is $V_{\text{LSR}} = 4.0 \text{ km s}^{-1}$ (Mardones et al. 1997). (c) Time variation contour map of the maser emission in the period from 1997 December 27 through 1998 January 20. The vertical dashed lines present dates of observations. Sensitivity of the observations was typically 45 mK in T_A^* : the contour intervals are 5% of the peak intensity.

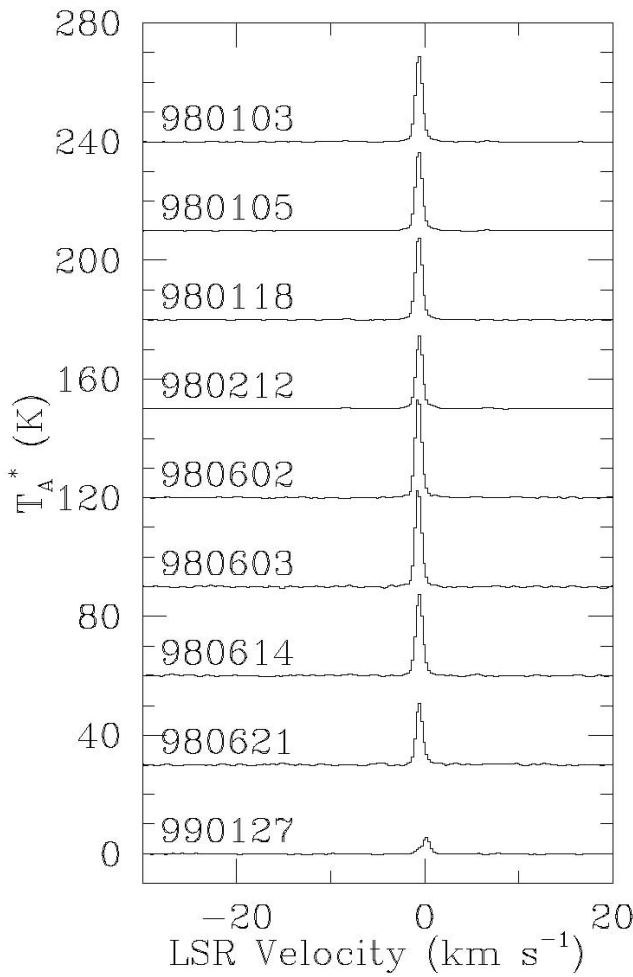


FIG. 21a

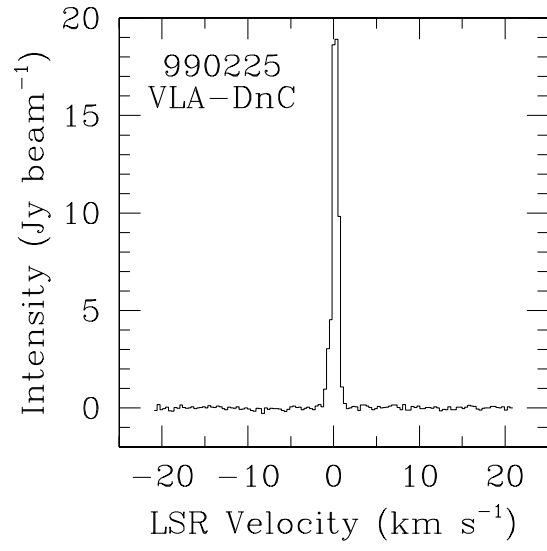


FIG. 21b

FIG. 21.— H_2O maser spectra for the source L483-FIR (IRAS 18148–0440) from (a) the Nobeyama 45 m telescope survey and (b) VLA DnC array observations. The ambient cloud velocity estimated from the $\text{NH}_3(1,1), (2,2)$ lines is $V_{\text{LSR}} = 5.4 \text{ km s}^{-1}$ (Anglada, Sepúlveda, & Gómez 1997).

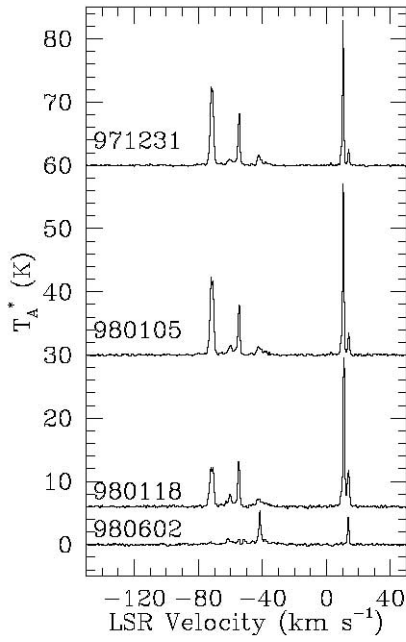


FIG. 22a

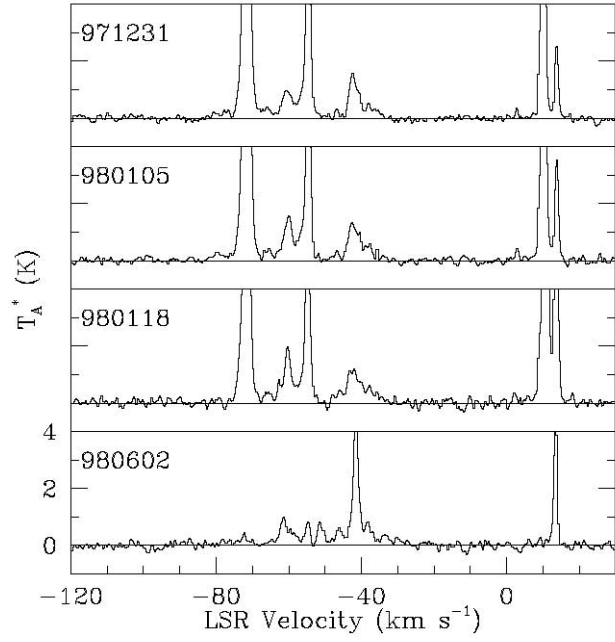


FIG. 22b

FIG. 22.—(a) and (b) H_2O maser spectra for the source IRAS 18162–2048 (HH 80–81) from the Nobeyama 45 m telescope survey. The ambient cloud velocity estimated from the $^{12}\text{CO } J = 1–0$ line is $V_{\text{LSR}} \sim -11 \text{ km s}^{-1}$ (Rodríguez et al. 1980) and from the NH_3 lines is roughly -12 km s^{-1} (Girart et al. 1994).

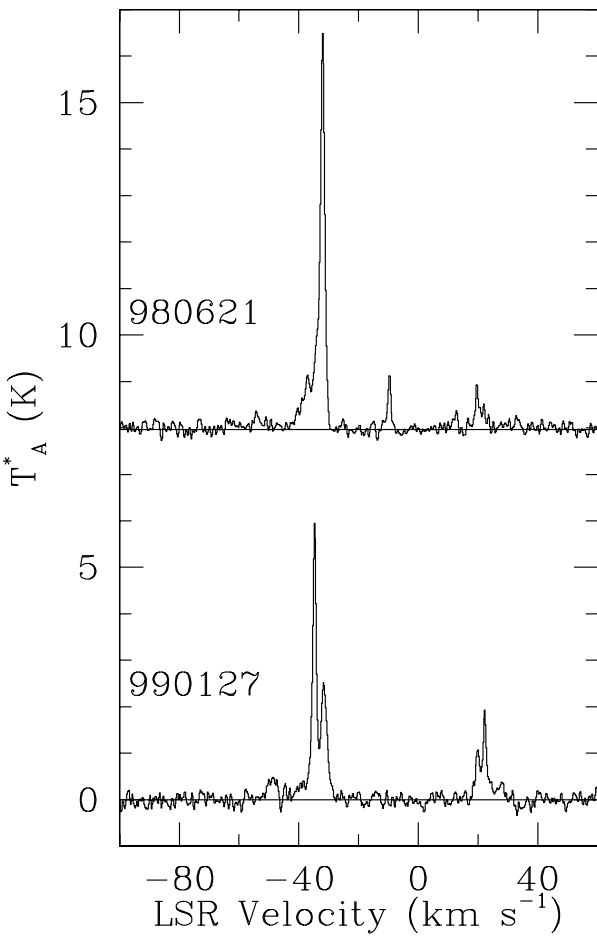


FIG. 23.— H_2O maser spectra for the source IRAS 18265–1517 (L379-IRS 1) from the Nobeyama 45 m telescope survey. The ambient cloud velocity estimated from the ^{12}CO $J = 2-1$ line is $V_{\text{LSR}} \sim 16 \text{ km s}^{-1}$ (Kelly & MacDonald 1996).

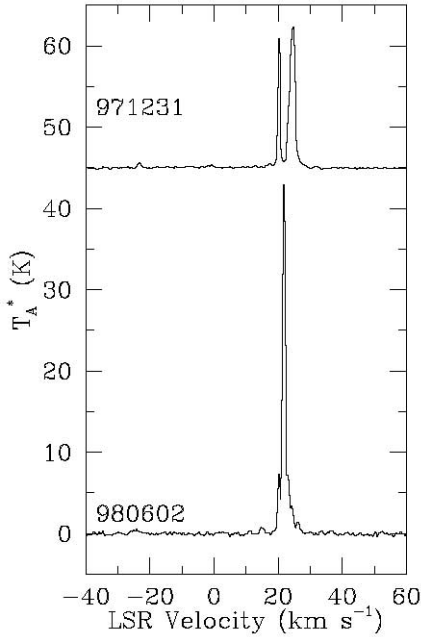


FIG. 24a

FIG. 24.— H_2O maser spectra for the source IRAS 18277–1516 (L379-IRS 2) from the Nobeyama 45 m telescope survey. The ambient cloud velocity estimated from the CO $J = 1-0$ line is $V_{\text{LSR}} = 4.0 \text{ km s}^{-1}$.

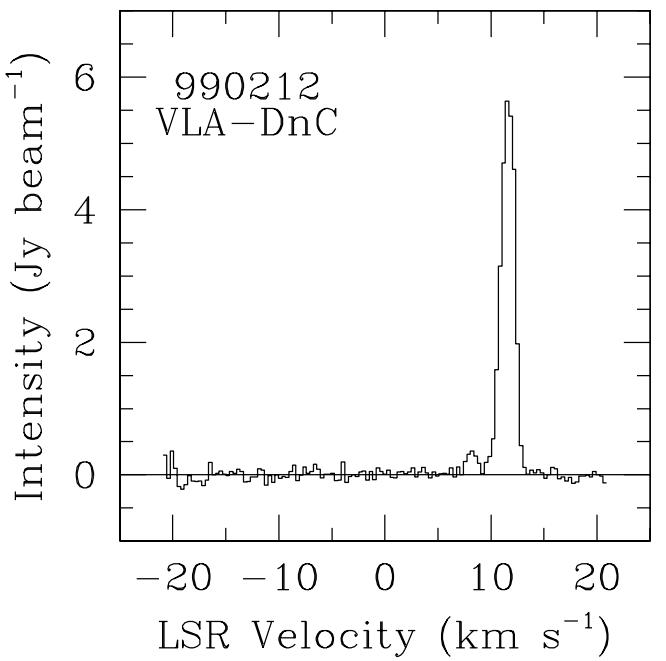


FIG. 25.— H_2O maser spectrum for the source S68N (Serpens SMM 9) observed by the VLA DnC array. The ambient cloud velocities estimated from the CS $J = 2-1$ line (Wolf-Chase et al. 1998) and the N_2H^+ $101-012$ line (Mardones et al. 1997) are 8.75 and 8.79 km s^{-1} , respectively.

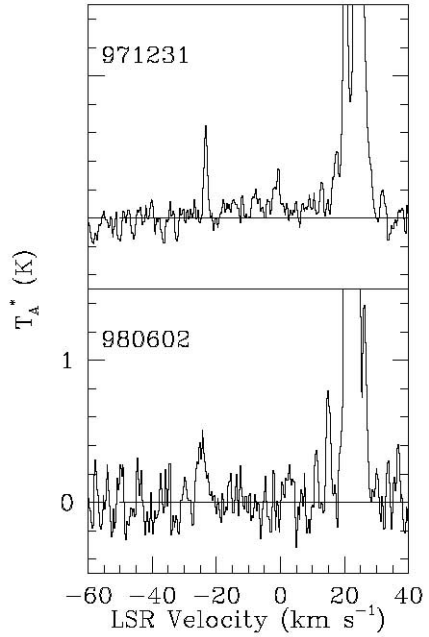


FIG. 24b

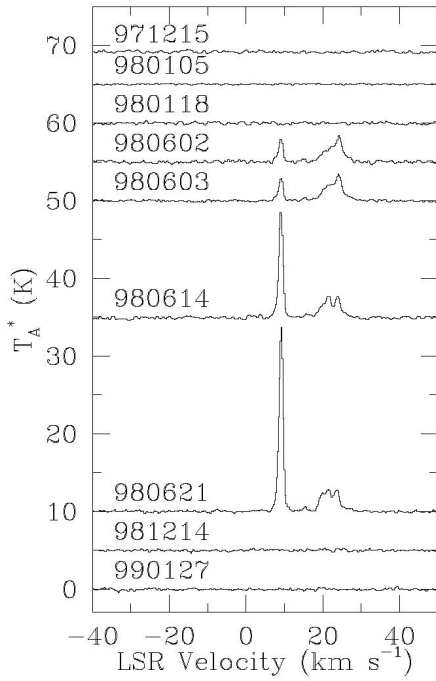


FIG. 26a

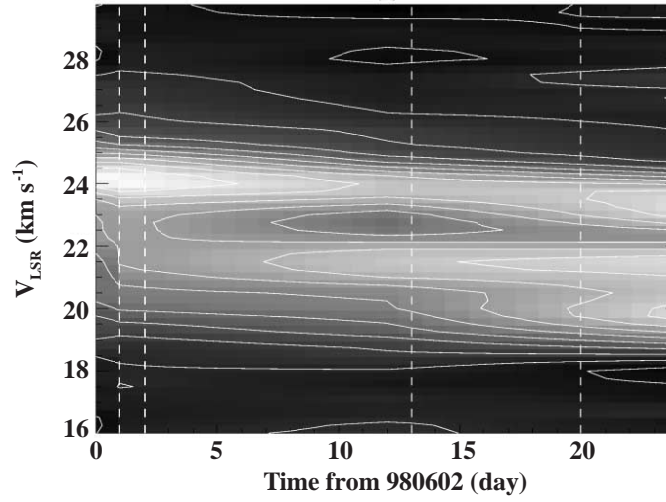


FIG. 26b

FIG. 26.—(a) H₂O maser spectra for the source Serpens FIRS 1 (Serpens SMM 1) from the Nobeyama 45 m telescope survey. The ambient cloud velocities estimated from the H₂CO 3₀₃–2₀₂ line (Hurt & Barsony 1996) and the N₂H⁺ 101–012 line (Mardones et al. 1997) are $V_{\text{LSR}} = 8.47$ and 8.75 km s^{-1} , respectively. (b) Time variation contour map of the maser emission in the period from 1998 June 3 through June 25. The vertical dashed lines present the dates of observations. Sensitivity of the observations was typically 55 mK in T_A^* : the contour intervals are 10% of the peak intensity.

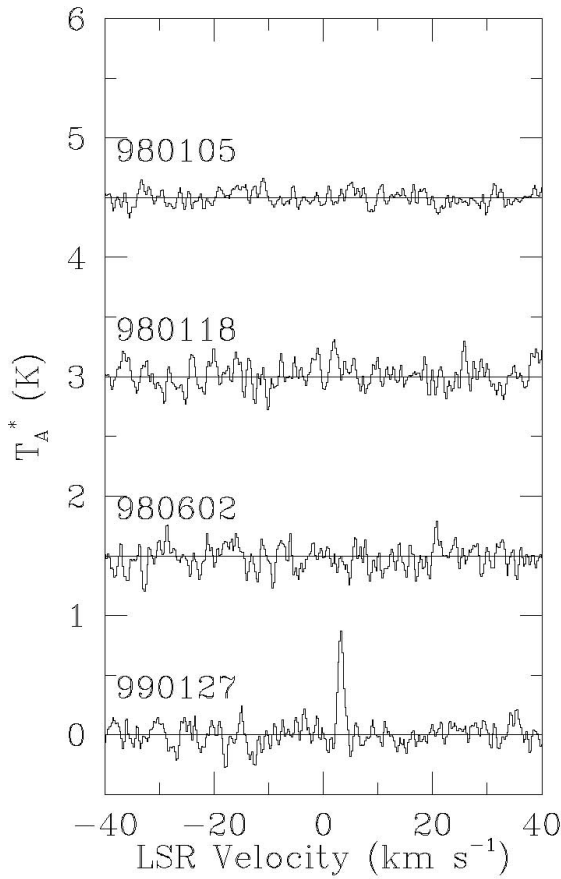


FIG. 27a

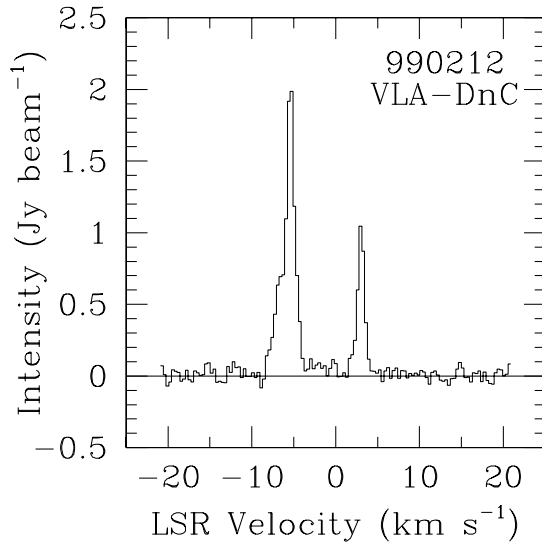


FIG. 27b

FIG. 27.—H₂O maser spectra for the source Serpens SMM 4 from (a) the Nobeyama 45 m telescope survey and (b) VLA DnC array observations. The ambient cloud velocities estimated from the H₂CO 3₀₃–2₀₂ line (Hurt & Barsony 1996) and the N₂H⁺ 101–012 line (Mardones et al. 1997) are 8.75 and 8.08 km s^{-1} , respectively.

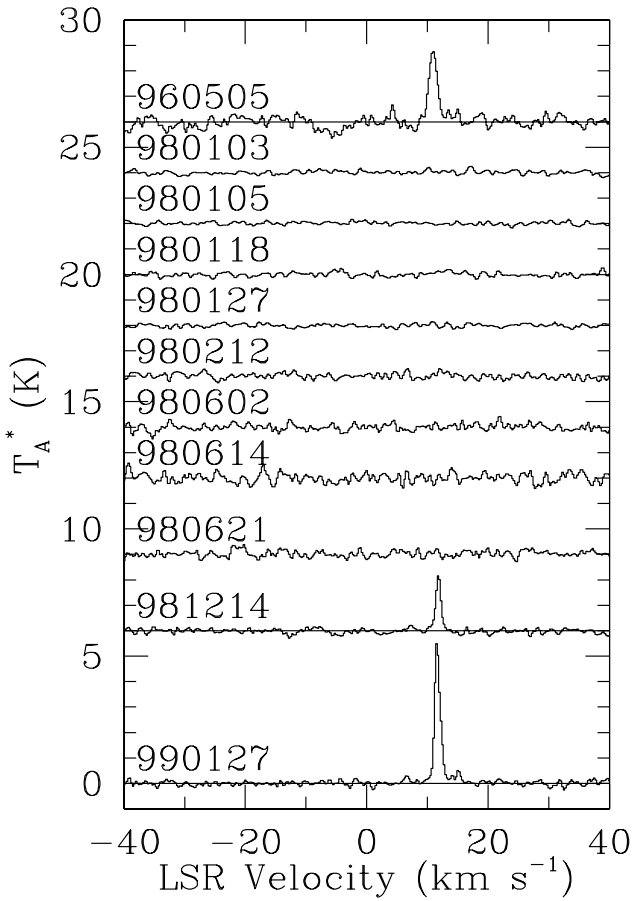


FIG. 28a

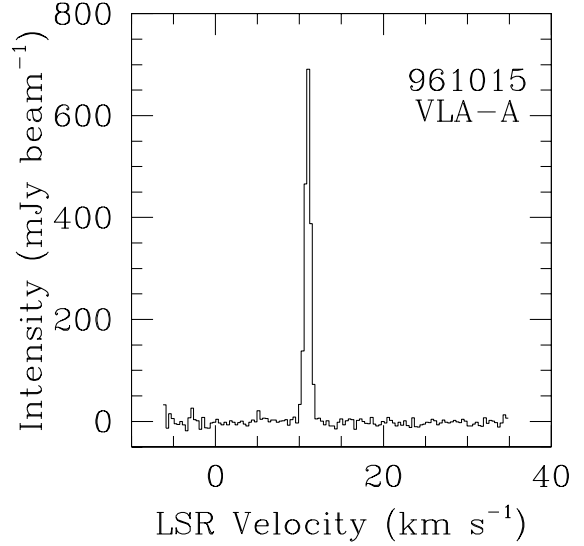


FIG. 28b

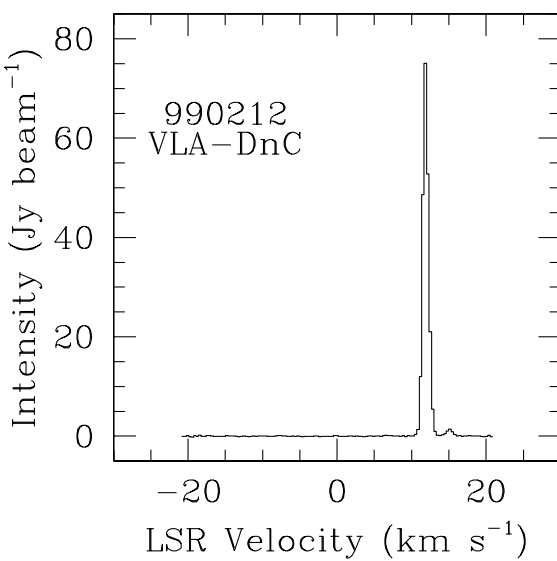


FIG. 28c

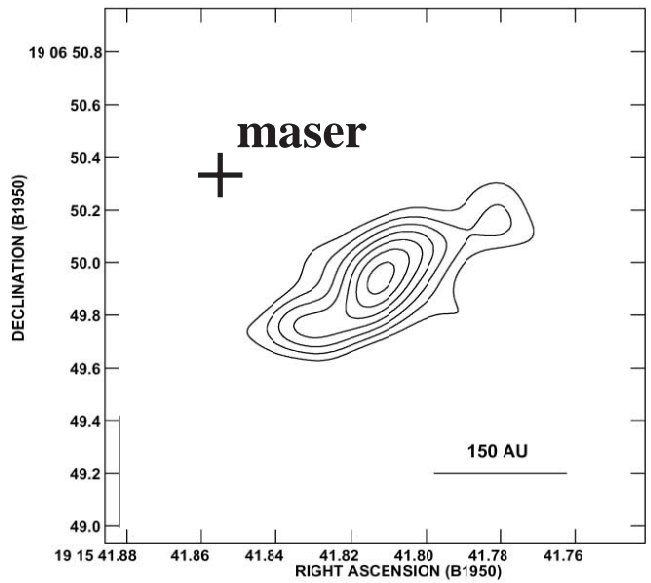


FIG. 28d

FIG. 28.—(a) H_2O maser spectra for the source L723-FIR (IRAS 19156+1906) from the Nobeyama 45 m telescope survey. The ambient cloud velocity estimated from the $^{13}\text{CO } J = 1-0$ line is $\sim 10.5 \text{ km s}^{-1}$ (Hayashi et al. 1991), from the CS $J = 2-1$ line is 10.5 km s^{-1} (Heyer et al. 1986), and from the NH_3 lines is $10.86 \pm 0.04 \text{ km s}^{-1}$ (Torrelles et al. 1986). Panels (b) and (c) present H_2O maser spectra obtained with (b) the VLA A array and (c) DnC array observations. (d) Position of the masers from the VLA A array observations (thick cross) indicated on the $\lambda = 3.6 \text{ cm}$ free-free emission image of the source L723 VLA 2 (Anglada et al. 1996). (e) Distribution of the masers obtained by the VLA observations: filled triangles, open squares, and filled circle indicate maser spots for $V_{\text{LSR}} = 10-11$, $11-12$, and $12-13 \text{ km s}^{-1}$, respectively.

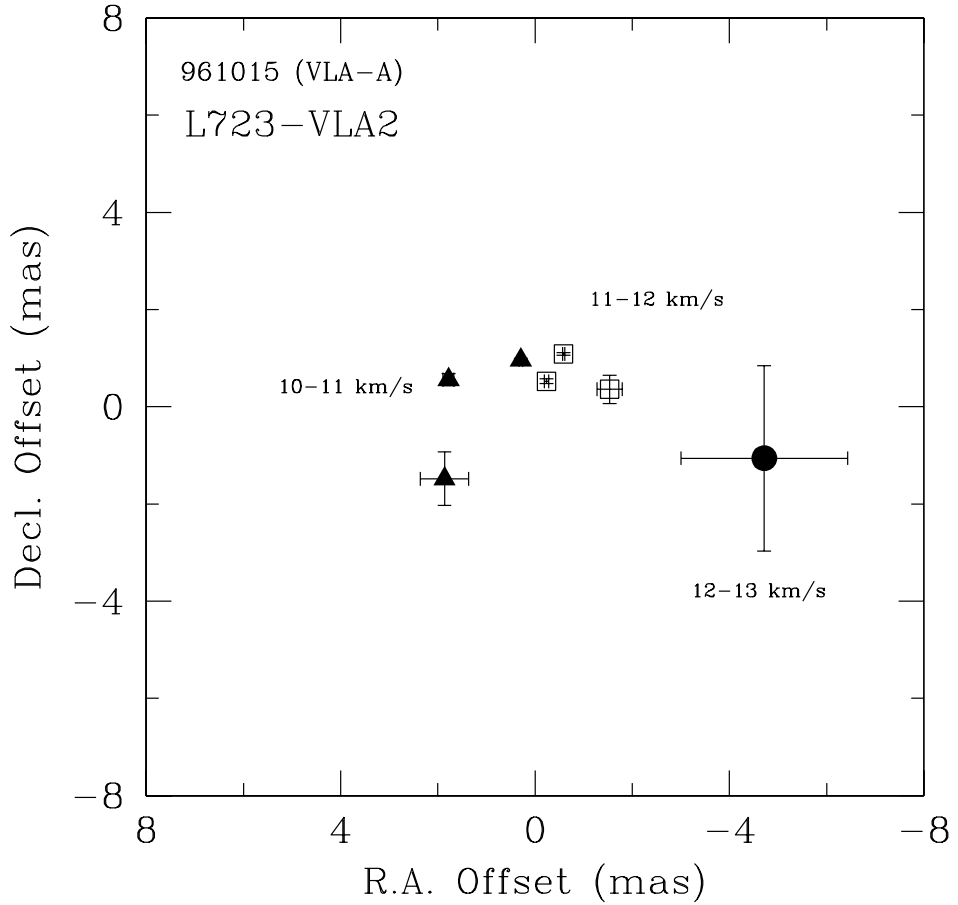


FIG. 28e

unlikely to be directly associated with the star itself. Genzel & Downes (1977), using the Efflesberg 100 m telescope, detected maser emission at the same velocity (1.4 km s^{-1}) in 1976. However, they suggested that the maser emission was from T Tauri itself, despite their large positional uncertainty ($\pm 10''$). The intensity of the maser decreased from 60 Jy in 1975 July to 3 Jy in 1976 October. It never repeated its former brilliance during the monthly 13 epoch monitoring with the Haystack 37 m telescope starting from 1991 December (Claussen et al. 1996) and during our monitoring program at Nobeyama.

Figure 9 presents an H_2O maser profile that we succeeded in detecting with the VLA CnB array in 1998 October. We determined the position of the maser: it was located at $0''.49$ south of the Class I source T Tau South. The velocity of the emission ($V_{\text{LSR}} = 5.9 \text{ km s}^{-1}$) differs from that of the previous reports, although, like them, this maser is blueshifted with respect to the systemic velocity of $V_{\text{LSR}} = 8.2 \text{ km s}^{-1}$. The emission lies within the nearly pole-on blueshifted biconical outflowing shells identified from interferometric ^{13}CO $J = 1-0$ observations (Momose et al. 1996). We suggest that the maser emission is associated with this outflow activity in T Tau South. Proper motion observations with the VLBA could confirm this suggestion.

4.3.4. NGC 2024 FIR 5/FIR 6 Region

The star-forming region of NGC 2024 (Orion B) contains seven dense cloud cores, FIR 1–FIR 7, which were detected by dust continuum emission at millimeter and submillimeter

wavelengths (Mezger et al. 1992). Many studies (Mangum, Wootten, & Barsony 1999 and references therein) suggested that the seven sources are isothermal condensations on their way to forming protostars. Through these investigations, FIR 5 and FIR 6 were suggested to be Class 0 sources (Wiesemeyer, Güsten, & Wright 1997a). FIR 5 and FIR 6 are known to drive a highly collimated one-sided molecular outflow (Richer, Hills, & Padman 1992; Sanders & Willner 1985; Richer et al. 1989) and a bipolar outflow (Richer 1990), respectively. Genzel & Downes (1977) reported the presence of H_2O maser emission ($V_{\text{LSR}} = 10 \text{ km s}^{-1}$) toward FIR 6 with the positional accuracy of $\pm 6''$.

Both FIR 5 and FIR 6 lie within the beam of the 45 m telescope. The region of NGC 2024 FIR 5 and FIR 6 is one of the eight displaying maser emission throughout the Nobeyama monitoring that contain Class 0 sources. As shown in Figure 13, the emission was seen around $V_{\text{LSR}} = 11$ and 14 km s^{-1} in the period from 1998 January to June. Instead of these velocities, we detected emission at $V_{\text{LSR}} = 3.3$ and 16.1 km s^{-1} with the VLA CnD array observations in 1999 February and at 2.4 km s^{-1} with the 45 m telescope in 1999 March. The VLA observations showed that the masers were associated not with FIR 6 but with FIR 5. On the basis of these results, we suggest that the maser emission detected in 1998 January and June was associated with FIR 5, although the LSR velocities were not necessarily identical to those of the VLA detection. The maser lies 7000 AU southeast of the close binary FIR 5. This

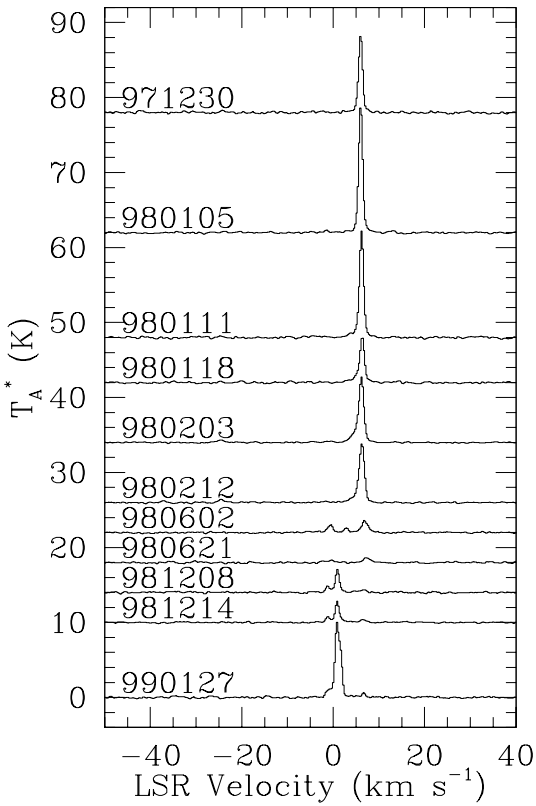


FIG. 29a

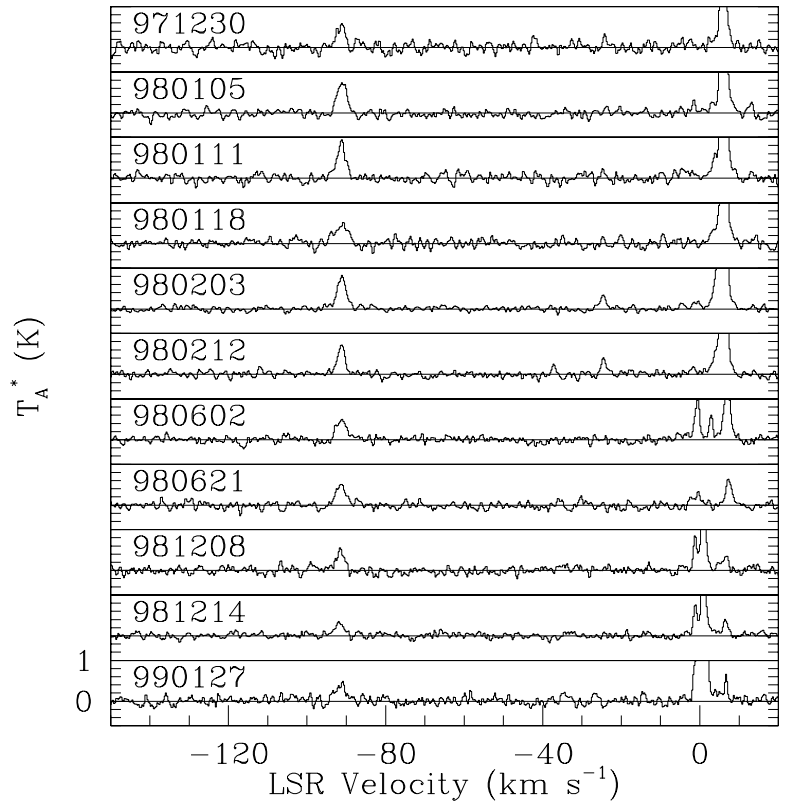


FIG. 29b

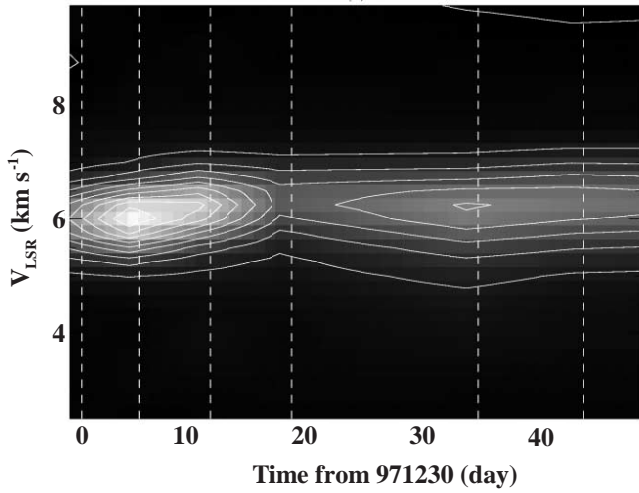


FIG. 29c

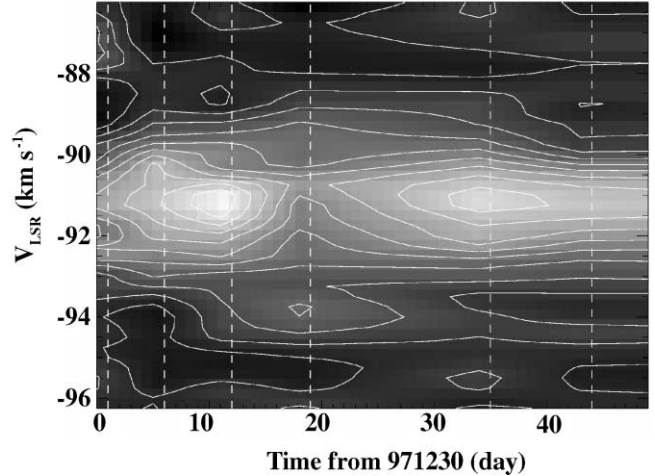


FIG. 29d

FIG. 29.—(a) and (b) H₂O maser spectra for the source IRAS 20050+2720 from the Nobeyama 45 m telescope survey. The ambient cloud velocity estimated from the CS $J = 3-2$ line is $V_{\text{LSR}} = 6 \text{ km s}^{-1}$ (Bachiller et al. 1995a). Panels (c) and (d) present time variation contour maps of the masers in IRAS 20050+2720 in the period from 1997 December 30 through 1998 February 18 for the emission (c) around the ambient cloud velocity and (d) at the blueshifted EHV emission. Sensitivity of the observations was typically 55 mK in T_A^* : the contour intervals are 5% and 10% of the peak intensity for panels (c) and (d), respectively. Panels (e) and (f) present the longer term time variation for the two components together with the best-fit lines (see text). Panels (g) and (h) present the spectra from the VLA DnC array observations for the components around the ambient cloud velocity and for the EHV emission, respectively.

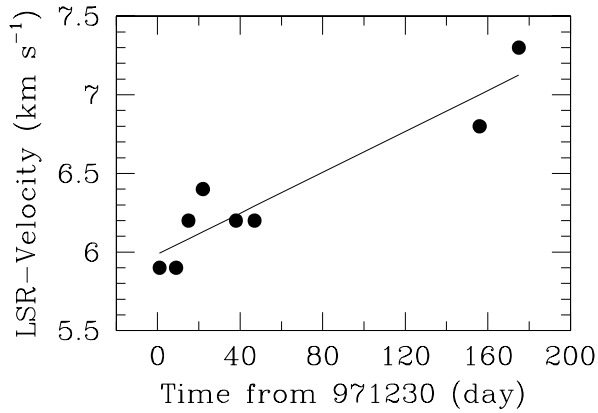


FIG. 29e

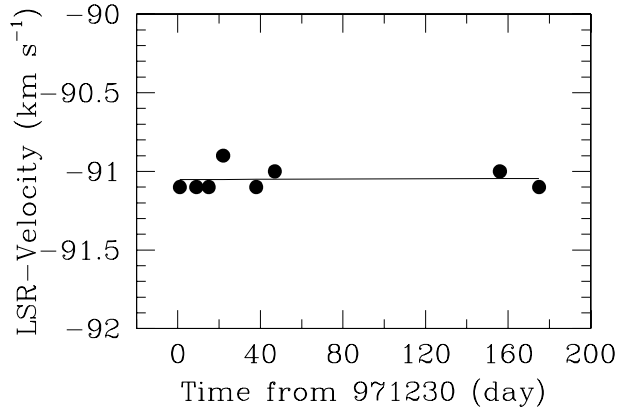


FIG. 29f

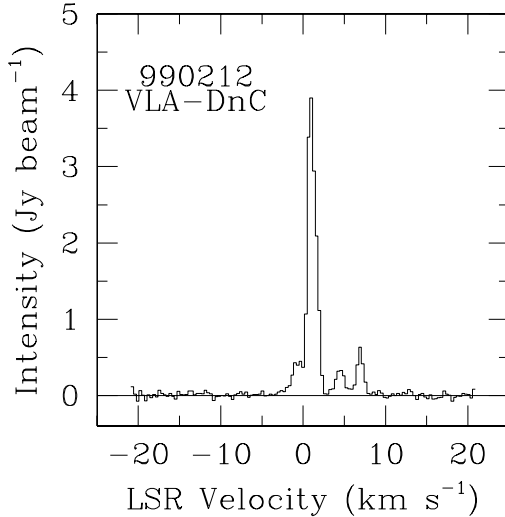


FIG. 29g

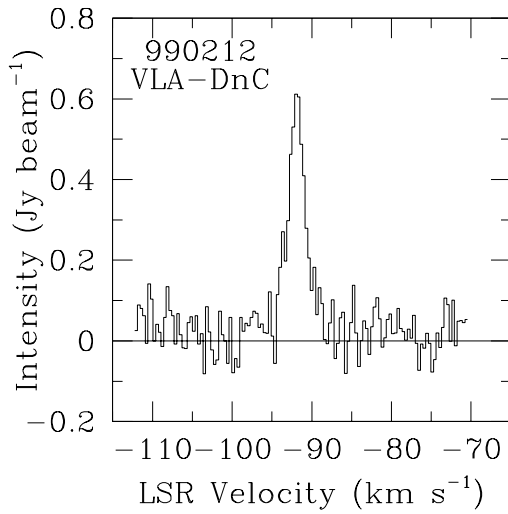


FIG. 29h

result supports the suggestion that FIR 5 could be a deeply embedded YSO rather than a PPSC, based on the fact that the region around FIR 5 contains the warmest gas (Mangum et al. 1999), although Chernin (1996) ruled out the possibility of FIR 5 being the driving source of the outflow from high-resolution BIMA array observations.

4.3.5. NGC 2071 North

This source was found by the unbiased CO outflow survey performed with the Nagoya University 4 m telescope (Iwata, Fukui, & Ogawa 1988). NGC 2071 North is located at 20' north of the well-known source NGC 2071 IRS in L1630. The exciting source, suggested to be IRAS 05451+0037, shows a far-infrared spectrum similar to T Tau and is considered to be a Class I object.

Maser emission from NGC 2071 North was first detected by the Nobeyama survey in 1999 March. The detected emission ($V_{\text{LSR}} = 13.2 \text{ km s}^{-1}$) is redshifted with respect to the ambient cloud velocity (Fig. 16).

4.3.6. GSS 30-IRS

Emission at 1.3 mm from the Class I source GSS 30-IRS 1 has been interpreted as arising from a circumstellar mass of $\sim 0.1 M_{\odot}$ (André & Montmerle 1994). Although a well-

defined bipolar reflection nebula is associated with IRS 1, the distribution of high-velocity CO gas does not reconcile with the morphology of the reflection nebula (Tamura et al. 1990). Lying at the terminus of the VLA 1623 outflow (André & Montmerle 1994), part of the high-velocity gas reported by Tamura et al. (1990) probably arises from that source. Zhang, Wootten, & Ho (1997) present interferometric CO isotopomer observations that show that the core is under disruption.

GSS 30-IRS 1 is the only Class I source that displayed maser emission throughout the Nobeyama observations (Fig. 17). As Claussen et al. (1996) have already reported, the maser emission is associated with GSS 30-IRS. Our VLA CnD array observations show the maser velocity and position to have remained unchanged since 1994, arising within 40 AU of IRS 1. Although the detections in 1997 December and 1998 January were marginal (10.6 σ detection in 1997 December and 7.9 σ detection in 1997 January), the masers here do show component variations. The 1997 December spectrum alone peaked at $V_{\text{LSR}} = -12.6 \text{ km s}^{-1}$, while all of the remaining spectra peaked at -14.6 km s^{-1} . We thus suggest that the faint emission seen in 1998 January is a precursor of the strong emission seen in 1998 June and surviving at least up to the 1999 February VLA observations.

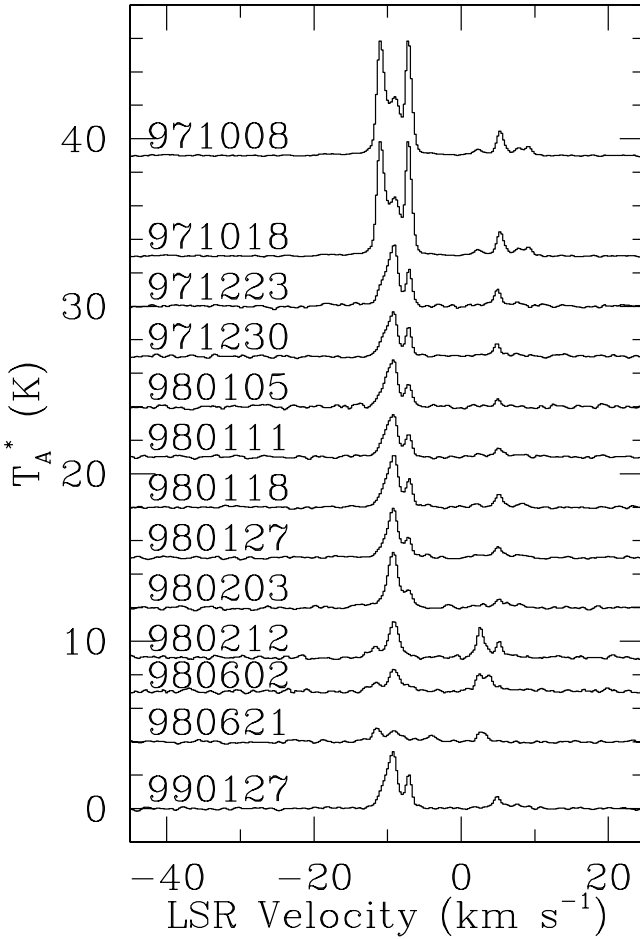


FIG. 30a

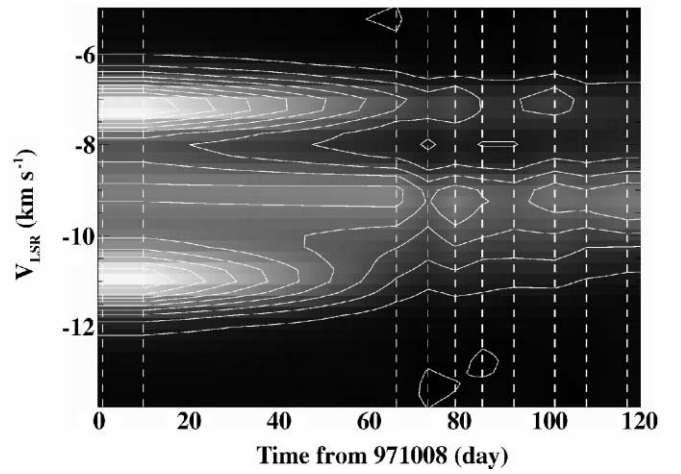


FIG. 30b

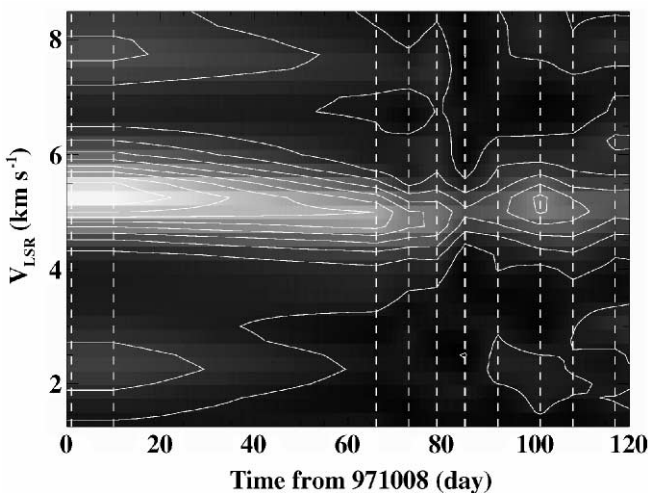


FIG. 30c

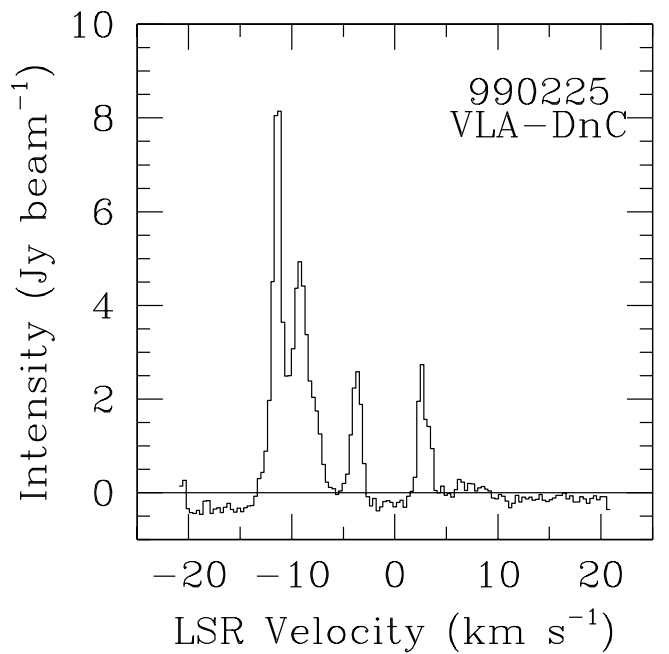


FIG. 30d

FIG. 30.—(a) H_2O maser spectra for the source S106 FIR from the Nobeyama 45 m telescope survey. The ambient cloud velocity estimated from the $\text{H}^{13}\text{CO}^+ J = 1-0$ line is -1.1 km s^{-1} (Furuya et al. 2000). Panels (b) and (c) present time variation contour maps of the maser emission in the period from 1997 October 8 through 1998 February 14 for (b) blueshifted and (c) redshifted emission. The vertical dashed lines indicate the dates of observations. Sensitivity of the observations was typically 30 mK in T_A^* : the contour intervals are 10% of the peak intensity. (d) H_2O maser spectrum observed with the VLA DnC array.

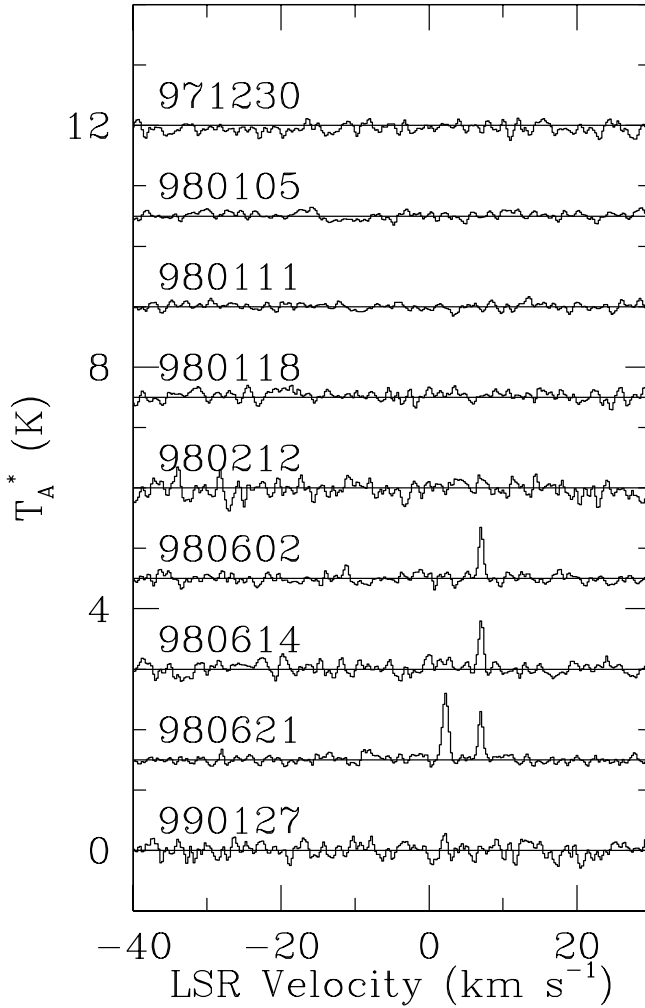


FIG. 31a

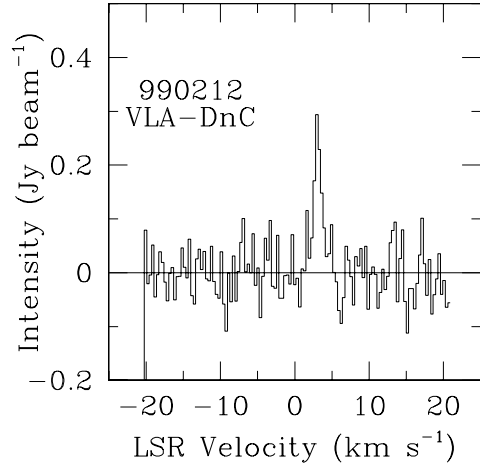


FIG. 31b

FIG. 31.— H_2O maser spectra for the source L1157-MM (IRAS 20386+6751) from (a) the Nobeyama 45 m telescope survey and (b) VLA DnC array observations. The ambient cloud velocities estimated from the CO $J = 1-0$ line (Umemoto et al. 1992) and the N_2H^+ 101–012 line (Mardones et al. 1997) are $V_{\text{LSR}} = 2.7$ and 2.69 km s^{-1} , respectively.

As a triple system comprised of variously evolved sources, GSS 30 can offer clues to the reasons for maser emission. IRS 1 emits $\sim 26 L_\odot$, while IRS 3 only emits $\sim 1 L_\odot$; both, however, show SED Class I spectra, and both have circumstellar masses; only the Class III sources IRS 2 and IRS 3 emit centimeter radio emission. The association of the maser with IRS 1 suggests that luminosity of the central star is a critical determinant of maser emission, as was shown in Paper I and Wilking et al. (1994) for the ensemble of masers.

4.3.7. VLA 1623

The Class 0 source VLA 1623 is the prototypical Class 0 source; it drives a large-scale CO outflow with principal axis roughly -60° (André et al. 1990; Dent, Matthews, & Walther 1995; Yu & Chernin 1997). High-resolution VLA radio continuum emission observations at $\lambda = 3.6 \text{ cm}$ revealed the presence of a series of clumps that are interpreted as knots of radio jet driving the large-scale CO outflow (Bontemps & André 1997), although the position angle

(P.A.) of the radio jet and that of CO outflows differ by roughly -30° . A recent subarcsecond $\lambda = 2.7 \text{ mm}$ continuum emission image indicated that VLA 1623 is a binary system with two circumstellar disks (Looney et al. 2000).

We detected weak ($\sim 0.9 \text{ Jy}$) maser emission with a single peak at $V_{\text{LSR}} = 8 \text{ km s}^{-1}$ in 1997 December (Figs. 18a and 18b), which is one of the weakest emissions in our detection with the 45 m telescope. We presented a time-velocity variation diagram for this emission in Figure 18c. In 1998 June, we detected the stronger emission ($\sim 6.7 \text{ Jy}$) at 9 km s^{-1} , whose intensity decreased to less than half within 13 days. Figure 18d presents the maser spectrum taken by the VLA observations in 1996 December, performed a year prior to the Nobeyama monitoring. We detected emission peaked at $V_{\text{LSR}} = 13.2 \text{ km s}^{-1}$, which is redshifted to the ambient cloud velocity. The velocity range of the VLA detection is slightly redshifted compared to that of the 45 m telescope. The 80 mas resolution VLA observations clearly reveal that the masers are associated with the western source of the binary sys-

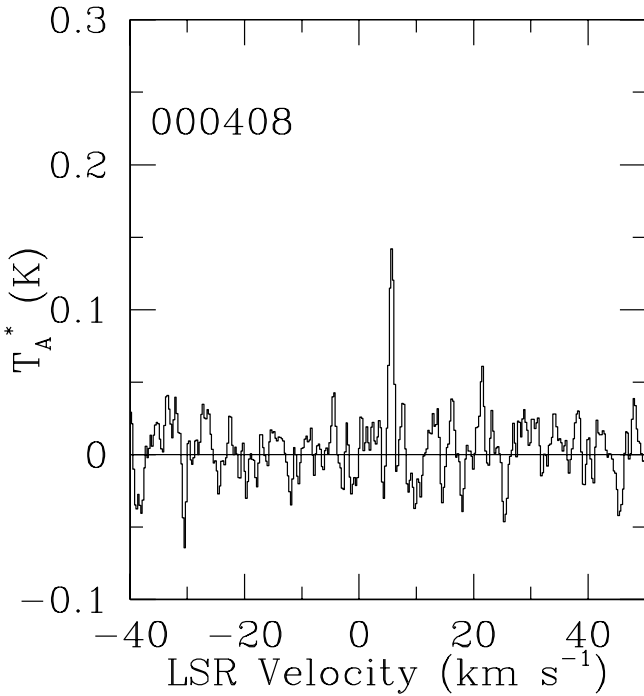


FIG. 32.— H_2O maser spectrum for the source GF 9-2 from the Nobeyama 45 m telescope survey. The ambient cloud velocity estimated from the C^{34}S $J = 2-1$ lines is $V_{\text{LSR}} = -2.7 \text{ km s}^{-1}$ (Wiesemeyer et al. 1997b).

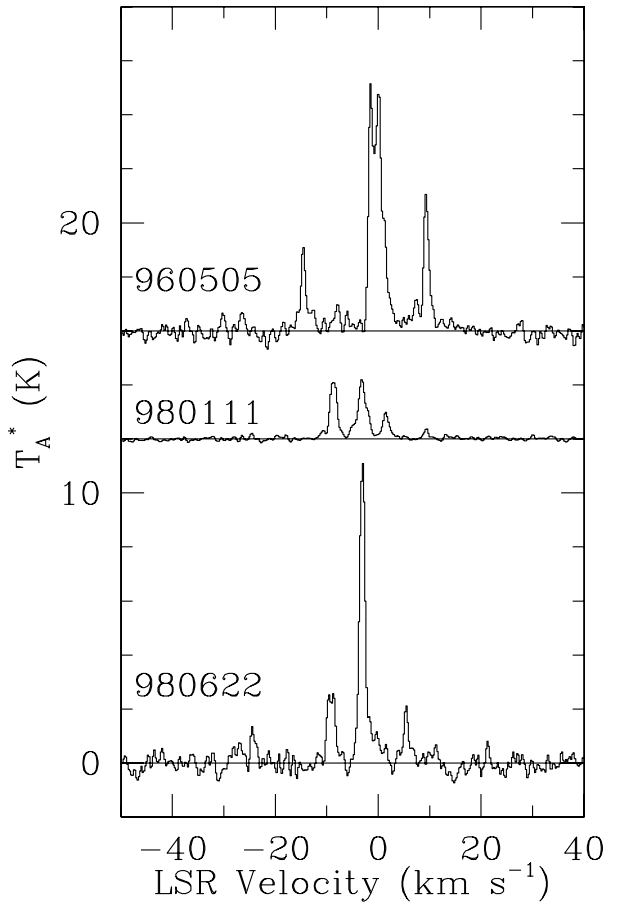


FIG. 33.— H_2O maser spectra for the source IC 1396N (IRAS 21391+5802) from the Nobeyama 45 m telescope survey. The ambient cloud velocity estimated from the ^{13}CO $J = 1-0$ line is $V_{\text{LSR}} \approx 0 \text{ km s}^{-1}$ (Patel et al. 1995).

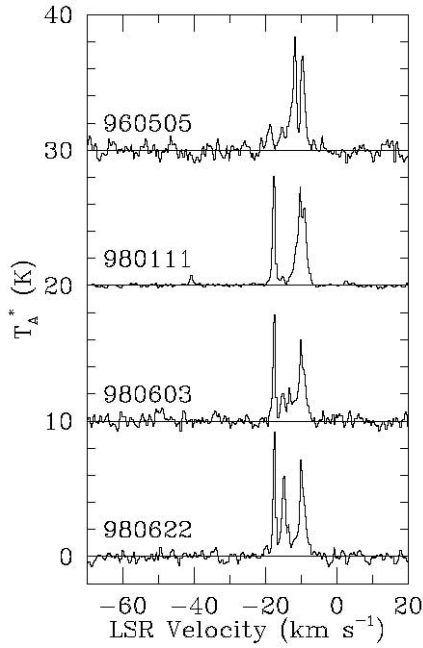


FIG. 34a

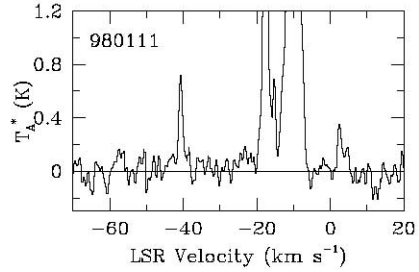


FIG. 34b

FIG. 34.—(a) and (b) H_2O maser spectra for the source LkH α 234 (IRAS 21418+6552) from the Nobeyama 45 m telescope survey. The ambient cloud velocity estimated from the C^{18}O $J = 3-2$ line is $V_{\text{LSR}} = -10 \text{ km s}^{-1}$ (Font, Mitchell, & Sandell 2001).

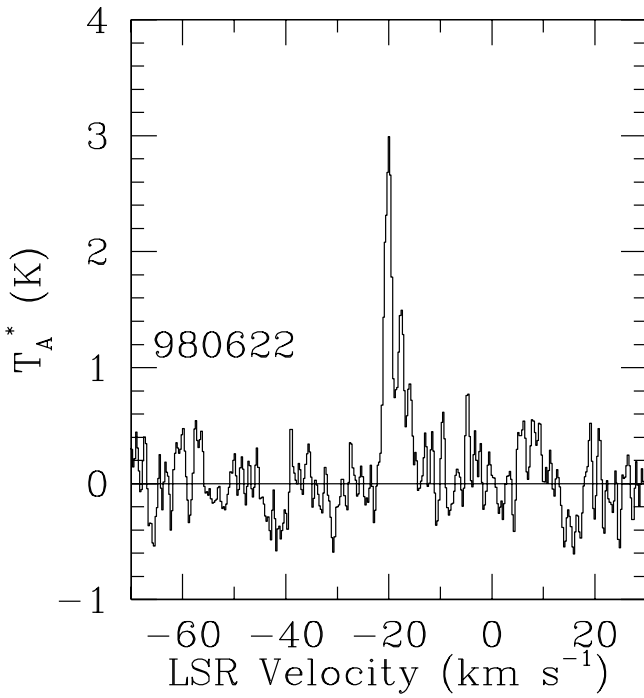


FIG. 35.— H_2O maser spectrum for the source S140-IRS (IRAS 22176+630) from the Nobeyama 45 m telescope survey. The ambient cloud velocity estimated from the CS $J = 1-0$ line is $V_{\text{LSR}} = -7.5 \text{ km s}^{-1}$ (Hayashi & Murata 1992).

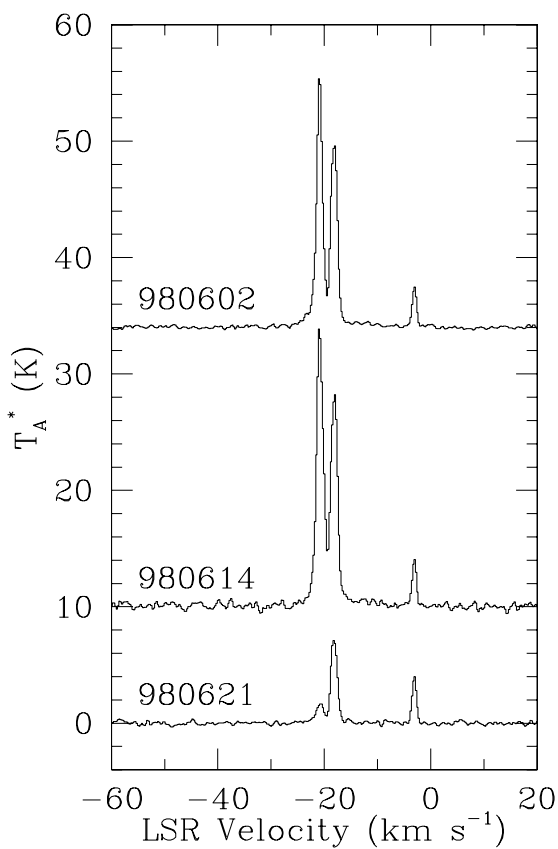


FIG. 36.— H_2O maser spectra for the source IRAS 22198+6336 (L1204A) from the Nobeyama 45 m telescope survey. The ambient cloud velocity estimated from the $J = 1-0$ transitions of ^{13}CO and CS is $V_{\text{LSR}} = -8.8 \text{ km s}^{-1}$ (Tafalla, Bachiller, & Martín-Pintado 1993).

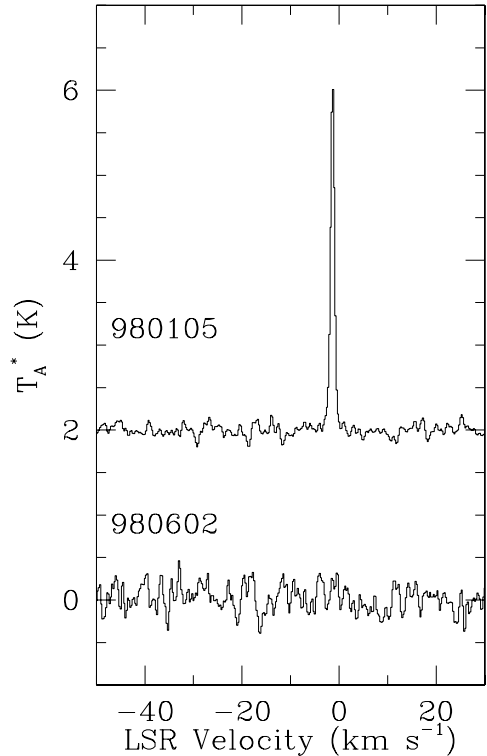


FIG. 37.— H_2O maser spectrum for the source IRAS 22266+6845 (L1221) from the Nobeyama 45 m telescope survey. The ambient cloud velocity estimated from the ^{13}CO $J = 1-0$ line is $V_{\text{LSR}} = -4.4 \text{ km s}^{-1}$ (Umemoto et al. 1991).

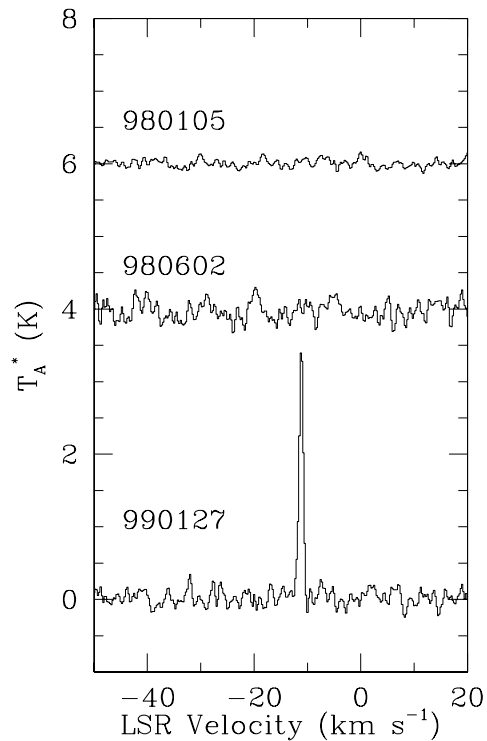


FIG. 38.— H_2O maser spectra for the source L1251A (IRAS 22343+7501) from the Nobeyama 45 m telescope survey. The ambient cloud velocities estimated from the NH_3 (1, 1), (2, 2) lines (Anglada et al. 1997) and the N_2H^+ 101–012 line (Mardones et al. 1997) are $V_{\text{LSR}} = -4.7$ and -5.02 km s^{-1} , respectively.

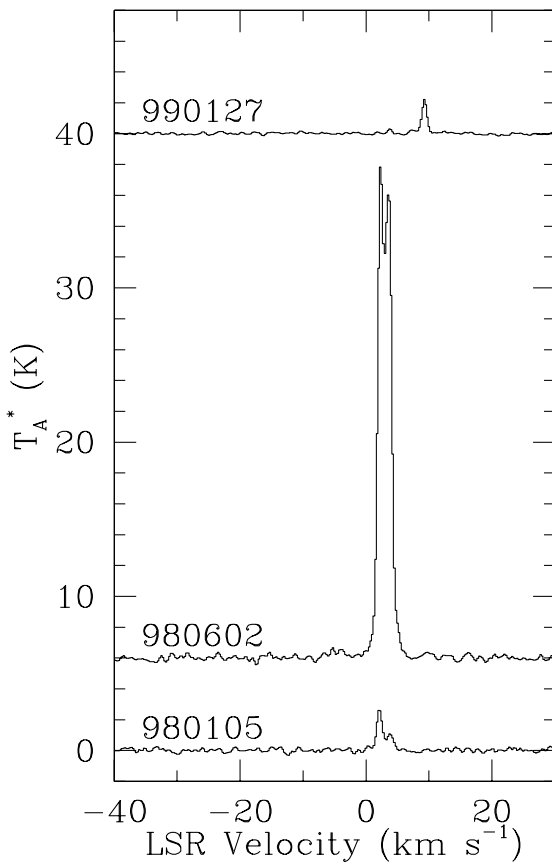


FIG. 39.— H_2O maser spectra for the source L1251B (IRAS 22376+7455) from the Nobeyama 45 m telescope survey. The ambient cloud velocities estimated from the NH_3 (1, 1), (2, 2) lines (Anglada et al. 1997) and the N_2H^+ 101–012 line (Mardones et al. 1997) are $V_{\text{LSR}} = -3.6$ and -3.53 km s^{-1} , respectively.

tem (VLA 1623 B; see Fig. 18e). A detailed presentation of the kinematics of the maser spots will be published elsewhere (R. S. Furuya et al. 2003, in preparation).

4.3.8. IRAS 16244–2431 (YLW 16A)

The Class I source IRAS 16244–2431 is an *IRAS* dense core (Myers et al. 1987) and is also known as YLW 16A (Young, Lada, & Wilking 1986). This source possesses a highly collimated one-sided CO outflow (Terebey, Vogel, & Myers 1989), suggesting that the outflow axis lies normal to the plane of sky (Sekimoto et al. 1997).

Maser emission from YLW 16A was first detected by Wilking & Claussen (1987). Subsequently, Claussen et al. (1996) reported that this source showed strong emission around $V_{\text{LSR}} = -12$ to -15 km s^{-1} in the latter half of 1990 and weak emission at -9 km s^{-1} in 1992. The beam of the 45 m telescope toward YLW 16A encompasses another source of YLW 16B (IRAS 16244–2432 NE): this source is also known to possess maser emission. Terebey et al. (1992) reported that YLW 16B showed weak maser emission at $V_{\text{LSR}} = 13.5 \text{ km s}^{-1}$. In 1997 December, we detected weak maser emission at -10.5 km s^{-1} at the 9.7σ level (Fig. 19). Considering the available velocity information, we suggest that the emission is associated with YLW 16A.

4.3.9. IRAS 16293–2422

IRAS 16293–2422 is among the first recognized Class 0 sources (AWB93). High-resolution continuum emission observations at centimeter and millimeter wavelengths revealed that the deeply embedded system is made up of two sources, MM 1 and MM 2, a suggested binary system with a projected separation of 840 AU (Wootten 1989; Mundy et al. 1992; Looney et al. 2000). This binary system shows two pairs of outflow lobes: the brighter one extending along an east-west direction and the other one along a northeast-southwest direction (Walker et al. 1988; Mizuno et al.

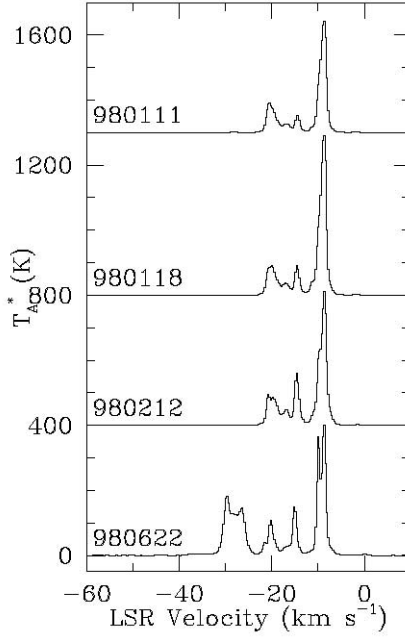


FIG. 40a

FIG. 40.—(a) and (b) H_2O maser spectra for the source Cepheus A (IRAS 22543+6145) from the Nobeyama 45 m telescope survey. The ambient cloud velocity estimated from the N_2H^+ 101–012 line is $V_{\text{LSR}} = -10.0 \text{ km s}^{-1}$ (Williams & Myers 1999).

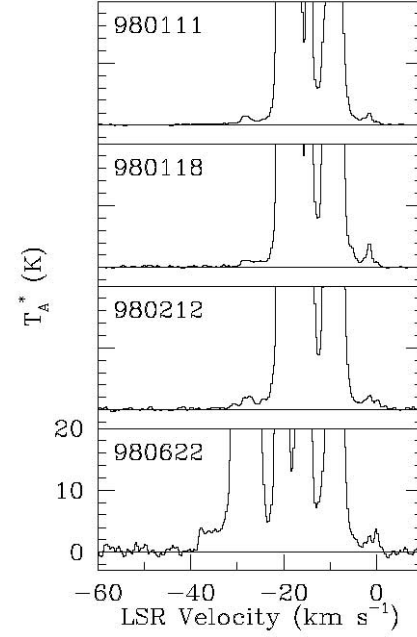


FIG. 40b

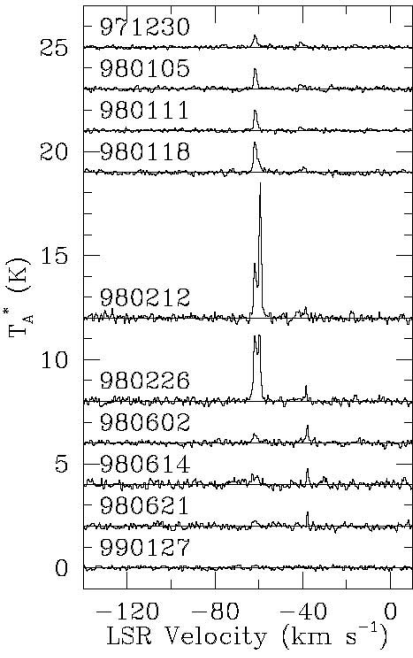


FIG. 41a

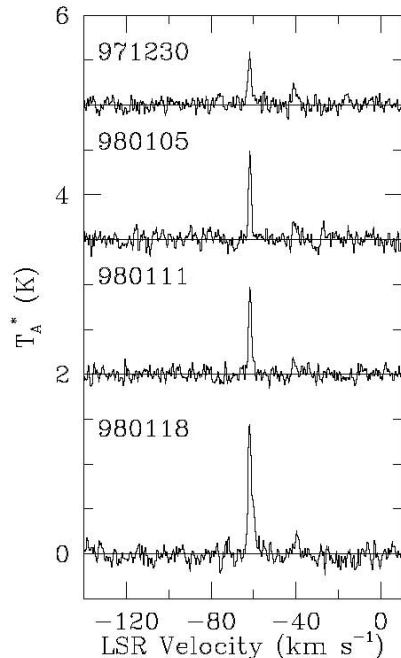


FIG. 41b

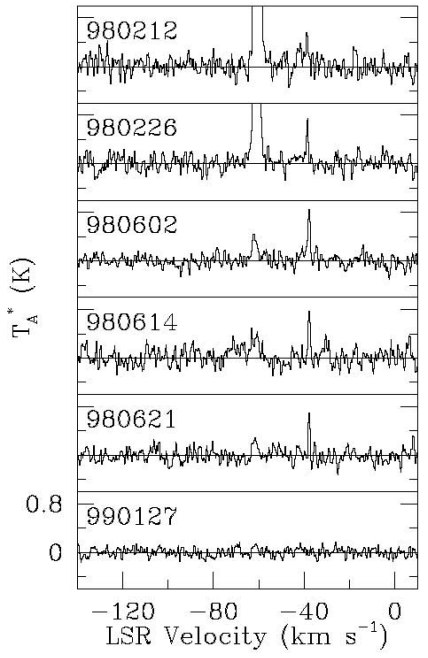


FIG. 41c

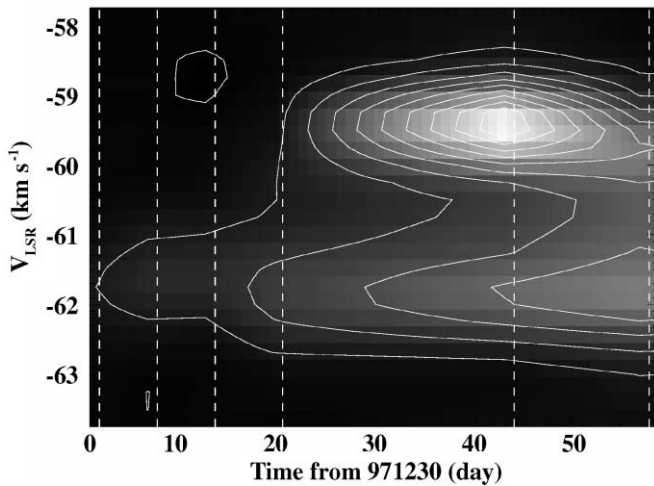


FIG. 41d

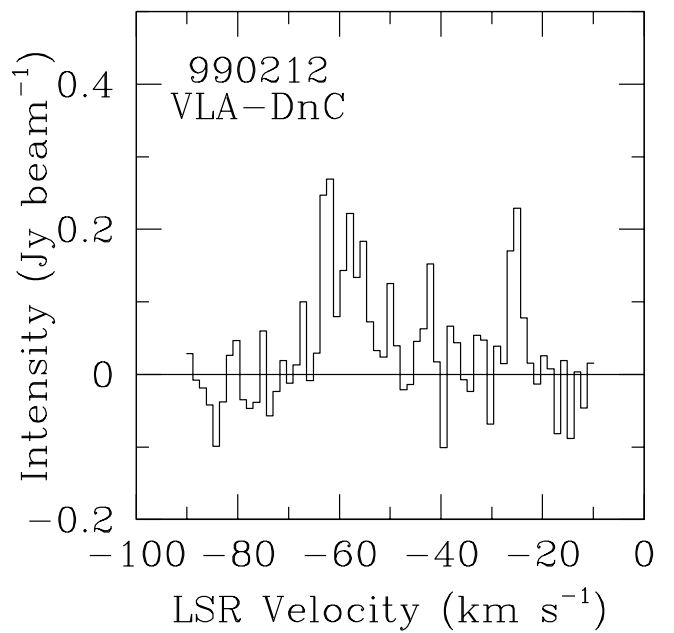


FIG. 41e

FIG. 41.—(a), (b), and (c) H₂O maser spectra for the source Cep E-MM (IRAS 23011+6126) from the Nobeyama 45 m telescope survey. The ambient cloud velocity estimated from the CO $J = 1-0$ lines is $V_{\text{LSR}} = -13 \text{ km s}^{-1}$ (Lefloch et al. 1996). (d) Time variation contour map of the maser emission around $V_{\text{LSR}} = -60 \text{ km s}^{-1}$ in the period from 1997 December 30 through 1998 February 13. The vertical dashed lines indicate the dates of observations. Sensitivity of the observations was typically 0.1 K in T_A^* ; the contour intervals are 10% of the peak intensity. (e) H₂O maser spectrum observed with the VLA DnC array.

TABLE 2
PARAMETERS OF H₂O MASER SPECTRA DETECTED BY THE NOBEYAMA 45 m TELESCOPE

Name (1)	Date (2)	Velocity (km s ⁻¹) (3)	T_A^* (K) (4)	ΔV (km s ⁻¹) (5)	$\int T_A^* dv$ (K km s ⁻¹) (6)	L_{H_2O} (L_\odot) (7)	Comments (8)
(1) IRAS 00338+6312.....	1998 Jan 5	-26.7	11.7	0.9	12.7	6.2E-10	
	1998 Feb 26	-26.7	7.7	0.8	9.1	4.4E-10	
	1998 Jun 3	-26.4	3.9	0.9	6.2	3.0E-10	
(2) NGC 281 West.....	1998 Jun 22	-34.2	40.7	2.1	79.7	3.0E-08	
		-32.1	18.7	1.2	22.7		
(6) RNO 15 FIR.....	1998 Jan 10	...	<0.026	
	1998 Jun 22	...	<0.21	
	1999 Jan 31	2.5	1.3	0.8	1.7	1.4E-11	
	1999 Mar 15	...	<0.24	
(9) NGC 1333 IRAS 2A	1998 Jan 4	4.6	0.3	2.3	0.6	3.6E-12	rms = 18 mK, 19 σ
		7.6	0.4	1.3	0.5		
	1998 Jan 10	7.6	0.4	1.4	0.7	2.3E-12	rms = 17 mK, 23 σ
	1998 Jun 1	4.6	0.8	2.1	2.0	6.5E-11	
	1998 Jun 14	4.9	0.9	1.7	2.3	5.5E-11	rms = 117 mK, 7.3 σ
	1998 Jun 22	...	<0.18	
	1999 Jan 31	7.0	4.6	1.2	7.0	2.3E-11	
	1999 Mar 15	2.4	3.2	1.4	7.7	2.5E-11	
(10) SVS 13A.....	1998 Jan 4	4.6	62.8	1.8	134	4.4E-10	
	1998 Jun 1	4.6	44.1	2.1	97.8	3.2E-10	
	1998 Jun 14	4.6	39.5	2.0	34.2	1.1E-10	
	1998 Jun 22	4.6	90.5	1.9	176.8	5.8E-10	
	1999 Jan 31	6.1	1.7	1.5	3.8	2.6E-11	
		13.6	2.2	1.8	4.3		
(11) NGC 1333 IRAS 4A	1997 Dec 30	7.6	6.7	1.2	11	5.2E-11	
(12) NGC 1333 IRAS 4B.....		12.1	3.2	1.0	5.0		
	1998 Jan 14	7.8	5.3	1.1	6.9	3.4E-11	
		9.7	1.3	2.2	1.6		
		12.4	1.3	1.2	1.8		
	1998 Jun 1	2.7	2.7	0.9	4.4	1.1E-10	
		7.8	3.0	1.2	4.7		
		16.7	21.6	1.0	26.0		
	1998 Jun 5	2.6	2.1	0.9	4.7	6.2E-11	
		16.8	11.9	0.9	14.4		
	1998 Jun 22	7.6	3.4	0.9	3.6	3.6E-11	
		16.7	3.8	1.1	7.6		
	1999 Jan 31	-5.9	9.7	1.0	10.9	1.3E-10 ^a	From IRAS 4B
		10.8	7.3	1.0	11.4		From IRAS 4A
		19.9	11.9	1.1	17.7		From IRAS 4B
	1999 Mar 15	-5.9	3.5	1.0	3.6	5.8E-10 ^b	From IRAS 4B
		1.1	1.5	1.1	2.3		From IRAS 4B
		10.5	3.2	1.4	6.9		From IRAS 4A
		18.3	3.5	1.2	5.1		From IRAS 4B
(16) B1-IRS.....	1998 Jun 1	15.7	6.3	1.7	12.4	8.6E-11	
		21.2	0.7	1.9	1.8		
	1998 Jun 5	15.7	1.4	1.7	3.5	2.1E-11	
	1998 Jun 14	15.7	3.7	1.7	7.2	4.4E-11	
	1998 Jun 22	15.7	8.9	1.2	14.3	8.6E-11	
	1999 Jan 31	16.1	2.3	0.8	2.2	1.3E-11	
	1999 Mar 15	...	<0.23	
(58) Orion A West	1998 Feb 26	6.2	9.6	1.2	16.7	2.3E-10	
	1998 Jun 1	4.0	33.1	1.0	38.2	8.1E-10	
		5.7	4.1	2.7	5.5		
		6.1	13.4	0.8	12.8		
		11.6	1.6	1.2	2.8		
	1998 Jun 22	3.8	39.5	1.0	44.9	6.8E-10	
		5.7	1.8	1.0	2.7		
		11.6	1.8	1.0	2.7		
	1999 Mar 15	-3.8	2.3	1.2	3.9	2.5E-09	
		3.8	107.0	1.2	155.0		

TABLE 2—Continued

Name (1)	Date (2)	Velocity (km s ⁻¹) (3)	T_A^* (K) (4)	ΔV (km s ⁻¹) (5)	$\int T_A^* dv$ (K km s ⁻¹) (6)	$L_{\text{H}_2\text{O}}$ (L_\odot) (7)	Comments (8)
		6.2	13.2	6.8	27.6		
		9.2	3.3	6.4	4.0		
(63) HH 1–2	1998 Jan 13	15.1	2.3	0.85	2.2	2.9E–11	
	1998 Feb 26	...	<0.011	
	1998 Jun 1	...	<0.09		
(66) IRAS 05375–0731	1998 Feb 26	4.6	3.9	0.8	2.3	3.1E–11	
	1998 Jun 1	7.0	0.8	0.9	0.9	1.2E–11	
	1999 Mar 15	...	<0.21	
(68) NGC 2024 FIR 5	1998 Jan 4	10.8	7.8	0.8	7.6	7.5E–11	
	1998 Jan 10	11.1	2.3	0.8	2.7	2.6E–11	
	1998 Jun 1	11.1	1.6	0.9	1.6	4.5E–11	
		13.8	1.2	1.1	3.3		
	1998 Jun 22	10.9	5.2	0.8	5.1	7.7E–11	
		13.9	1.3	1.3	2.8		
	1999 Mar 15	2.4	3.2	1.4	7.8	7.7E–11	
(71) IRAS 05413–0104	1998 Jan 18	−1.9	2.5	1.3	4.0	1.4E–10	
		2.7	3.4	1.3	6.4		
	1998 Feb 26	−2.0	4.2	1.1	6.7	2.3E–10	
		2.7	7.4	1.0	9.5		
	1998 Jun 1	−2.1	3.2	1.3	4.9	1.4E–10	
		2.9	2.7	1.6	5.0		
	1999 Mar 15	4.9	1.7	0.9	1.0	1.4E–11	
(76) NGC 2071 IRS	1998 Jun 1	−0.5	14.4	1.1	19.1	3.5E–09	
		2.2	12.3	1.5	19.8		
		4.0	12.2	2.5	19.5		
		11.1	128	1.2	197.5		
	1998 Jun 5	−0.5	14.5	1.1	18.8	3.7E–09	
		2.2	15.4	2.1	21.8		
		4.0	12.9	2.3	27.5		
		11.1	132.3	1.1	204.9		
	1998 Jun 22	−0.5	11.3	1.0	14.5	2.0E–09	
		4.0	6.6	2.8	18.8		
		9.7	54.1	1.0	57.1		
		11.0	32.2	0.7	55.5		
		23.2	1.6	1.0	1.5		
	1999 Mar 15	1.9	13.1	1.0	16.7	2.7E–09	
		4.3	3.0	1.9	5.9		
		7.8	2.9	1.5	5.3		
		11.6	92.9	1.0	158.1		
		18.6	2.3	1.0	2.6		
		22.9	1.7	1.6	3.2		
		25.1	1.8	2.9	5.3		
(77) NGC 2071 North	1998 Jan 13	...	<0.093	
	1998 Jun 1	...	<0.13	
	1999 Mar 15	13.2	1.1	1.3	1.7	2.3E–11	
(96) GSS 30-IRS	1997 Dec 31	−12.6	0.37	1.2	0.7	1.2E–12	rms = 35 mK
	1998 Jan 18	−14.6	0.49	1.1	1.2	2.1E–11	rms = 62 mK
	1998 Jun 1	−14.6	21.8	0.8	24.3	4.2E–11	
	1998 Jun 2	−14.6	22.8	0.8	23.5	4.0E–11	
	1998 Jun 13	−14.6	20.9	0.8	20.9	3.6E–11	
(101) VLA 1623	1997 Dec 27	8.1	0.33	1.0	0.7	1.2E–12	rms = 48 mK, 7.5 σ
	1997 Dec 31	...	<0.03	
	1998 Jan 5	7.8	0.4	1.3	0.9	1.5E–12	
	1998 Jan 11	7.8	0.4	1.1	0.6	1.0E–12	rms = 22 mK, 183 σ
	1998 Jan 14	7.8	0.6	1.1	0.7	1.2E–12	rms = 27 mK, 13 σ
	1998 Jun 1	9.0	2.4	1.0	3.7	6.4E–12	
	1998 Jun 2	9.0	2.1	1.0	3.6	6.2E–12	
	1999 Jun 13	9.3	1.1	1.0	1.6	2.8E–12	

TABLE 2—Continued

Name (1)	Date (2)	Velocity (km s ⁻¹) (3)	T_A^* (K) (4)	ΔV (km s ⁻¹) (5)	$\int T_A^* dv$ (K km s ⁻¹) (6)	$L_{\text{H}_2\text{O}}$ (L_\odot) (7)	Comments (8)
(124) YLW 16A.....	1997 Dec 27	-10.5	0.4	0.9	0.3	5.2E-13	rms = 41 mK
	1998 Jan 11	...	<0.04	
	1998 Jun 13	...	<0.07	
(139) IRAS 16293–2422	1997 Dec 27	0.3	7.6	2.1	10.3	1.8E-10	
		1.9	25.5	1.6	29.3		
		3.5	24.2	1.7	35.3		
		5.9	22.6	0.9	23.2		
		7.3	4.9	0.4	7.2		
	1998 Jan 3	1.9	25.5	1.2	35.2	1.6E-10	
		3.2	15.9	1.9	23.4		
		5.9	25.7	0.9	27.6		
		7.3	4.5	1.6	5.9		
		1.9	27.6	1.1	36.3	1.6E-10	
	1998 Jan 5	3.2	14.9	2.2	22		
		5.9	29.5	0.9	33.2		
		1.9	35.5	0.95	42.4	1.6E-10	
		3.2	11.0	3.5	17.0		
		5.9	29.3	0.9	32.2		
	1998 Jan 14	1.9	44.8	0.9	55.9	1.8E-10	
		3.2	10.3	3.0	13.8		
		5.9	32.6	0.9	37.4		
		1.9	52.6	0.9	73.9	1.9E-10	
		5.9	32.3	0.9	37.8		
	1998 Jun 1	-2.4	61.9	1.9	140	5.5E-10	
		1.5	18.6	2.3	49.7		
		5.4	114.4	1.0	131.2		
		-2.4	51.1	1.9	113	4.6E-10	
		2.6	15.8	2.4	42		
	1998 Jun 2	5.4	100	1.0	115		
		-2.4	58.1	1.1	84.5	5.0E-10	
		2.6	43.3	1.19	72.2		
		5.4	111.8	1.0	136.6		
(147) L483-FIR.....	1998 Jan 3	-0.5	29.2	0.9	30.3	1.3E-10	
	1998 Jan 5	-0.5	26.9	0.9	27.5	1.2E-10	
	1998 Jan 18	-0.5	26.9	0.9	29.0	1.2E-10	
	1998 Feb 12	-0.5	24.5	0.9	24.7	1.0E-10	
	1998 Jun 2	-0.7	34.2	0.9	33.5	1.4E-10	
	1998 Jun 3	-0.7	33.4	0.9	32.1	1.3E-10	
	1998 Jun 14	-0.5	27.5	0.9	28.3	1.2E-10	
	1998 Jun 21	-0.5	20.6	0.9	20.8	8.7E-11	
	1999 Jan 27	0.3	5.5	0.9	6.6	2.8E-11	
(148) HH 80–81.....	1997 Dec 31	-72.0	12.4	2.5	35.4	1.7E-08	
		-60.7	1.0	4.0	3.5		
		-54.8	8.1	1.3	13.5		
		-42.3	1.6	3.1	4.4		
		10.2	22.9	1.0	25.7		
		13.8	2.5	1.2	3.3		
		-72.0	12.3	5.3	18.5	1.9E-08	
		-70.9	11.6	4.6	17.6		
		-59.9	1.6	2.5	5.1		
		-54.7	7.9	1.4	13.0		
	1998 Jan 5	-42.6	1.4	3.6	5.7		
		3.0	0.5	1.0	0.8		
		10.2	26.9	1.0	31.9		
		14.0	3.5	1.2	4.6		
		-72.3	6.1	3.6	9.1	1.6E-08	
		-70.9	6.3	3.0	9.5		
		-60.4	2.0	1.9	4.3		
		-54.7	7.1	1.3	12.0		
	1998 Jan 18	-42.1	1.2	4.5	5.2		
		10.8	22.7	1.3	34.3		
		14.0	5.8	1.7	10.9		

TABLE 2—Continued

Name (1)	Date (2)	Velocity (km s ⁻¹) (3)	T_A^* (K) (4)	ΔV (km s ⁻¹) (5)	$\int T_A^* dv$ (K km s ⁻¹) (6)	L_{H_2O} (L_\odot) (7)	Comments (8)
	1998 Jun 2	-61.2 -54.7 -51.5 -41.5 13.5	1.0 0.8 0.8 5.4 4.4	2.1 1.6 2.2 1.4 0.9	3.5 1.5 1.7 10.0 4.9	4.2E-09	
(149) IRAS 18265–1517	1997 Dec 31	-32.1 -9.7 19.7 1998 Jun 2 -34.8 -31.8 19.8 22.3	8.4 1.1 0.9 5.9 2.5 1.1 1.9	1.7 1.0 1.0 1.4 2.4 2.3 1.3	22.3 0.6 3.2 10.6 7.3 1.9 4.2	7.0E-09 6.6E-11	
(153) Serpens FIRS	1997 Dec 15 1998 Jan 5 1998 Jan 18 1998 Jun 2 1998 Jun 3 1998 Jun 14 1998 Jun 21 1998 Dec 14 1999 Jan 27	...	<0.06 <0.03 <0.06 9.0 24.3 9.0 15.4 24.0 9.2 21.6 24.0 9.2 21.4 23.7
(156) Serpens SMM 4	1998 Jan 5 1998 Jan 18 1998 Jun 2 1999 Jan 27	...	<0.03 <0.06 <0.09 3.3
(161) IRAS 18277–1516	1997 Dec 31 1998 Jun 2	-23.2 20.2 24.5 20.1 21.8	0.6 15.5 17.1 7.4 44.9	1.1 0.8 2.0 0.8 0.9	1.0 14.8 37.5 6.0 55.7	1.4E-10 1.7E-10	
(166) L723-FIR	1996 May 5 1998 Jan 3 1998 Jan 5 1998 Jan 18 1998 Jan 27 1998 Feb 12 1998 Jun 2 1998 Jun 14 1998 Jun 21 1998 Dec 14 1999 Jan 27	11.0 ...	2.7 <0.09 <0.2 <0.04 <0.04 <0.06 <0.12 <0.08 <0.12 11.7 11.7	1.7 ...	5.0 ...	3.0E-11 ...	
(173) IRAS 20050+2720	1997 Dec 27 1998 Jan 5 1998 Jan 11 1998 Jan 18 1998 Feb 3	-91.1 -91.1 -91.1 -90.9 -91.1	0.6 10.1 0.7 16.6 0.9 6.2 14.2 0.5 1.2 0.8 0.3 6.2	2.5 1.0 2.9 1.0 2.1 1.0 18.9 3.8 9.6 2.5 1.6 0.6 8.7	1.8 12.9 1.7 20.9 2.6 18.9 1.9 3.8E-10 9.6 2.7 0.6 15.1	4.8E-10 7.4E-10 7.1E-10 3.8E-10 6.1E-10	

TABLE 2—Continued

Name (1)	Date (2)	Velocity (km s ⁻¹) (3)	T_A^* (K) (4)	ΔV (km s ⁻¹) (5)	$\int T_A^* dv$ (K km s ⁻¹) (6)	L_{H_2O} (L_\odot) (7)	Comments (8)
	1998 Feb 12	-91.1 -37.2 -24.5 6.2	0.7 0.3 0.4 7.8	2.2 1.1 1.4 1.4	2.0 0.2 0.6 13.1	5.2E-10	
	1998 Jun 2	-91.0 -0.4 2.9 6.8	0.5 1.0 0.6 1.6	3.4 1.4 1.1 1.6	1.4 1.7 0.8 2.8	2.2E-10	
	1998 Jun 21	-91.1 7.3	0.5 0.6	2.8 1.6	1.3 1.1	7.9E-11	
	1998 Dec 8	-91.6 -1.3 0.9 7.0	0.6 0.9 3.1 0.35	1.9 1.3 1.0 2.0	1.1 1.2 3.5 0.8	2.2E-10	
	1998 Dec 14	-91.9 -1.3 0.9	0.6 1.0 3.9	2.6 1.3 1.0	1.1 1.0 4.9	2.3E-10	
	1999 Jan 27	-90.9 0.9 6.7	0.5 10 0.7	2.2 1.5 0.8	1.4 17.2 1.0	6.5E-10	
(174) S106 FIR.....	1997 Oct 8	-15.6 -11.8 0.6 3.0 4.7	9.1 6.7 1.0 0.45 0.45	1.4 1.1 1.1 1.4 1.2	17.7 8.3 1.5 0.5 0.6	6.9E-10	
	1997 Oct 18	-13.9 -12.1 -10.2 -0.7 2.2 6.0	6.9 3.5 7.0 0.38 1.4 0.5	1.5 4.3 1.1 1.6 1.2 2.6	9.6 5.1 8.5 0.6 2.1 1.3	6.6E-10	
	1997 Dec 23	-9.1 -6.9 4.9	3.7 2.1 1.0	2.0 1.1 1.1	7.9 2.7 1.5	2.9E-10	
	1997 Dec 30	-9.1 -7.2 4.9	2.6 1.7 0.8	2.0 1.0 1.0	5.3 3.3 1.3	2.4E-10	
	1998 Jan 5	-9.4 -7.2 4.9	3.4 2.0 0.7	1.9 1.1 1.2	7.0 2.6 1.9	2.8E-10	
	1998 Jan 11	-9.1 -7.2 4.9	3.4 2.0 0.7	1.9 1.1 1.2	7.0 2.6 1.9	2.8E-10	
	1998 Jan 18	-9.1 -7.2 4.9	2.8 1.3 0.5	2.0 1.4 0.8	6.1 1.9 0.6	2.1E-10	
	1998 Feb 3	-9.1 -7.2 4.9	2.9 2.0 0.6	1.8 1.1 1.3	5.6 1.9 1.1	2.1E-10	
	1998 Feb 12	-9.1 -7.2 5.2	3.3 1.1 0.5	1.7 3.0 1.2	6.6 1.5 0.7	2.1E-10	
	1998 Jun 2	-11.7 -9.2 2.4 5.2	0.7 2.1 1.7 0.9	2.0 1.6 1.2 1.1	1.2 4.1 2.6 1.5	2.3E-10	
	1998 Jun 21	-11.5 -9.3 2.4 3.8	0.5 1.3 1.0 0.9	1.7 1.8 1.5 2.2	0.9 3.1 1.2 1.9	1.7E-10	
	1999 Jan 27	-11.3 -9 2.6	0.73 0.6 0.53	1.5 2.3 1.5	1.2 1.8 0.9	9.4E-10	

TABLE 2—Continued

Name (1)	Date (2)	Velocity (km s ⁻¹) (3)	T_A^* (K) (4)	ΔV (km s ⁻¹) (5)	$\int T_A^* dv$ (K km s ⁻¹) (6)	L_{H_2O} (L_\odot) (7)	Comments (8)
(176) L1157-MM	1997 Dec 30	...	<0.04
	1998 Jan 5	...	<0.03
	1998 Jan 11	...	<0.04
	1998 Jan 18	...	<0.05
	1998 Feb 12	...	<0.05
	1998 Feb 18	...	<0.05
	1998 Jun 2	7.0	0.9	0.7	0.9	1.1E-11	
	1998 Jun 14	7.0	0.9	0.7	0.9	1.0E-11	
	1998 Jun 21	2.3	1.1	1.0	1.2	2.6E-11	
		7.1	0.8	0.7	0.8		
	1999 Jan 27	...	<0.8
(178) GF 9-2.....	2000 Apr 8	5.7	0.14	0.9	0.12	3.2E-13	
(189) IC 1396N.....	1996 May 5	-11.6	3.3	0.9	5.1	1.5E-09	
		1.5	9.2	1.5	8.8		
		3.2	8.9	3.1	16.3		
		12.1	5.0	1.1	9.7		
	1998 Jan 11	-8.9	2.1	1.6	4.1	4.3E-10	
		-3.3	2.2	1.8	4.8		
		1.3	0.9	1.4	1.9		
		9.4	0.4	0.9	0.7		
	1998 Jun 22	-8.8	2.5	1.9	5.5	1.0E-09	
		-3.0	11.1	1.3	18		
		5.3	2.1	0.9	3.8		
(190) LkH α 234.....	1996 May 5	-11.9	7.9	1.1	12.6	1.7E-09	
		-9.5	6.8	1.4	12.1		
	1998 Jan 11	-40.7	0.7	1.2	1.3	2.1E-09	rms = 32 mK
		-17.8	7.8	0.9	9.4		
		-10.3	7.2	1.6	12.6		
		-9.1	5.8	1.9	7.8		
		2.4	0.35	1.3	0.6		
	1998 Jun 3	-17.6	8.2	0.8	7.6	1.8E-09	
		-15.1	2.0	1.4	2.8		
		-13.5	2.4	1.2	3.1		
		-10.1	6.0	1.8	12.9		
	1998 Jun 22	-17.5	9.3	0.9	9.6	2.3E-09	
		-14.8	6.1	1.1	9.6		
		-10.0	7.2	1.6	15.0		
(192) S140-IRS.....	1998 Jun 22	-19.9	3.0	1.7	4.9	4.7E-10	
		-17.5	1.5	2.4	3.8		
(193) L1204A	1998 Jun 2	-20.9	21.8	1.2	32.5	3.6E-09	
		-18.2	15.6	1.5	28.4		
		-2.9	3.4	1.0	4.4		
	1998 Jun 14	-21.0	24.1	1.5	41.6	4.3E-09	
		-18.1	17.9	1.6	33.1		
		-3.1	3.9	1.0	4.0		
	1998 Jun 21	-20.7	1.6	1.8	3.2	9.9E-10	
		-18.2	7.0	1.4	11		
		-3.0	4.0	1.0	4.0		
(195) IRAS 22266+6845	1998 Jan 5	-1.3	4.1	0.9	4.3	1.2E-11	
	1998 Jun 2	...	<0.15
(198) L1251A	1998 Jan 5	...	<0.02
	1998 Jun 2	...	<0.13
	1999 Jan 27	-11.0	3.5	0.9	3.9	1.0E-11	
(199) L1251B	1999 Jan 5	9.2	2.1	0.9	2.8	7.5E-12	
	1998 Jun 2	2.4	31.7	3.2	34.7	2.1E-10	
		3.5	30	2.7	43.4		
	1999 Jan 27	2.2	2.6	1.1	2.89	1.2E-11	
		3.9	1.1	1.4	1.4		

TABLE 2—Continued

Name (1)	Date (2)	Velocity (km s ⁻¹) (3)	T_A^* (K) (4)	ΔV (km s ⁻¹) (5)	$\int T_A^* dv$ (K km s ⁻¹) (6)	L_{H_2O} (L_\odot) (7)	Comments (8)
(200) Cep A.....	1998 Jan 11	-28.0	1.5	3.0	4.4	3.3E-08	
		-20.5	90.3	2.2	211.5		
		-17.0	27.3	1.1	57.5		
		-14.6	54.2	1.2	71.6		
		-8.6	341.9	1.7	640.3		
		-1.6	2.0	2.3	4.9		
	1998 Jan 18	-20.0	91.0	2.5	229.5	4.0E-08	
		-16.9	38.1	2.7	66.0		
		-8.6	492.1	1.6	912.7		
		-1.3	3.8	1.3	7.8		
	1998 Feb 12	-27.5	2.2	3.1	8.6	4.4E-08	
		-20.8	159.7	1.1	202.1		
		-17.0	47.8	1.2	84.9		
		-14.6	96.0	2.7	236.5		
		-8.6	411.9	1.9	785.4		
		-1.3	2.4	2.4	7.9		
(200) Cep A.....	1998 Jun 22	-29.7	181.2	1.9	250.8	6.4E-08	
		-29.1	138.0	7.3	171.6		
		-26.4	146.8	3.4	260.5		
		-21.6	39.6	6.2	40.9		
		-20.2	109.7	1.3	157.3		
		-15.1	150.1	1.1	245.8		
		-10.0	364.8	0.1	368.5		
		-8.6	399.9	1.1	438.9		
		...	<0.09	
		...	<0.09	
(201) Cep E-MM.....	1997 Dec 30	-61.9	0.6	1.7	1.1	7.5E-11	
		-41.2	0.24	1.6	0.4		
		-61.8	1.0	1.5	1.7	6.1E-11	
		-61.8	1.0	1.6	1.8	6.4E-11	
		-61.7	1.4	1.8	3.7	1.3E-10	
		-61.7	2.6	2.1	3.9	4.5E-10	
		-59.3	6.4	1.1	8.7		
		-61.9	3.2	2.8	5.5	4.1E-10	
		-59.7	3.3	1.9	5.0		
		-38.3	0.8	0.8	1.0		
		-62.2	0.8	2.3	1.5	1.1E-10	
		-37.4	0.7	1.0	1.6		
		-37.9	0.8	1.0	1.2	4.3E-11	
		-37.9	0.7	0.7	0.2	7.2E-12	
	1999 Jan 27	...	<0.09	

^a Sum of L_{H_2O} from IRAS 4A (3.7E-11 L_\odot) and 4B (9.3E-11 L_\odot).^b Sum of L_{H_2O} from IRAS 4A (2.2E-11 L_\odot) and 4B (3.6E-11 L_\odot).

1990). The presence of H₂O masers was first reported by Wilking & Claussen (1987). Subsequent VLA observations (Wootten 1989; Terebey et al. 1992; Wootten 1993) revealed that maser emission is only associated with MM 1. Wootten (1993) showed that the northeast-southwest outflow may be followed through maser emission to within 100 AU of MM 1. Wootten et al. (2002) used proper motions observed with the VLBA to confirm this and trace the masers down to perhaps 1 AU from MM 1 itself. No maser has ever been found associated with MM 2.

Figures 20a and 20b show the strong maser emission from IRAS 16293–2422 with isotropic maser luminosity of an order of $\sim 10^{-10} L_\odot$. This is the most luminous maser emission in Class 0 sources. All of the detected emission lies around the ambient cloud velocity. Although this source displayed maser emission throughout the Nobeyama monitoring, the duration of each component seldom exceeds a

few months. For instance, examine the decay of the velocity component at ~ 3.5 km s⁻¹ in 1998 January (Figs. 20b and 20c).

4.3.10. L483-FIR

The source IRAS 18148–0440, first identified by Parker et al. (1988), in L483 is one of the early proposed Class 0 sources (AWB93). Recent VLA NH₃ line observations revealed the presence of the infall motion (Fuller & Wootten 2000), which had been suggested from the studies of spectral line shape (Myers et al. 1995; Mardones et al. 1997). L483-FIR is known to drive a well-collimated bipolar outflow (Parker et al. 1988; Parker, Padman, & Scott 1991; Fuller et al. 1995; Hatchell, Fuller, & Ladd 1999; Tafalla et al. 2000; Park et al. 2000). The characteristics of the highly collimated outflow together with the infall motion are common

TABLE 3
PARAMETERS OF H₂O MASERS DETECTED BY THE VLA

Name (1)	$\theta_{\text{maj}} \times \theta_{\text{min}}$ (arcsec) (2)	P.A. (deg) (3)	V_{LSR} (km s ⁻¹) (4)	Peak (Jy beam ⁻¹) (5)	rms (Jy beam ⁻¹) (6)	R.A. (B1950.0) (7)	Decl. (B1950.0) (8)
1996 Oct 15: VLA A							
(166) L723-FIR	0.094 × 0.084	-9.2	11.9	0.75	0.014	19 15 41.852	19 06 50.336
1996 Dec 30: VLA A							
(101) VLA 1623	0.18 × 0.092	-6.2	13.2	0.28	0.012	16 23 24.8625	-24 17 46.210
1998 Oct 24: VLA CnB							
(6) RNO 15-FIR	1.0 × 0.4	84.5	3.0	2.4	0.34	03 24 35.74	30 02 28.54
(16) B1-IRS	0.9 × 0.5	82.2	15.8	3.3	0.34	03 30 10.122	30 57 29.80
(28) T Tau South	0.9 × 0.5	78.5	5.9	2.8	0.33	04 19 04.241	19 25 04.05
1999 Feb 12: VLA DnC							
(96) GSS 30-IRS	5.7 × 1.7	51.5	-14.2	19.6	1.0	16 23 19.956	-24 16 20.10
(147) L483 FIR	4.2 × 1.5	73.6	0.3	18.9	1.8	18 14 50.700	-04 40 49.90
(151) S68N	4.0 × 1.4	78.0	11.5	5.6	0.27	18 27 15.753	01 14 39.07
(156) Serpens SMM 4	4.2 × 1.4	71.8	-5.3	2.0	0.08	18 27 24.123	01 11 06.53
			3.0	1.0	0.08	18 27 24.123	01 11 06.53
(166) L723 FIR	3.8 × 1.3	71.3	11.8	75.1	0.33	19 15 41.800	19 06 49.90
(173) IRAS 20050+2720 MMS 1	3.9 × 1.2	68.9	-92.0	0.61	0.16	20 05 01.960	27 20 15.30
			1.0	3.9	0.15	20 05 01.622	27 20 15.90
			4.6	0.3	0.15	20 05 01.622	27 20 15.90
			6.9	0.63	0.15	20 05 01.622	27 20 15.90
(174) S106 FIR	3.7 × 1.3	74.7	-11.2	8.1	0.23	20 25 32.535	37 12 50.80
			-9.2	4.9	0.23	20 25 32.535	37 12 50.80
			-3.6	2.6	0.23	20 25 32.535	37 12 50.80
			2.6	2.7	0.23	20 25 32.535	37 12 50.80
(176) L1157-MM	3.1 × 2.5	60.9	3.0	0.29	0.08	20 38 39.247	67 51 35.40
(201) Cep E-MM	3.6 × 1.3	78.3	-61.8	0.38	0.07	23 01 09.807	61 26 15.70
1999 Feb 25: VLA DnC							
(9) NGC 1333 IRAS 2A	3.1 × 2.6	-79.3	-16.8	4.0	0.24	03 25 50.041	31 04 18.10
			7.2	33.9	0.24	03 25 50.041	31 04 18.10
(10) NGC 1333 SVS 13A	3.1 × 2.7	-88.3	6.3	112	14	03 25 58.175	31 05 45.30
			12.8	506	14	03 25 58.198	31 05 45.60
(11) NGC 1333 IRAS 4A	3.1 × 2.7	-82.3	10.9	39.3	0.26	03 26 04.897	31 03 13.90
			12.2	18.7	0.26	03 26 04.897	31 03 13.90
(12) NGC 1333 IRAS 4B	3.1 × 2.7	-82.3	-5.9	25.3	0.26	03 26 06.461	31 02 50.20
			1.3	11.9	0.26	03 26 06.461	31 02 50.20
			14.2	4.3	0.26	03 26 06.461	31 02 50.20
			15.5	4.4	0.26	03 26 06.461	31 02 50.20
			18.8	44.8	0.26	03 26 06.461	31 02 50.20
(16) B1-IRS	3.1 × 2.6	-74.2	13.5	1.1	0.13	03 30 10.806	30 57 51.00
			15.8	14.0	0.13	03 30 10.806	30 57 51.00
(66) IRAS 05375-0731	2.9 × 2.3	-83.5	0.3	0.24	0.14	05 37 31.020	-07 32 00.60
(68) NGC 2024 FIR 5	3.0 × 2.3	-75.0	3.3	1.9	0.13	05 39 13.690	-01 57 25.90
			16.1	26.4	0.13	05 39 13.690	-01 57 25.90

NOTE.—Units of right ascension are hours, minutes, and seconds, and units of declination are degrees, arcminutes, and arcseconds.

in Class 0 sources. However, Park et al. (2000) pointed out, from an HCO⁺ $J = 1-0$ line image taken by the BIMA array, that there have been at least three mass-loss events to date. Tafalla et al. (2000) argued that this source is more evolved than other Class 0 sources and concluded that it is in transition to become a Class I object. This is because the outflow velocity is low and because of the lack of emission from shock-excited molecules and the presence of a near-IR

scattering nebula that are more common in more evolved outflows in Class I.

Figure 21a presents the maser emission toward L483-FIR: the emission was seen at $V_{\text{LSR}} \sim -0.5$ km s⁻¹ throughout the Nobeyama observations. The emission is blueshifted with respect to the cloud velocity and was exceptionally stable compared with maser emission from the other Class 0 sources: a clear velocity shift cannot be seen throughout the

TABLE 4
PROPERTIES OF SAMPLES IN THE 45 m TELESCOPE H₂O MASER SURVEY

Name (1)	Alternative Name (2)	D (pc) (3)	L_{bol} (L_{\odot}) (4)	M_{env} (M_{\odot}) (5)	$T_{\text{bol}}^{\text{a}}$ (K) (6)	F_{CO} ($M_{\odot} \text{ km s}^{-1} \text{ yr}^{-1}$) (7)	L_{CO} (L_{\odot}) (8)	$S_{3.5 \text{ cm}}$ (mJy) (9)	$L_{\text{H}_2\text{O,min}}$ (L_{\odot}) (10)	$L_{\text{H}_2\text{O,max}}$ (L_{\odot}) (11)	Evolutionary Class (13)	Reference ^b (14)	
(1) L1287.....	00338+6312	850	1100	...	3.8E-4	0.5	...	0.49	3.0E-10	6.2E-10	I	2, 6, 38, 144	
(3) L1448-IRS 2		300	6.0	0.9	55	1.0E-4	0.3	0	141	
(4) L1448-IRS 3	L1448N	300	11	2.3	70	1.0E-4	0.32	0.92	0	7, 13, 22, 28, 70, 82, 108, 141, 151	
(5) L1448C	L1448-MM	300	9.0	1.4	55	1.7E-4	0.52	0.062	0	7, 22, 24, 82, 108, 141, 151	
(6) RNO 15-FIR	03245+3002	350	10	12	71	1.1E-6	0.02	0.24	0.12	1.4E-11	0 or I	37, 75	
(9) NGC 1333 IRAS 2		~17	0.35~1.7	41	2.4E-5	0.016	0.06	0.25	2.3E-12	2.5E-11	0	63, 70, 97	
(10) NGC 1333 SSV 13A	HH 12	220	7.0	0.13~2.7	30	1.1E-5	0.0049	0.26	0.45	2.6E-11	5.8E-10	0	12, 63, 70, 97, 99, 101
(11) NGC 1333 IRAS 4A		220	14	1.5~7.0	34	1.9E-5	0.012	0.36	0.49	2.2E-11	3.7E-11	0	63, 70, 97
(12) NGC 1333 IRAS 4B		220	14	0.36~2.7	36	...	0.07	<0.10	3.6E-11	9.3E-11	0	63, 70, 97	
(13) NGC 1333 IRAS 7	HH 6-VLA	220	9.0	0.06~0.35	...	3.1E-5	0.016	0.48	0.83	0	50, 63, 97, 106
(15)	03282+3035	300	1.5	1.4	23	6.8E-5	0.09	0	22, 82	
(16) BI-IRS	03301+3057	300	2.2	1.5	25	9.0E-6	0.01	...	1.3E-11	8.6E-11	0	53	
(17) HH 211-MM		315	5.0	1.5	30	1.8E-4	0.28	0	47, 82	
(18) B5-IRS	03445+2234	300	9.4	~0.35	...	4.1E-5	0.08	1	15, 22, 82, 103, 124, 132	
(19) L148-9-IRS	04016+2610	140	3.6	1.0	238	5.2E-6	...	0.26	0.34	...	1	7, 72, 80, 84, 103, 108, 149	
(21) L149.5	04108+2803.B	140	0.7	0.03	205	<1.6E-6	1	22, 103, 124	
(22)	04113+2758	140	2.8	0.0036~0.4	606	1	82, 155	
(23)	04158+2805	140	0.2	0.05	528	<2.3E-6	1	22	
(24)	04166+2706	140	0.4	0.2	139	3.1E-6	0 or I	22	
(25)	04169+2702	140	0.76	0.2	170	5.7E-6	0.01	1	22, 87	
(26)	0418+2655	140	0.5	<0.05	278	2.2E-6	1	22	
(27)	04181+2654	140	0.7	<0.06	346	<1.4E-6	1	22	
(28) T Tau South	04190+1924	140	15	0.02	501	1.7E-4	0.17	4.3~5.8	1	24, 77, 80, 90, 101, 110,	
(29) IRAM 04191+1522		140	0.15	0.5	18	1.5E-5	0.02	...	0.14	...	0	1	
(31)	04239+2436	140	1.48	0.03	236	0.12	1	30, 72, 101	
(32) DG Tau	04240+2559	140	8.4	0.03	1440	7.6E-6	...	1.2	II	61, 70, 80, 101, 110	
(35) L1524 (HH 6-10)	04263+2426	140	6.98	0.9	409	4.5E-6	...	0.8	0.60	...	1	7, 21, 84	
(36) HL Tau	04287+1807	140	6.0	0.059	576	1.6E-5	0.0015	0.25	1	7, 70, 72, 78, 108, 110, 139, 155	
(37) L1551-NE	04289+1802	140	3.9	0.04~0.15	75	1.5E-5	1	80, 101, 155	
(39) TMC 2A	04292+2422	140	1.2	...	910	1	84	
(40)	04295+2251	140	0.6	<0.07	447	<1.8E-6	1	22, 80	
(41) G+G Tau	04296+1725	140	2.3	0.0 ^e	621	II	59, 110	
(43) L1536	04302+2247	140	0.33	0.05	202	3.1E-6	...	0.14	1	22, 72	
(42) L1551-IRS 5	04287+1801	140	21	0.18~0.28	97	1.1E-3	2.1	3.5~4.3	1.48	...	1	7, 24, 44, 70, 71, 76, 80, 98, 101, 105,	
(44)	04320+1746	140	0.3	...	321	III	108, 114, 155	
(45) TMR-1	04361+2547	140	3.8	0.15	144	6.1E-6	0.01	...	0.14	...	1	22, 72	
(46) TMC A	04365+2535	140	2.4	0.2	172	1.6E-5	0.02	1	22, 26, 84, 87, 103, 120	
(47) L1527	04368+2557	140	1.6	0.023~0.4	59	7.9E-6	0.01	0 or I	22, 30, 103, 120, 155	
(48) TMC 1	04381+2540	140	0.7	0.05	139	5.7E-6	0.01	1	22, 26, 84	
(49) TMC 1C	04385+2550	140	>0.4	0.007	636	1	82	
(50) L1513	04489+3032	140	0.3	<0.02	399	<1.1E-6	1	22	
(55) HH 114-MMS	05115+0707	460	26.3	5.5	0.25	...	0	31, 100	
(56) R NO 40-IRS	05173-0555	460	17	~3.0~9.0	0.12	0 or I	17, 46, 55, 66	

TABLE 4—Continued

Name (1)	Alternative Name (2)	D (pc) (3)	L_{bol} (L_{\odot}) (4)	M_{env} (M_{\odot}) (5)	$T_{\text{bol}}^{\text{a}}$ (K) (6)	F_{CO} ($M_{\odot} \text{ km s}^{-1} \text{ yr}^{-1}$) (7)	L_{CO} (L_{\odot}) (8)	$S_{6 \text{ cm}}$ (mJy) (9)	$L_{\text{H}_2\text{O},\text{min}}$ (L_{\odot}) (10)	$L_{\text{H}_2\text{O},\text{max}}$ (L_{\odot}) (11)	Evolutionary Class (12)	Reference ^b (14)
(57) RNO 43-MM.....	05295+1247	460	8.0	0.6	36	1.2E-3	0.67	0.24	0.42	...	0 or I	3, 7, 20, 24, 149
(58) Orion A West.....	05302-0537	450	40	0.86	2.3E-10	2.5E-10	1	75, 125, 145
(59) OMC-3-MMS 6.....	450	<60	12	~30	0.15	0	32, 91
(60) OMC-3-MMS 9.....	450	<94	10	...	1.2E-4	...	0.79	10, 32, 91
(61) OMC2-FIR 4.....	450	0.64	32, 91
(62) HH 34.....	460	28	0.42	...	4.2E-5	...	0.16	I ^c	29, 92, 100
(63) HH 1-2 MMS 3.....	05339-0647	440	70	0.8	...	2.4E-5	0.03	1.17	1.2	2.9E-11	...	0 or I
(64) L1641 North.....	05338-0624	480	144	1.9	52	9.0E-4	...	0.6	0.48	3, 4, 74, 108, 138
(65) HH 4-255.....	05369-0728	480	26	4.0E-4	0.12	0.32	0.43	3, 7, 39
(66) L1641-S3 MMS 1.....	05375-0731	460	67	0.047	0.017	1.2E-11	3.1E-11	1
(68) NGC 2024 FIR 5.....	415	~10	15	29	2.6E-11	7.7E-11	0
(69) NGC 2024 FIR 6.....	415	~15	6	~30	27, 95, 73
(70) HH 24-MMS.....	450	5.0	4.0	20	0.2	0	3, 23, 101, 69
(71) HH 212.....	05413-0104	460	12	0.2	24	1.4E-11	2.3E-10	0 or I	33, 66, 148, 149, 140
(72) B354.....	05417+0907	460	15	~4.0	...	1.0E-5	...	0.2	82, 84, 103, 123
(73) L1630-SSV 63E.....	05435-0014	450	21	2.9	0.36	1	43, 3, 69
(74) HH 25-MMS.....	05435-0014	450	6.0	0.5	34	0.16	0.25	...	0 or I	3, 23, 43, 69
(75) HH 26-IR.....	05435-0015	450	...	1.5	0.14	1	43, 69
(76) NGC 2071 IRS 1.....	05445+0020	450	401	...	108	9.1E-3	24	7.9	4.52	2.0E-09	3.7E-09	B?
(77) NGC 2071 North.....	05451+0037	450	40	0.03	2.3E-11	...	1
(78) HH 111-VLA.....	05491+0247	460	25	0.49	...	5.0E-5	0.055	...	0.95	0
(79) RNO 73-MM.....	06308+0402	1600	3900	2.3E-4	0.07	112
(80) NGC 2264G VLA2.....	06384+0958	800	12	2	25	2.7E-4	0.96	0.27	0.34	0
(84) S287B.....	06571-0441	1400	440	<0.18	0.16	Ae/Be
(86) L1641.....	06572-0742	1100	1400	4.41	4.12	B2-B3 ZAMS
(89) HH 120.....	08076-3556	400	8.9	2.3	74	18
(92) L1719B.....	16191-1936	160	1.8	<0.15	701	4.0E-7	58
(93) ROX 6.....	EL 13/SR 4	160	3.1	4.7E-3 ^d	2438
(96) GSS 30-IRS 1.....	160	26	0.06	174	0.56	...	1.2E-12	4.2E-11	1
(99) ROX 10B.....	160	15.8	9.8E-3 ^d	4786	22, 68, 83, 121, 147
(101) VLA 1623.....	160	1.0	0.6	<35	5.0E-5	0.075	0.39-0.58	86
(108) SR 24.....	HH 224	160	21.3	...	4605	0
(110) WL 12.....	160	4.1	0.03	366	6.0E-6	0.02	2, 7, 22, 24, 68, 70, 146, 152
(114) GY 2/3.....	160	92
(115) EL 29.....	160	41	0.09	409	2.0E-6	0.01	0.3	22, 83, 111
(120) GY 236.....	160	83
(122) WL 6.....	160	1.02	<0.02	467	2.5E-6	83
(123) IRS 43.....	160	10.1	0.05	229	1.5E-5	0.02	3.26	22, 83
(124) YLW 16A.....	160	13	0.05	157	3.4E-6	0.05	0.82	...	5.2E-13	22, 68, 108, 111, 123, 124, 137
(125) IRS 46.....	160	0.8	...	633	22, 83, 111
(126) GY 284.....	160	83
(128) IRS 48.....	160	11.1	0.06	611	3.0E-5	0.04	22, 83
(129) IRS 51/YLW 45.....	16246-2436	160	1.3	0.06	628	5.5E-6	22, 83
(130) ROX 30C.....	160	0.9	6.0E-3 ^d	4169	II or III

TABLE 4—Continued

Name (1)	Alternative Name (2)	D (pc) (3)	L_{bol} (L_{\odot}) (4)	M_{env} (M_{\odot}) (5)	$T_{\text{bol}}^{\text{a}}$ (K) (6)	F_{CO} ($M_{\odot} \text{ km s}^{-1} \text{ yr}^{-1}$) (7)	L_{CO} (L_{\odot}) (8)	$S_{6 \text{ cm}}$ (mJy) (9)	$L_{\text{H}_2\text{O,min}}$ (L_{\odot}) (10)	$L_{\text{H}_2\text{O,max}}$ (L_{\odot}) (11)	Evolutionary Class (12)	Reference ^b (14)
(131) IRS 55	ROX 31	160	0.9	2179	1	86
(135) ROX 34	SR 13	160	0.8	9.0E-3 ^d	1839	II	86
(136) ROX 44		160	2.3	1.58E-02 ^d	2354	II	22
(137)	16285-2355	160	1.4	0.3	580	6.3E-6	0.01	1	22
(138) IRS 67	L1689S	160	2.5	0.07	454	1.0E-5	0.01	1	22
(139) ρ Oph East	16293-2422	160	2.3	43	3.2E-4	0.43	2.95	...	1.6E-10	5.5E-10	0	7, 22, 24, 70, 108, 123, 143
(140) L43-RNO 91	16316-1540	170	3.7	8.3	79	5.0E-7	I or II	19, 66, 84, 103
(141) L260	16422-0929	160	0.66	0.03	...	3.0E-7	1	22, 82
(147) L48 FIR	18148-0440	200	9.0	<0.3	48	1.5E-5	0.02	0.20	0.31	2.8E-11	1.4E-10	0 or I
(148) HH 80/81	18162-2048	1700	16602	32	4.2E-09	1.9E-08	...
(149) L379-IRS 1	18265-1517	2000	8200 ± 900	6.6E-09	7.0E-08	B0-5 ZAMS?	60
(150) HH 106/107	18269+0116	310	6.6	0.065	92
(151) S68N	...	310	6.0	1.7	40	2.0E-4 ^c	0.11	3.6	0	36, 56, 122, 142
(152) FU Orionis	...	310	<8	0.75	56
(153) Serpens FIRs 1	SMM 1	310	12.3	51	3.0E-4 ^f	0.6	2.7	...	1.3E-10	3.3E-10	0	34, 36, 56, 57, 113, 122, 128
(154) Serpens SMM 5	IRS 53	310	>0.8	0.52	25, 56, 122
(156) Serpens SMM 4	...	310	9.0	5.0	35	3.0E-4 ^f	0.6	...	6.5E-12	...	0	36, 56, 57, 122
(157) Serpens SMM 6	SVS 20	310	>0.6	0.48	25, 56, 122
(159) Serpens SMM 3	...	310	8.0	3.5	38	3.0E-4 ^f	0.6	0	36, 56, 57, 122
(160) Serpens SMM 2	...	310	6.0	0.82	38	3.0E-4 ^f	0.6	0	36, 56, 57, 122
(162) HH 108-IRS	18331-0035	310	<8.0	4.5	54	30
(163) HH 108-MMS	...	310	1.0	3.6	0	30
(164) HH 100-IR	...	130	12.0	0.027	373	Ae/Be	92
(165) R CTA	18585-3701	130	92	...	736	5.0E-5	0.44	11.0	108
(166) L723 FIR	19156+1906	300	3.0	0.6	39	3.7E-4	0.04	0.28	0.36	1.5E-11	4.6E-11	0
(167) L673-RNO 109	19180+1116	300	1.0	9
(168) L673A	19180+1114	300	0.4	...	55	4.3E-5	0.012	9
(169) L778	19244+2352	250	0.57	1.9E-6	0.0011	16, 84
(170) B335-IRS	19345+0727	250	3.0	0.8	37	(1.2~3.6)E-5	0.019	<0.16	0.21	3, 7, 24, 22, 54, 104
(171) HH 165	1548C27	900	52	0.45	92
(173) MMS 1	20050+2720	700	305	17.1	62	5.0E-3	16	14, 30, 136, 138
(174) S106 FIR	...	600	<1080	4.2	>24	<1.7E-6	<0.1	1.7E-10	9.4E-10	0 or I
(175) L1152	20353+6742	440	3.3	0.05	...	4.7E-6	41, 42, 94
(176) L1157-MM	20386+6751	440	11	0.5	44	2.4E-5	0.03	0.15	0.18	1.0E-11	2.6E-11	0 or I
(177) L1082C	20503+6006	440	0.6	<7.2E-6	0.15	75, 118, 130, 153
(178) GF 9-2	...	200	0.3	0.5	<20	<0.1	3.2E-13	...	1
(179) L1082A	20520+6003	440	3.0	0.09	...	2.5E-5	0.02	0	133, 134
(180) L1082B	20520+5958	440	0.8	0.02	...	2.8E-6	1	84, 103
(181) L11228	20582+7724	100	28	0.04	...	0.15	...	1	22
(182) L1174	20597+6800	440	2.4	0.2	...	2.8E-5	0.03	48
(184) L1172-D	21017+6742	440	0.95	6.6E-6	0.0036	1	22, 84, 103
(187) B361	21106+4712	350	4.7	0.4	...	1.5E-5	0.02	0.09	0.06	...	1	75, 82
(189) IC 1396N	21391+5802	750	235	8.3	...	4.0E-5	0.02	...	4.3E-10	1.5E-09	...	89, 107, 116, 125
(190) LkH α 234	21418+6552	1000	~1300	1.7E-09	2.3E-09	...	125

TABLE 4—Continued

Name (1)	Alternative Name (2)	D (pc) (3)	L_{bol} (L_{\odot}) (4)	M_{env} (M_{\odot}) (5)	$T_{\text{bol}}^{\text{a}}$ (K) (6)	F_{CO} ($M_{\odot} \text{ km s}^{-1} \text{ yr}^{-1}$) (7)	L_{CO} (L_{\odot}) (8)	$S_{6 \text{ cm}}$ (mJy) (9)	$S_{3.5 \text{ cm}}$ (mJy) (10)	$L_{\text{H}_2\text{O,max}}$ (L_{\odot}) (11)	Evolutionary Class (13)	Reference ^b (14)
(192) SL40-JRS.....	22176+6317	910	337	...	72	5.3E-3	8.4	5.2	...	4.7E-10
(193) L1204A.....	22198+6336	900	<35	7.89	9.9E-10	4.3E-09	...
(195) L1221.....	22266+6845	200	2.7	8.1E-5	0.03	1.2E-11	...	131
(196) L1203.....	22267+6244	450	<110	0.40	0.75
(197) L1206.....	22272+6358	900	710	4.5E-5	0.01	116
(198) L1251A.....	22343+7501	200	9.3	...	108	...	0.006	0.28	0.31	1.0E-11	...	1 or II
(199) L1251B.....	22376+7455	200	14	...	91	5.0E-5	...	0.84	1.34	7.5E-12	2.1E-10	3, 4, 127
(200) Cep A HW2.....	22543+6145	700	13700	...	35	45.0	...	3.3E-08	6.4E-08	B0.5ZAMS
(201) Cep E-MM.....	23011+6126	730	17	...	40	1.2E-5	1.9	7.2E-12	4.5E-10	0
(202) Cep C.....	23037+6123	750	129	...	57	138
(203) L1262.....	23238+7401	200	2.3	0.09	104	1.1E-5	0.01	0.21	0.33	1
												3, 4, 22, 103, 124

^a References for low-mass YSOs are Chen et al. 1995, 1997; Mardones et al. 1997; AWB00; the reference for high-mass YSOs is Williams & Myers 1999.^b References for cols. (3), (4), (5), (7)–(10), and (13).^c No circumstellar envelope, only a circumbinary disk exists.^d Mass estimated from 1.3 mm continuum emission, which is mass of the circumstellar disks rather than M_{env} (Nürnberger et al. 1998).^e Since individual outflow parameters have not been revealed as a result of the severe contamination, the typical value reported in Davis et al. 1999 is given.

- REFERENCES.—(1) André, Motte, & Bacmann 1999. (2) AWB93. (3) Anglada et al. 1998. (4) Anglada et al. 1997. (5) Anglada et al. 1992. (8) Anglada et al. 1989. (9) Armstrong & Weintraub 1989. (10) Aso et al. 2000. (11) Avery, Hayashi, & White 1990. (12) Bachiller et al. 1995c. (15) Bally & Alten 1996. (16) Beichman et al. 1986. (17) Beltrán et al. 2002. (18) Beltrán et al. 2001. (19) Bene, Richer, & Padman 1996. (21) Bieging, Cohen, & Schwartz 1984. (22) Bontemps et al. 1996. (23) Bontemps, André, & Ward-Thompson 1995. (24) Cabrit & Bertout 1992. (25) Casali et al. 1993. (26) Chandren et al. 1996. (27) Chernin 1996. (28) Chernin & Masson 1995. (29) Chernin & Masson 1995. (30) Chini et al. 2001. (31) Chini et al. 1997a. (32) Chini et al. 1997b. (33) Claussen et al. 1998. (34) Curiel et al. 1993. (35) Davidson 1987. (36) Davis et al. 1999. (37) Davis et al. 1997. (38) Fiebig et al. 1997. (39) Fukui et al. 1989. (40) Fuller & Wootten 2000. (41) Furuya et al. 2000. (42) Furuya et al. 1999. (43) Gibb 1999. (44) Giovanardi et al. 2000. (45) Gómez et al. 1994. (46) Gregersen et al. 2000. (47) Gueth & Guilloteau 1999. (48) Haikala & Laureij 1989. (49) Hatchell et al. 1999. (50) Henkel, Haschick, & Güsten 1986. (51) Henning & Launhardt 1998. (52) Hirano et al. 1998. (53) Hirano et al. 1997. (54) Hirano et al. 1992. (55) Hoardapp & Ladd 1995. (56) Hurt & Barsony 1996. (57) Hurt et al. 1996. (58) Iwata et al. 1988. (59) Kawabe et al. 1993. (60) Kelly & MacDonald 1996. (61) Kitamura, Kawabe, & Saito 1996. (62) Kitamura et al. 1990. (63) Knee & Sandell 2000. (64) Lada & Fisch 1996. (65) Ladd & Hodapp 1997. (66) Lee et al. 2000. (67) Lefloch et al. 1996. (68) Leous et al. 1991. (69) Lis, Menten, & Zylka 1999. (70) Looney et al. 2000. (71) Looney, Mundy, & Welch 1997. (72) Lucas, Blundell, & Roche 2000. (73) McMullin, Mundy, & Blake 1994a. (74) Mangum et al. 1999. (75) Mehah et al. 1998. (76) Momose et al. 1998. (77) Momose et al. 1996. (78) Monin, Pudritz, & Lazareff 1996. (79) Morgan, Snell, & Strom 1990. (80) Moriarty-Schieven et al. 1994. (81) Moro-Martín et al. 1999. (82) Mothé & André 2001. (83) Mothé et al. 1998. (84) Myers et al. 1988. (85) Noriega-Crespo, Garnavich, & Molinarri 1998. (86) Nürnberger et al. 1998. (87) Ohashi et al. 1997. (88) Park et al. 2000. (89) Patel et al. 2000. (90) Ray et al. 1997. (91) Reipurth, Rodriguez, & Chini 1999. (92) Reipurth et al. 1993. (93) Reipurth & Olberg 1991. (94) Richer 1990. (95) Richer 1991. (96) Rodriguez et al. 2000. (97) Rodriguez et al. 1999. (98) Rodriguez et al. 1998. (99) Rodriguez et al. 1997. (100) Rodriguez & Reipurth 1996. (101) Rodriguez & Reipurth 1994. (102) Rodriguez et al. 1990. (103) Rodriguez et al. 1989. (104) Saito et al. 1999. (105) Saito et al. 1996. (106) Sandell & Knee 2001. (107) Saraceno et al. 1996b. (108) Saraceno et al. 1996a. (109) Saito & Fukui 1989. (110) Schuster et al. 1993. (111) Sekimoto et al. 1997. (112) Snell, Dickman, & Huang 1990. (113) Snell & Bally 1986. (114) Snell, Loren, & Plambeck 1980. (115) Stanke, McCaughan, & Zinnecker 2000. (116) Sugitani et al. 1989. (117) Tafalla et al. 2000. (118) Tafalla & Bachiller 1995. (119) Tafalla et al. 1993. (120) Tamura et al. 1996. (121) Tamura et al. 1992. (124) Terebey et al. 1989. (125) Tofani et al. 1995. (126) Torres et al. 1998b. (127) Torrelles et al. 1998a. (128) Torrelles et al. 1985. (129) Torrelles et al. 1992. (131) Umemoto et al. 1991. (132) Velusamy & Langer 1998. (133) Wiesemeyer et al. 1999. (134) Wiesemeyer et al. 1997b. (135) Wilking & Claussen 1987. (136) Williams & Myers 1999. (138) Wilner, Ho, & Rodriguez 1996. (140) Wiseman et al. 2001. (141) Wolf-Chase, Barsony, & O'Linger 2000. (142) Wolf-Chase et al. 1998. (143) Wootten 1989. (144) Yang et al. 1991. (145) Yu et al. 2000. (146) Yu & Chernin 1997. (147) Zhang et al. 1997. (148) Zinnecker, McCaughan, & Rayner 1998. (149) Zinnecker et al. 1991. (150) Anglada et al. 1992. (151) Currie et al. 1990. (152) Dent et al. 1995. (153) Gueth et al. 1996. (154) Torrelles et al. 1996. (155) Saito et al. 2001.

monitoring. From VLA DnC array observations, we found that the maser emission is associated with the *IRAS* source.

4.3.11. Serpens Star-forming Region

The Serpens star-forming region lies in the extended molecular cloud at $\sim 7'$ west of the high-mass star-forming region of S68 (Loren, Evans, & Knapp 1979); this region was originally mapped in the near-infrared (NIR) band (Strom et al. 1976) and in the FIR band (Nordh et al. 1982). The Serpens region is known to be an active site of low- and intermediate-mass star formation showing a remarkably high stellar density and high star formation efficiency (Eiroa & Casali 1992). Millimeter continuum emission maps revealed that there exist at least six cold dust continuum peaks and most of them lack NIR counterparts (Casali, Eiroa, & Duncan 1993). Subsequent multitransition H₂CO line studies of these continuum peaks, FIRS 1, SMM 2, SMM 3, SMM 4, and S68N, showed the presence of high-temperature gas, suggesting the presence of central heating sources (Hurt, Barsony, & Wootten 1996). Using the HIRES data, Hurt & Barsony (1996) found that all five sources studied by the H₂CO lines share the defining characteristics of Class 0 protostars. Addressing the outflow activity in this region, CO $J = 2-1$ maps obtained with the JCMT (White, Casali, & Eiroa 1995; Davis et al. 1999) showed a number of high-velocity CO lobes that extend radially outward from the clusters of submillimeter sources, although identification of each driving source was hampered by the severe contamination.

S68N (Serpens SMM 9).—This source was found by 1.3 mm continuum emission observations (Eiroa & Casali 1992; Casali et al. 1993; McMullin et al. 1994b), and there is no clear *IRAS* counterpart (Harvey, Wilking, & Joy 1984; Zhang et al. 1988; McMullin et al. 1994), suggesting that S68N is a Class 0 source (Hurt & Barsony 1996). A compact (~ 0.12 pc) molecular outflow was found by interferometric CS $J = 2-1$ line observations (Wolf-Chase et al. 1998; Testi et al. 2000). Wolf-Chase et al. (1998) revealed that its outflow momentum flux ($\sim 2 \times 10^{-4} M_{\odot} \text{ km s}^{-1} \text{ yr}^{-1}$) is comparable to that of the highest values among Class 0 sources. From VLA observations, A. Wootten (1995; private communication) found that H₂O masers are located at the center of the outflow, coincident with the submillimeter source.

S68N did not show H₂O maser activity in the period from 1998 January to 1999 January. In 1999 February, we detected emission at $V_{\text{LSR}} = 11.5 \text{ km s}^{-1}$ with the VLA DnC array observations (Fig. 25), just 16 days after the negative detection with the 45 m telescope. The velocity of the emission was redshifted with respect to the ambient cloud velocity and is slightly different from the previous detection by A. Wootten (1995, private communication; $V_{\text{LSR}} = 8.5$ and 12.4 km s^{-1}); however, the position of the masers was coincident with the previous observations.

Serpens FIRS 1 (Serpens SMM 1).—The most luminous source in this field, the Class 0 object FIRS 1 (Harvey et al. 1984) is the driving source of highly collimated, nonthermal radio jets (Curiel et al. 1993), the large-scale molecular outflow (White et al. 1995), and the Herbig-Haro object (HH 460; Torrelles et al. 1992; White et al. 1995; Testi et al. 2000). During our monitoring with the 45 m telescope, Serpens FIRS 1 displayed its maser activity only in 1998 June (Fig. 26a). The detected profiles represent two velocity components. One narrow velocity component around $V_{\text{LSR}} = 9 \text{ km s}^{-1}$ is almost at the ambient cloud velocity,

while the other component, which appears to be a superposition of several velocity components, is redshifted with respect to the systemic velocity.

Serpens SMM 4.—Maser emission from the Class 0 source Serpens SMM 4 was newly detected with the 45 m telescope in 1999 January (Fig. 27a). The maser emission is blueshifted with respect to the ambient cloud velocity. Subsequent VLA observations, carried out only 16 days after the Nobeyama detection, revealed that this source showed a second component at $V_{\text{LSR}} = -5.3 \text{ km s}^{-1}$ (Fig. 27b). Both components are blueshifted with respect to the ambient cloud velocity.

4.3.12. L723-FIR

L723 is known to show a quadrupolar molecular outflow (Hayashi, Hasegawa, & Kaifu 1991). At the center of the outflow, two radio continuum sources were found by VLA observations at 3.6 cm, separated by $15''$ (4500 AU in projection; Anglada et al. 1991). The northeastern source was also detected at FIR, submillimeter, and millimeter wavelengths (Cabrit & André 1991; Reipurth et al. 1993). From these flux measurements, the northeastern source was identified as “Class 0,” and its bolometric luminosity was estimated to be $\sim 3 L_{\odot}$ (Davidson 1987). Subsequent higher resolution VLA observations revealed that the northeastern radio continuum source is probably a thermal radio jet driving the larger pair of CO outflow lobes (Anglada et al. 1996).

Figure 28a presents a series of H₂O maser spectra obtained with the 45 m telescope. H₂O maser emission from L723 was first detected by Claussen et al. (1996) using the Haystack 37 m telescope during the process of publishing their supplement paper. We confirmed that this source shows maser activity at least in 1996 May and October and in the period from 1998 December to 1999 February (Figs. 28a–28c). On the other hand, no significant emission above 0.3 Jy was seen during the period from 1998 January to June. In 1996 October, we succeeded in determining the position of the masers using the VLA A configuration. The 90 mas resolution VLA image clearly indicated that the masers are associated with the radio jet VLA 2, located at $\sim 0''.4$ northwest of VLA 2 (Fig. 28d). In Figure 28e we present a distribution of the L723 masers. The important point is that the maser emission is located very close to the central powering object; however, it is hard to discuss the origin of the masers from this map alone.

4.3.13. IRAS 20050+2720

IRAS 20050+2720 is one of the luminous Class 0 protostars (Bachiller 1996; $L_{\text{FIR}} \approx 388 L_{\odot}$ reported in Molinari et al. 1996) surrounded by a large cluster of low-mass stars (e.g., Wilking & Claussen 1987; di Francesco et al. 1998). A recent SCUBA image revealed the presence of a bright central object IRAS 20050+2720 SMM 1 and two associated objects (Chini et al. 2001). This source shows a quadrupolar molecular outflow, although driving sources have not been identified. One of the pair of outflow lobes shows an EHV jetlike flow (Bachiller, Fuente, & Tafalla 1995a; Codella, Bachiller, & Reipurth 1999). The terminal velocity of the EHV flow traced by the CO $J = 2-1$ line is $\sim 160 \text{ km s}^{-1}$ from the ambient cloud velocity: the presence of the EHV flow suggests that this source is in its most powerful outflow phase.

Our Nobeyama survey revealed that IRAS 20050+2720 shows principally two groups of velocity components. One group consists of a few velocity components around the systemic velocity, while the other is a newly detected EHV emission at $V_{\text{LSR}} = -91 \text{ km s}^{-1}$ (Figs. 29a and 29b). The EHV emission was blueshifted with respect to the cloud velocity, while no EHV emission was detected on the redshifted side. Furthermore, we detected weak, blueshifted, intermediate-velocity components at $V_{\text{LSR}} = -24$ and -36 km s^{-1} in 1998 February. In panels (c) and (d), we present time-velocity contour maps of the main components and the EHV emission for the period from 1997 December through 1998 February, respectively. In order to investigate longer term variation, we plot diagrams of time versus peak velocity of the masers in panels (e) and (f). Together with the data taken in 1998 June, one can recognize a velocity drift (estimated acceleration of $2.4 \text{ km s}^{-1} \text{ yr}^{-1}$) for the low-velocity component (Fig. 29e), while any definite similar drift cannot be seen in the EHV emission (Fig. 29f). However, we cannot exclude the possibility that a new component was born, resulting in an apparent velocity drift, because a typical lifetime of the masers in Class 0 is about 2 weeks, as will be discussed in § 5.1, and because the maser profiles drastically changed in 1998 June, as shown in Figure 29a. In 1999 February, we carried out VLA observations: Figures 29g and 29h show the detected spectra. From comparison with the SCUBA image, we find that the EHV emission is located at the source MMS 1, while the main components are slightly shifted at positions $4''55$ northeast ($4''50$ east and $0''60$ north) from the EHV emission. This result suggests that the powering source of the EHV CO outflow is the brightest source MMS 1. Furthermore, we suggest a possibility that the low-velocity components trace the gas that is currently being accelerated by the EHV jet, whereas the EHV masers trace the gas that has already been accelerated.

4.3.14. S106 FIR

S106 FIR was identified to be a very young intermediate-mass Class 0 source (Richer et al. 1993). This source has an extraordinarily compact AU-scale protostellar jet—a *microjet*—traced by H₂O masers using the VLBA, while this source shows no CO outflow evidenced by a sensitive multi-transition search (Furuya et al. 2000). From these results, Furuya et al. (2000) concluded that S106 FIR is the first protostar discovered in an evolutionary stage prior to the formation of a CO outflow.

Figure 30a shows the maser emission from S106 FIR: this source is one of the eight Class 0 sources observed to display maser emission throughout the Nobeyama monitoring. All of the observed spectra show a doubly peaked shape with respect to the ambient cloud velocity. However, the duration of each component is not likely to persist more than several months, similar to IRAS 16293–2422. For instance, one can see the decay of the velocity component at roughly -9 km s^{-1} in late 1997 (Figs. 30a and 30b).

4.3.15. L1157-MM

The deeply embedded source IRAS 20386+6751 in L1157 is a prototypical Class 0 source, showing a highly collimated powerful CO outflow (Umemoto et al. 1992) and infall motions (Choi, Panis, & Evans 1999; Gregersen et al. 2000). Despite the low-luminosity of its exciting source

($L_{\text{bol}} \simeq 11 L_{\odot}$), L1157-MM shows evidence for strong interaction between stellar winds and ambient gas (e.g., Mikami et al. 1992; Tafalla & Bachiller 1995; Zhang et al. 1995; Bachiller et al. 1995c; Gueth, Guilloteau, & Bachiller 1996; Gueth et al. 1997). H₂O maser emission from L1157-MM was first detected through the Haystack survey (Claussen et al. 1996). Subsequently, Meehan et al. (1998) detected emission at $V_{\text{LSR}} = 8.67 \text{ km s}^{-1}$ in 1995 August and at 5.0 km s^{-1} in 1997 April using the VLA: they concluded that the position of the masers is coincident with that of the 3.6 cm radio continuum source.

Figure 31 presents the maser emission in L1157-MM: this source did not show maser activity at least in 1997 January and February. In the first half of 1998 June, we detected maser emission at $V_{\text{LSR}} = 7.0 \text{ km s}^{-1}$, which is redshifted with respect to the ambient cloud velocity. One week after the detection, this source displayed a second component around the cloud velocity. In 1999 February 12, we detected emission at $V_{\text{LSR}} = 3.0 \text{ km s}^{-1}$ with the VLA CnD array observations, although we confirmed no maser activity on 1999 January 27 with the 45 m telescope. The position of the emission (Table 3) is coincident with the previous detection (Meehan et al. 1998). L1157-MM typifies the highly time variable nature of the masers in low-mass protostars.

4.3.16. GF 9-2

This source is an embedded Class 0 protostar located in the GF 9 filament in L1082 ($d = 150 \text{ pc}$), where several YSOs exist at $\sim 0.75 \text{ pc}$ intervals. From observations with the *Infrared Space Observatory (ISO)* and the IRAM 30 m telescope, the SED of this source was identified as Class 0 (Wiesemeyer, Güsten, & Wright 1999). They reported that T_{bol} is less than 20 K and that the bolometric luminosity is $0.3 L_{\odot}$: this source is one of the coldest and the dimmest sources among known Class 0 objects. Since no CO outflow has been reported (Wiesemeyer et al. 1997b; 1999; AWB00), we tried to detect outflow wing emission by observing the $J = 1-0$ transition with the Nobeyama 45 m telescope toward selected points around the object. We detected weak redshifted wing emission (R. S. Furuya et al. 2000, unpublished data); thus, a molecular outflow appears to accompany the protostar.

In Figure 32 we present very weak H₂O maser emission detected at $V_{\text{LSR}} = 8.4 \text{ km s}^{-1}$ at the 8σ level. The emission is redshifted with respect to the ambient cloud velocity, as was the weak CO flow. GF 9-2 is the lowest luminosity object known to possess H₂O masers. The presence of the masers is evidence that this source is seen at an early protostellar stage.

4.3.17. Cep E-MM

This source lies in the Cep E molecular cloud, which is a part of the Cepheus OB3 association. The Cep E-MM outflow was first reported by Fukui et al. (1989), although they did not show a map of the outflow. Its driving source was identified as IRAS 23011+0126, and its SED was identified as Class 0 (Erlöf et al. 1996). The outflow was extensively studied using CO lines (Lefloch, Eislöffel, & Lazareff 1996; Ladd & Hodapp 1997; Hatchell et al. 1999). From CO $J = 2-1$ observations, Lefloch et al. (1996) revealed the presence of molecular bullets: it was extensively studied in the $J = 4-3$ line (Hatchell et al. 1999). The total extent of CO outflow, including the HH objects, is less than $70''$

(Lefloch et al. 1996; Hatchell et al. 1999), which is almost the same as the beam size of the Nobeyama 45 m telescope.

Figures 41a–41c present the maser spectra toward Cep E-MM: this source displayed only blueshifted high-velocity emission at $V_{\text{LSR}} = -62$ and -38 km s^{-1} , while no emission was seen either around the cloud velocity or on the redshifted side. This source displayed a drastic change of its maser spectrum from 1997 December through 1998 February (Fig. 41a–41d). In particular, the velocity component around $V_{\text{LSR}} = -60 \text{ km s}^{-1}$ showed a rapid increase within 2.5 months ($\sim 1.7 \text{ Jy}$ in 1997 December 30; $\sim 25 \text{ Jy}$ in 1998 February 12). All of the detected maser emission peaked in the velocity range of the CO outflow wings. Figure 41e shows the spectrum of the masers taken by the VLA. The maser emission is located at the peak position of $850 \mu\text{m}$ continuum emission (Ladd & Hodapp 1997).

4.4. Properties of Maser Sources

In Table 4 we compiled the properties of 142 YSOs, including high-mass objects, which displayed maser emission during our survey or at sometime in the past, or which exhibited no maser emission but were observed. In columns (1) and (2) we give the most common YSO name and the alternative YSO name, respectively. Column (3) gives a distance to the source. Column (4) gives a bolometric luminosity (L_{bol}) of the source. Column (5) gives mass of the circumstellar envelope (M_{env}): most of them were derived from flux measurements in dust continuum emission at 1.3 mm by either single-dish telescopes or interferometers. Column (6) gives a bolometric temperature (T_{bol}) of the source. We referred to either Chen et al. (1995, 1997), Mardones et al. (1997), or AWB00 for low-mass YSOs and to Williams & Myers (1999) for high-mass objects. Columns (7) and (8) give momentum flux (F_{CO}) and mechanical luminosity (L_{CO}) of the CO outflow, respectively, which were mainly derived from observations of the $J = 2-1$ transition. For some sources, we consulted papers of other transitions of the CO molecule, its isotopomer, and/or other molecular lines. If kinematic parameters for more than two outflow lobes were given in original papers, we give the sum of them (e.g., CO outflows in the NGC 1333 region reported by Knee & Sandell 2000). Columns (9) and (10) give intensities of radio continuum emission at $\lambda = 6$ and 3.8 cm measured by the VLA observations, respectively. Columns (11) and (12) give the minimum and maximum luminosities of H_2O masers, respectively, obtained by the 45 m telescope on the basis of Table 2, taking into account the results from the VLA observations (§ 4.3). Column (13) gives an evolutionary identification of the YSO. In the case of a low-mass YSO, an SED class is given. Column (14) gives references for columns (3), (4), (5), (7)–(10), and (13). All four figures in Paper I and Figures 43–46 were produced on the basis of Table 4.

5. DISCUSSION

5.1. Time Variability of H_2O Masers

The data presented in § 4 clearly indicate that the well-known highly time variable nature of maser emission is also common in low-mass protostars. In this subsection we wish to give a more detailed presentation of maser duration, briefly discussed in § 4.2 of Paper I. Figure 42 presents a histogram of duration of each velocity component for low-

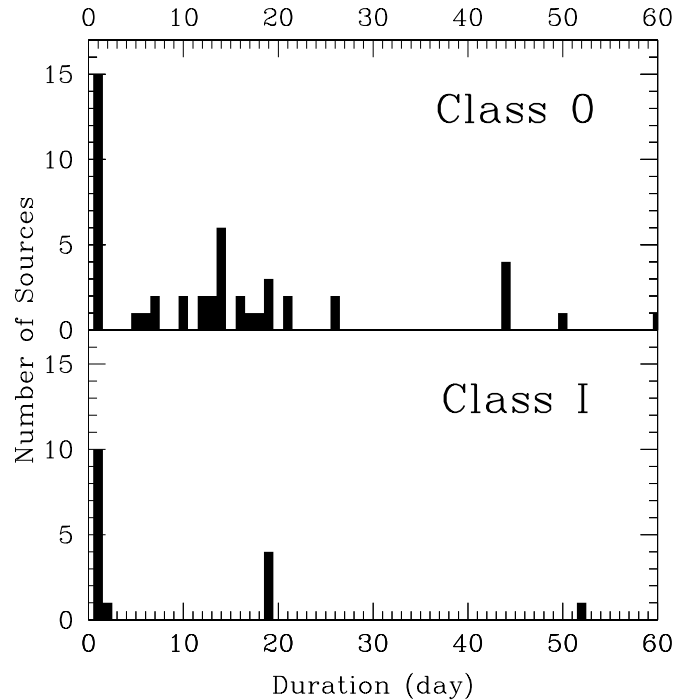


FIG. 42.—Histogram of duration for each velocity component of H_2O maser spectra obtained with the Nobeyama 45 m telescope and VLA for Class 0 sources (top) and Class I sources (bottom).

mass Class 0 and Class I sources (for the classification of sources we adopted the bolometric temperature). We show the distribution of duration up to 60 days because we could not obtain enough data points in 60–120 day bins owing to the irregularly allocated observations. Most of the 45 m telescope observations were conducted in the period from 1997 late December through 1998 early February, in 1998 June, and in the period from 1999 late January through 1999 early March. This provides us with a sufficient number of bins to discuss duration less than ~ 60 days and that of ~ 120 –180 days, while we do not have enough data in the ~ 60 –120 day bins. Therefore, we decided to discuss only short time variations, less than 60 days. As in Paper I, we assigned the duration of 1 day in the case that a velocity component was only detected once.

Wilking et al. (1994) reported that the maser emission is time variable with a detectable maser phase lasting from greater than 13 months down to less than 1 month. In Figure 42 we note that the most frequent value for Class 0 sources appears to be around 2 weeks (except the 1 day bin). Such short time variations can be explained by a small change in pumping rate assuming that the masers are unsaturated (Burke, Giuffrida, & Haschick 1978): one of the most plausible pumping mechanisms is collisional pumping in shocks driven by protostellar jets. In fact, Furuya et al. (2000) discovered a *micro-bow shock* in the Class 0 source S106 FIR: the bow shock traced by the H_2O masers is thought to be caused by the impact of a protostellar jet on the ambient cloud medium. The width of the micro-bow shock is $\sim 1 \text{ AU}$, and the shock velocity is $\sim 40 \text{ km s}^{-1}$. This leads to a shock crossing time of approximately 6 days. Therefore, we suggest that the short time variation less than 1 month is caused by some instability of the shocked region where the masers are collisionally excited.

5.2. Excitation Conditions of the Masers

In Paper I we could gain some insight into the maser phenomena in low-mass YSOs by comparing the physical properties of the YSOs with and without H₂O masers. Using the present sample, more extended than that of Paper I, we wish to investigate properties of H₂O masers as a probe of jet and outflow phenomena in low-mass YSOs. For statistical discussion, we limited the sample to the sources less luminous than $100 L_{\odot}$. This is because our observed sources more luminous than $100 L_{\odot}$ were not systematically selected, which might lead to wrong conclusions as a result of low statistics.

In Figure 43, observed isotropic H₂O maser luminosity is plotted as a function of source bolometric luminosity. A weak correlation can be seen in the sample of low-mass stars (*filled symbols*). This correlation is essentially the same as that between $L_{\text{H}_2\text{O}}$ and the FIR luminosities proposed by FPT92 for high-mass sources ($L_{\text{FIR}} \sim 10\text{--}10^6 L_{\odot}$) and by Wilking et al. (1994) for low-mass sources ($L_{\text{FIR}} \sim 1\text{--}10^2 L_{\odot}$) selected from the *IRAS* PSC. Wilking et al. (1994) and Claussen et al. (1996) proposed that sources more luminous than $25 L_{\odot}$ in L_{FIR} tend to always show H₂O maser emission. The high sensitivity of the 45 m telescope revealed that the correlation holds down to approximately $1 L_{\odot}$, although the correlation seems weak.

As expected from the correlation in Figure 43, we confirmed a significant correlation between $L_{\text{H}_2\text{O}}$ and luminosities of 6 cm radio continuum emission (Fig. 44). Here we defined the radio continuum luminosity as $4\pi d^2 S_{6\text{cm}}$, where d is a source distance and $S_{6\text{cm}}$ is the flux density at $\lambda = 6.0$

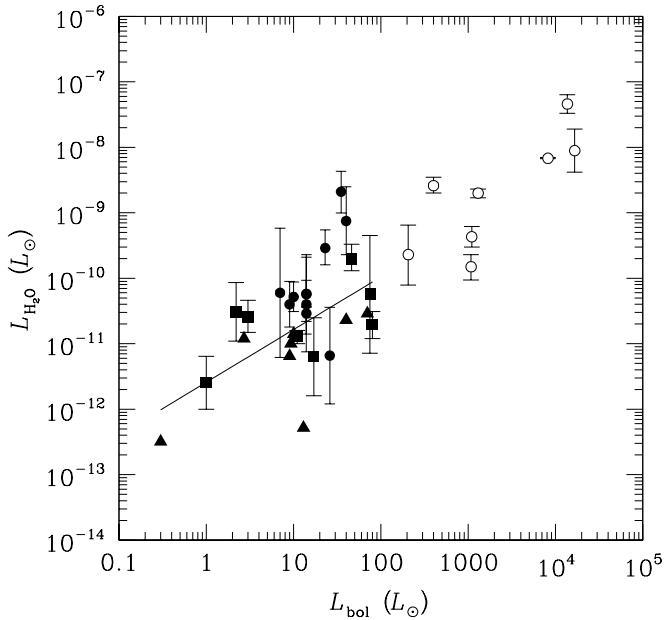


FIG. 43.—Observed isotropic H₂O maser luminosities ($L_{\text{H}_2\text{O}}$) vs. source bolometric luminosities (L_{bol}) for all the sources detected in the Nobeyama survey. Filled and open symbols present sources less and more luminous than $100 L_{\odot}$, respectively. The circles indicate the H₂O masers detected at all observing epochs. The squares indicate the H₂O masers that have not been detected at one or more epochs. The associated bars indicate the range of the luminosities for detected spectra in our observations. The triangles represent the maser luminosities for the sources that have been detected only once during the monitoring. The best-fit curve of $L_{\text{H}_2\text{O}} = 2.58 \times 10^{-12} (L_{\text{bol}})^{0.81}$ is shown by a line (correlation coefficient; $\rho = 0.28$).

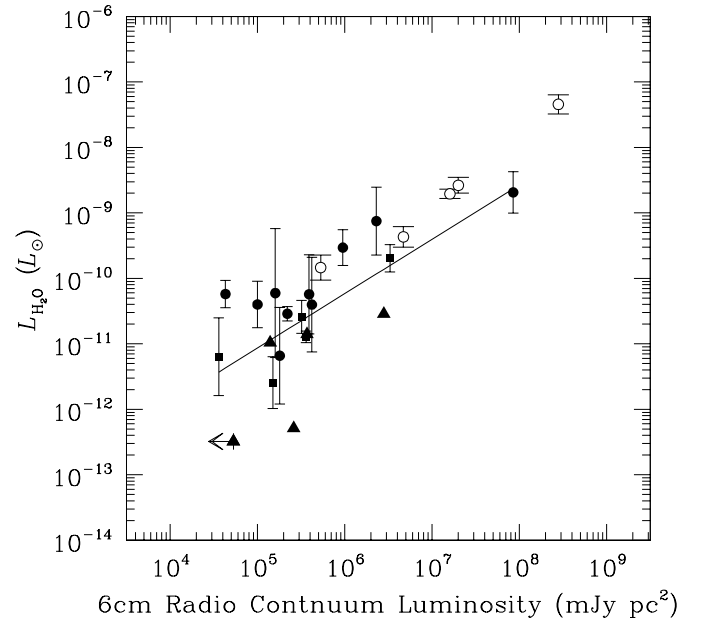


FIG. 44.—Plots of observed isotropic H₂O maser luminosities ($L_{\text{H}_2\text{O}}$) vs. 6 cm radio continuum luminosities ($4\pi d^2 S_{6\text{cm}}$). The symbols are the same as in Fig. 43. The best-fit curve of $L_{\text{H}_2\text{O}} = 5.93 \times 10^{-16} (4\pi d^2 S_{6\text{cm}})^{0.83}$ is shown by a line ($\rho = -0.47$). A filled triangle with an upper limit is the source GF 9-2, which we did not use to fit the curve.

cm measured with the VLA. This correlation seems to be reasonable because the radio continuum luminosities are known to correlate with L_{bol} (e.g., Meehan et al. 1998). The radio continuum emission emanating from protostars is thought to be free-free emission from shock-ionized gas produced by neutral protostellar jets (Torrelles et al. 1985; Rodríguez et al. 1989).⁴ From these results, we conclude that H₂O maser emission is one of the best probes to investigate activity of protostellar jets in the vicinity of central protostars ($\lesssim 100$ AU).

In Figure 45 we present plots of $L_{\text{H}_2\text{O}}$ against the mechanical luminosities of CO outflows (L_{CO}) and momentum fluxes (F_{CO}). As we reported in Paper I, no correlations can be seen for low-mass YSOs, while FPT92 reported that $L_{\text{H}_2\text{O}}$ correlates well with L_{CO} in their sample of high-mass YSOs. It should be noted that CO outflows are thought to be driven by jets and are generated by sweeping up material in the cloud cores. Therefore, these CO outflow parameters should be related not only to the activity of protostellar jets but also to the amount of material remaining in the cloud core that will be dispersed by the jets. Since the remaining material is not likely to be related to the jet activity, it is reasonable to expect no correlation in Figure 45.

Figures 44 and 45 suggest that H₂O masers in low-mass YSOs are more closely related to the 100 AU scale thermally ionized jets than to the $10^4\text{--}10^5$ AU scale CO outflows. This idea is supported by the VLA and VLBA observations: the masers in low-mass YSOs tend to be located within several hundred AU from the central objects (as shown in § 4) and are excited in the shocked layer between the ambient cloud

⁴ For 12 sources, we estimated the flux densities at 6 cm from those at 3.8 cm assuming optically thin free-free emission with the relation of $S_{\nu} \propto \nu^{\alpha}$, where $\alpha = -0.1$ (Curiel, Cantó, & Rodríguez 1987).

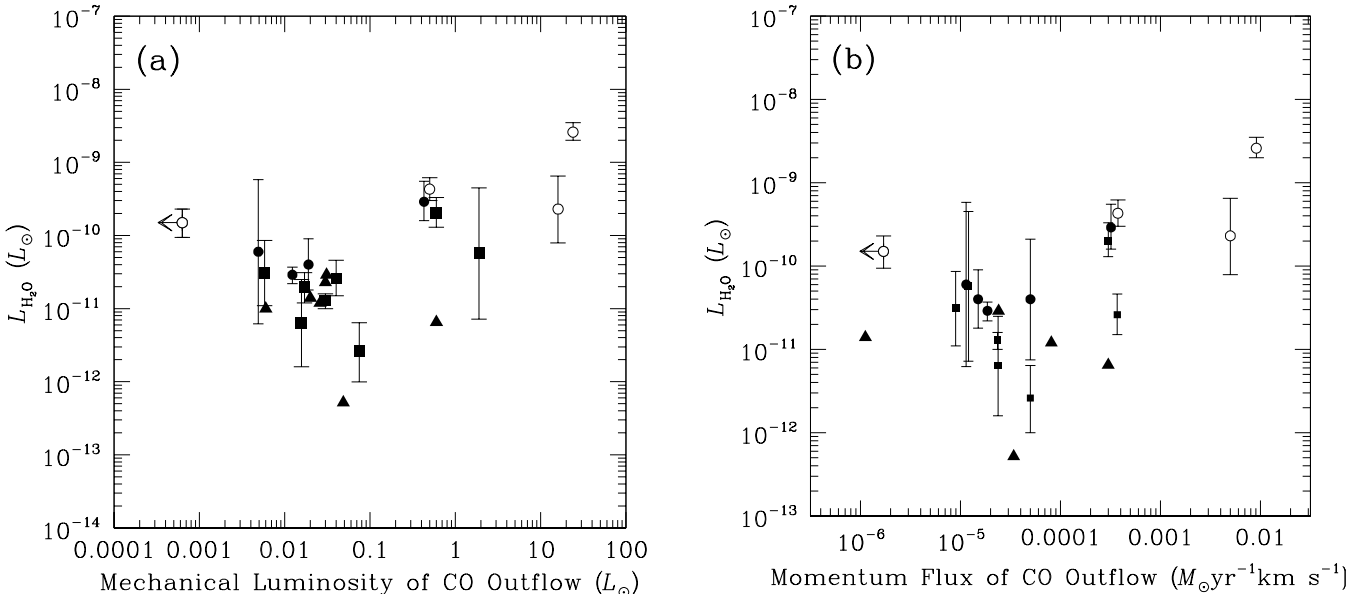


FIG. 45.—(a) Plots of observed isotropic H_2O maser luminosities ($L_{\text{H}_2\text{O}}$) vs. mechanical luminosity of CO outflows (L_{CO}). (b) Plots of observed isotropic H_2O maser luminosities ($L_{\text{H}_2\text{O}}$) vs. momentum flux of CO outflows (F_{CO}). The symbols are the same as in Fig. 43, and an open circle with an upper limit is the source S106 FIR.

and protostellar jets (e.g., Chernin 1995; Claussen et al. 1998; Furuya et al. 2000).

In Figure 46 we present a newly found correlation between $L_{\text{H}_2\text{O}}$ and circumstellar envelope mass (M_{env}),

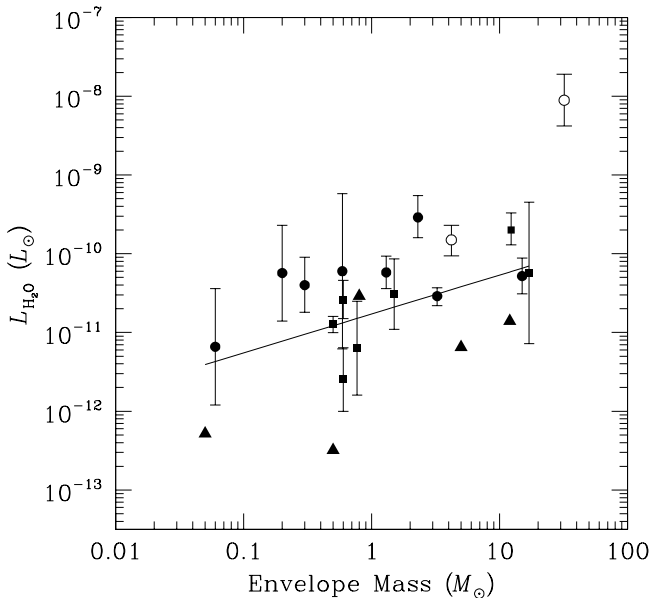


FIG. 46.—Plots of observed isotropic H_2O maser luminosities ($L_{\text{H}_2\text{O}}$) vs. circumstellar envelope mass (M_{env}). The symbols are the same as in Fig. 43. The best-fit curve of $L_{\text{H}_2\text{O}} = 1.72 \times 10^{-11} M_{\text{env}}^{0.49}$ is also shown by a line ($\rho = -0.53$).

although $L_{\text{H}_2\text{O}}$ and M_{env} are thought to depend on physical conditions on small ($\lesssim 100$ AU) and large ($\gtrsim 1000$ AU) scales, respectively. The cause of this correlation may be speculated on as follows. Since the material in the circumstellar envelope will eventually accrete to the star, M_{env} probably relates to the mass accretion rate onto the star. Furthermore, the mass accretion rate is thought to be linked to the mass ejection activity on smaller scales. Considering these facts, we suggest that the correlation between $L_{\text{H}_2\text{O}}$ and M_{env} essentially reflects that between $L_{\text{H}_2\text{O}}$ and the mass accretion rate. This interpretation is likely to be supported by the fact that $L_{\text{H}_2\text{O}}$ correlates well with the 100 AU scale radio continuum luminosity (Fig. 44), but $L_{\text{H}_2\text{O}}$ does not correlate with the 1000 AU scale CO outflow activity (Fig. 45). However, we could not find any definite reason why $L_{\text{H}_2\text{O}}$ varies as the square root of M_{env} .

We are grateful to all of the staff at the Nobeyama 45 m telescope and at the VLA. In particular, R. S. F. thanks N. Ukita and K. Sunada for their support during the monitoring project at Nobeyama. R. S. F. thanks all the observers at the 45 m telescope, who gave us their observing time for the maser survey as a backup project. F. Motte helped R. S. F. to prepare Figure 1. L. Looney and G. Anglada helped R. S. F. to prepare figures that show positions of the masers. L. Testi provided the values of circumstellar envelope masses in the Serpens cloud core in Table 4, which were not published in Testi & Sargent (1998). R. S. F. thanks C. M. Walmsley for discussion and encouragement. R. S. F. is supported by postdoctoral fellowship program at INAF, Osservatorio Astrofisico di Arcetri.

REFERENCES

- André, P., Martín-Pintado, J., Despois, D., & Montmerle, T. 1990, A&A, 236, 180
- André, P., & Montmerle, T. 1994, ApJ, 420, 837
- André, P., Motte, F., & Bacmann, A. 1999, ApJ, 513, L57
- André, P., Ward-Thompson, D., & Barsony, M. 1993, ApJ, 406, 122 (AWB93)
- . 2000, in Protostars and Planets IV, ed. V. Mannings, A. P. Boss, & S. S. Russell (Tucson: Univ. Arizona Press), 59 (AWB00)
- Anglada, G., Rodríguez, L. F., Cantó, J., Estalella, R., & Torrelles, J. M. 1992, ApJ, 395, 494
- Anglada, G., Rodríguez, L. F., Girart, J. M., Estalella, R., & Torrelles, J. M. 1994, ApJ, 420, L91
- Anglada, G., Rodríguez, L. F., & Torrelles, J. M. 1996, ApJ, 473, L123
- Anglada, G., Rodríguez, L. F., Torrelles, J. M., Estalella, R., Ho, P. T. P., Cantó, J., Lopez, R., & Verdes-Montenegro, L. 1989, ApJ, 341, 208
- Anglada, G., Sepúlveda, I., & Gómez, J. F. 1997, A&AS, 121, 255
- Anglada, G., Villuendas, E., Estalella, R., Beltrán, M. T., Rodríguez, L. F., Torrelles, J. M., & Curiel, S. 1998, AJ, 116, 2953
- Anglada, G., et al. 1991, ApJ, 376, 615
- Armstrong, J. T., & Weinewisser, G. 1989, A&A, 210, 373
- Aso, Y., Tatematsu, K., Sekimoto, Y., Nakano, T., Umemoto, T., Koyama, K., & Yamamoto, S. 2000, ApJS, 131, 465
- Avery, L. W., Hayashi, S. S., & White, G. J. 1990, ApJ, 357, 524
- Bachiller, R. 1996, ARA&A, 34, 111
- Bachiller, R., del Rio Alvarez, S., & Menten, K. M. 1990, A&A, 236, 461
- Bachiller, R., Fuente, A., & Tafalla, M. 1995a, ApJ, 445, L51
- Bachiller, R., Guilloteau, S., Dutrey, A., Planesas, P., & Martín-Pintado, J. 1995b, A&A, 299, 857
- Bachiller, R., Guilloteau, S., Gueth, F., Tafalla, M., Dutrey, A., Codella, C., & Castets, A. 1998, A&A, 339, L49
- Bachiller, R., Liechti, S., Walmsley, C. M., & Colomer, F. 1995c, A&A, 295, L51
- Bally, J., & Alten, V. 1996, ApJ, 473, 921
- Bally, J., Devine, D., & Reipurth, B. 1996, ApJ, 473, L49
- Beichman, C., Myers, P. C., Emerson, J. P., Harris, S., Mathieu, R., Benson, P. J., & Jennings, R. E. 1986, ApJ, 307, 337
- Beltrán, M. T., Estalella, R., Anglada, G., Rodríguez, L. F., & Torrelles, J. M. 2001, AJ, 121, 1556
- Beltrán, M. T., Estalella, R., Ho, P. T. P., Calvet, N., Anglada, G., & Sepúlveda, I. 2002, ApJ, 565, 1069
- Bence, S. J., Padman, R., Isaak, K. G., Wiedner, M. C., & Wright, G. S. 1998, MNRAS, 299, 965
- Bence, S. J., Richer, J. S., & Padman, R. 1996, MNRAS, 279, 866
- Bieging, J. H., Cohen, M., & Schwartz, P. R. 1984, ApJ, 282, 699
- Blake, G. A., Sandell, G., van Dishoeck, E. F., Groesbeck, T. D., Mundy, L. G., & Aspin, C. 1995, ApJ, 441, 689
- Bontemps, S., & André, P. 1997, in IAU Symp. 182, Herbig-Haro Flows and the Birth of Low Mass Stars, ed. B. Reipurth & C. Bertout (Dordrecht: Kluwer), 63
- Bontemps, S., André, P., Terebey, S., & Cabrit, S. 1996, A&A, 311, 858
- Bontemps, S., André, P., & Ward-Thompson, D. 1995, A&A, 297, 98
- Burke, B. F., Giuffrida, T. S., & Haschick, A. D. 1978, ApJ, 226, L21
- Cabrit, S., & André, P. 1991, ApJ, 379, L25
- Cabrit, S., & Bertout, C. 1992, A&A, 261, 274
- Casali, M. M., Eiroa, C., & Duncan, W. D. 1993, A&A, 275, 195
- Cernis, K. 1990, Ap&SS, 166, 315
- Chandler, C. J., Terebey, S., Barsony, M., Moore, T. J. T., & Gautier, T. N. 1996, ApJ, 471, 308
- Chen, H., Myers, P. C., Ladd, E. F., & Wood, D. O. S. 1995, ApJ, 445, 377
- Chen, H., Tafalla, M., Greene, T. P., Myers, P. C., & Wilner, D. J. 1997, ApJ, 475, 163
- Chernin, L. M. 1995, ApJ, 440, L97
- . 1996, ApJ, 460, 711
- Chernin, L. M., & Masson, C. R. 1995, ApJ, 443, 181
- Chini, R., Reipurth, B., Sievers, A., Ward-Thompson, D., Haslam, C. G. T., Kreysa, E., & Lemke, R. 1997a, A&A, 325, 542
- Chini, R., Reipurth, B., Ward-Thompson, D., Bally, J., Nyman, L.-A., Sievers, A., & Billawala, Y. 1997b, ApJ, 474, L135
- Chini, R., Ward-Thompson, D., Kirk, J. M., Nielbock, M., Reipurth, B., & Sievers, A. 2001, A&A, 369, 155
- Choi, M., Panis, J., & Evans, N. J. 1999, ApJS, 122, 519
- Claussen, M. J., Marvel, K. B., Wootten, A., & Wilking, B. A. 1998, ApJ, 507, L79
- Claussen, M. J., Wilking, B. A., Benson, P. J., Wootten, A., Myers, P. C., & Terebey, S. 1996, ApJS, 106, 111
- Codella, C., Bachiller, R., & Reipurth, B. 1999, A&A, 343, 585
- Comoretto, G., et al. 1990, A&AS, 84, 179
- Curiel, S., Cantó, J., & Rodríguez, L. F. 1987, Rev. Mexicana Astron. Astrofís., 14, 595
- Curiel, S., Raymond, J. C., Moran, J. M., Rodríguez, L. F., & Cantó, J. 1990, ApJ, 365, L85
- Curiel, S., Rodríguez, L. F., Moran, J. M., & Cantó, J. 1993, ApJ, 415, 191
- Davidson, J. A. 1987, ApJ, 315, 602
- Davis, C. J., Eislöffel, J., Ray, T. P., & Jenness, T. 1997, A&A, 324, 1013
- Davis, C. J., Matthews, H. E., Ray, T. P., Dent, W. R. F., & Richer, J. S. 1999, MNRAS, 309, 141
- Dent, W. R. F., Matthews, H. E., & Walther, D. M. 1995, MNRAS, 277, 193
- di Francesco, J., Evans, N. J., II, Harvey, P. M., Mundy, L. G., & Butner, H. M. 1998, ApJ, 509, 324
- Dyck, H. M., Simon, T., & Zuckerman, B. 1982, ApJ, 255, L103
- Edwards, S., & Snell, R. L. 1982, ApJ, 261, 151
- Eiroa, C., & Casali, M. M. 1992, A&A, 262, 468
- Eislöffel, J., Smith, M. D., Davis, C. J., & Ray, T. P. 1996, AJ, 112, 2086
- Felli, M., Palagi, F., & Tofani, G. 1992, A&A, 255, 293 (FPT92)
- Fiebig, D., Duschl, W. J., Menten, K. M., & Tscharnatur, W. M. 1996, A&A, 310, 199
- Font, A. S., Mitchell, G. F., & Sandell, G. 2001, ApJ, 555, 950
- Fukui, Y., Iwata, T., Mizuno, A., Bally, J., & Lane, A. P. 1993, in Protostars and Planets III, ed. E. H. Levy & J. I. Lunine (Tucson: Univ. Arizona Press), 603
- Fukui, Y., Iwata, T., Mizuno, A., Ogawa, H., & Takaba, H. 1989, Nature, 342, 161
- Fuller, G. A., Lada, E. A., Masson, C. R., & Myers, P. C. 1995, ApJ, 453, 754
- Fuller, G. A., & Wootten, A. 2000, ApJ, 534, 854
- Furuya, R. S., Kitamura, Y., Saito, M., Kawabe, R., & Wootten, H. A. 1999, ApJ, 525, 821
- Furuya, R. S., Kitamura, Y., Wootten, H. A., Claussen, M. J., & Kawabe, R. 2001, ApJ, 559, L143 (Paper I)
- Furuya, R. S., Kitamura, Y., Wootten, H. A., Claussen, M. J., Saito, M., Marvel, K. B., & Kawabe, R. 2000, ApJ, 542, L135
- Furuya, R. S., et al. 2002, in IAU Symp. 206, Cosmic Masers: From Protostars to Black Holes, ed. V. Migenes & E. Lüdke (San Francisco: ASP), in press
- Genzel, R., & Downes, D. 1977, A&AS, 30, 145
- Gibb, A. G. 1999, MNRAS, 304, 1
- Giovannardi, C., Rodríguez, L. F., Lizano, S., & Cantó, J. 2000, ApJ, 538, 728
- Giralt, J. M., et al. 1994, ApJ, 435, L145
- Gómez, J. F., Curiel, S., Torrelles, J. M., Rodríguez, L. F., Anglada, G., & Girart, J. M. 1994, ApJ, 436, 749
- Gregeresen, E. M., Evans, N. J., II, Mardones, D., & Myers, P. C. 2000, ApJ, 533, 440
- Gueth, F., & Guilloteau, S. 1999, A&A, 343, 571
- Gueth, F., Guilloteau, S., & Bachiller, R. 1996, A&A, 307, 891
- Gueth, F., Guilloteau, S., Dutrey, A., & Bachiller, R. 1997, A&A, 323, 943
- Haikala, L. K., & Laurejts, R. J. 1989, A&A, 223, 287
- Harju, J., Walmsley, C. M., & Wouterloot, J. G. A. 1993, A&AS, 98, 51
- Harvey, P. M., Wilking, B. A., & Joy, M. 1984, ApJ, 278, 156
- Hatchell, J., Fuller, G. A., & Ladd, E. F. 1999, A&A, 346, 278
- Hayashi, M., & Murata, Y. 1992, PASJ, 44, 391
- Hayashi, S. S., Hasegawa, T., & Kaifu, N. 1991, ApJ, 377, 492
- Henkel, C., Haschick, A. D., & Güstein, R. 1986, A&A, 165, 197
- Henning, T., & Launhardt, R. 1998, A&A, 338, 223
- Henning, T., Martin, K., Reimann, H.-G., Launhardt, R., Leisawitz, D., & Zinnecker, H. 1994, A&A, 288, 282
- Herbig, G. H. 1974, Lick Obs. Bull., 658, 1
- Herbig, G. H., & Jones, B. F. 1983, AJ, 88, 1040
- Heyer, M. H., Snell, R. L., Goldsmith, P. F., Strom, S. E., & Strom, K. M. 1986, ApJ, 308, 134
- Hirano, N., Hayashi, S. S., Umemoto, T., & Ukita, N. 1998, ApJ, 504, 334
- Hirano, N., Kameya, O., Kasuga, T., Umemoto, T. 1992, ApJ, 390, L85
- Hirano, N., Kameya, O., Mikami, H., Saito, S., Umemoto, T., & Yamamoto, S. 1997, ApJ, 478, 631
- Ho, P. T. P., & Barrett, A. H. 1980, ApJ, 237, 38
- Hodapp, K.-W., & Ladd, E. F. 1995, ApJ, 453, 715
- Hurt, R. L., & Barsony, M. 1996, ApJ, 460, L45
- Hurt, R. L., Barsony, M., & Wootten, A. 1996, ApJ, 456, 686
- Iwata, T., Fukui, Y., & Ogawa, H. 1988, ApJ, 325, 372
- Jennings, R. E., Cameron, D. H. M., Cudlip, W., & Hirst, C. J. 1987, MNRAS, 226, 461
- Kawabe, R., Ishiguro, M., Omodaka, T., Kitamura, Y., & Miyama, S. M. 1993, ApJ, 404, L63
- Kelly, M. L., & MacDonald, G. H. 1996, MNRAS, 282, 401
- Kitamura, Y., Kawabe, R., & Saito, M. 1996, ApJ, 465, L137
- Kitamura, Y., Kawabe, R., Yamashita, T., & Hayashi, M. 1990, ApJ, 363, 180
- Knapp, G. R., & Morris, M. 1976, ApJ, 206, 713
- Knee, L. B. G., & Sandell, G. 2000, A&A, 361, 671
- Lada, C. J. 1987, in IAU Symp. 115, Star Formation: From OB Associations to Protostars, ed. M. Peimbert & J. Jugaku (Dordrecht: Kluwer), 1
- Lada, C. J., & Fich, M. 1996, ApJ, 459, 638
- Ladd, E. F., & Hodapp, K.-W. 1997, ApJ, 474, 749
- Langer, W. D., Castets, A., & Lefloch, B. 1996, ApJ, 471, L111
- Lay, O., Carlstrom, J. E., & Hills, R. E. 1995, ApJ, 452, L73
- Lee, C.-F., Mundy, L. G., Reipurth, B., Ostriker, E. C., & Stone, J. M. 2000, ApJ, 542, 925
- Lefloch, B., Castets, A., Cernicharo, J., Langer, W. D., & Zylka, R. 1998, A&A, 334, 269

- Lefloch, B., Eislöffel, J., & Lazareff, B. 1996, *A&A*, 313, L17
 Leous, J. A., Feigelson, D., André, P., & Montmerle, T. 1991, *ApJ*, 379, 683
 Lis, D. C., Menten, K. M., & Zylka, R. 1999, *ApJ*, 527, 856
 Liseau, R., & Sandell, G. 1986, *ApJ*, 304, 459
 Looney, L. W., Mundy, L. G., & Welch, W. J. 1997, *ApJ*, 484, L157
 —. 2000, *ApJ*, 529, 477
 Loren, R. B., Evans, N. J., II, & Knapp, G. R. 1979, *ApJ*, 234, 932
 Lucas, P. W., Blundell, K. M., & Roche, P. F. 2000, *MNRAS*, 318, 526
 Maihara, T., & Kataza, H. 1991, *A&A*, 249, 392
 Mangum, J. F., Wootten, A., & Barsony, M. 1999, *ApJ*, 526, 845
 Mardones, D., Myers, P. C., Tafalla, M., Wilner, D. J., Bachiller, R., & Garay, G. 1997, *ApJ*, 489, 719
 McMullin, J. P., Mundy, L. G., & Blake, G. A. 1994a, *ApJ*, 437, 305
 McMullin, J. P., Mundy, L. G., Wilking, B. A., Hezel, T., & Blake, G. A. 1994b, *ApJ*, 424, 222
 Meehan, L. S. G., Wilking, B. A., Claussen, M. J., Mundy, L. G., & Wootten, A. 1998, *AJ*, 115, 1599
 Mezger, P. G., Sievers, A. W., Haslam, C. G. T., Kreysa, E., Lemke, R., Mauersberger, R., & Wilson, T. L. 1992, *A&A*, 256, 631
 Mikami, H., Umemoto, T., Yamamoto, S., & Saito, S. 1992, *ApJ*, 392, L87
 Mizuno, A., Fukui, Y., Iwata, T., Nozama, S., & Takano, T. 1990, *ApJ*, 356, 184
 Molinari, S., Brand, J., Cesaroni, R., & Palla, F. 1996, *A&A*, 308, 573
 Momose, M., Ohashi, N., Kawabe, R., Hayashi, M., & Nakano, T. 1996, *ApJ*, 470, 1001
 Momose, M., Ohashi, N., Kawabe, R., Nakano, T., & Hayashi, M. 1998, *ApJ*, 504, 314
 Monin, J.-L., Pudritz, R. E., & Lazareff, B. 1996, *A&A*, 305, 572
 Morgan, J. A., Snell, R. L., & Strom, K. M. 1990, *ApJ*, 362, 274
 Moriarty-Schieven, G. H., Wannier, P. G., Keene, J., & Tamura, M. 1994, *ApJ*, 436, 800
 Moro-Martín, A., Cernicharo, J., Noriega-Crespo, A., & Martín-Pintado, J. 1999, *ApJ*, 520, L111
 Motte, F., & André, P. 2001, *A&A*, 365, 440
 Motte, F., André, P., & Neri, R. 1998, *A&A*, 336, 150
 Mundy, L., McMullin, J. P., Grossman, A. W., & Sandell, G. 1993, *Icarus*, 106, 11
 Mundy, L., Wootten, A., Wilking, B. A., Blake, G. A., & Sargent, A. I. 1992, *ApJ*, 385, 306
 Myers, P. C., Bachiller, R., Caselli, P., Fuller, G. A., Mardones, D., Tafalla, M., & Wilner, D. J. 1995, *ApJ*, 449, L65
 Myers, P. C., Fuller, G. A., Mathieu, R. D., Beichman, C. A., Benson, P. J., Schild, R. E., & Emerson, J. P. 1987, *ApJ*, 319, 340
 Myers, P. C., Heyer, M., Snell, R. L., & Goldsmith, P. F. 1988, *ApJ*, 324, 907
 Myers, P. C., & Ladd, E. F. 1993, *ApJ*, 413, L47
 Nisenson, P., Stachnik, R. V., Karovska, M., & Noyes, R. 1985, *ApJ*, 297, L17
 Nordh, H. L., Fridlund, C. V. M., van Duinen, R. J., Sargent, A. I., Aalders, J. W. G., & Beintema, D. 1982, *A&A*, 115, 308
 Noriega-Crespo, A., Garnavich, P. M., & Molinari, S. 1998, *AJ*, 116, 1388
 Nürnberger, D., Brandner, W., Yorke, H. W., & Zinnecker, H. 1998, *A&A*, 330, 549
 Ohashi, N., Hayashi, M., Ho, P. T. P., Momose, M., Tamura, M., Hirano, N., & Sargent, A. I. 1997, *ApJ*, 488, 317
 Park, Y.-S., Panis, J.-F., Ohashi, N., Choi, M., & Minh, Y. C. 2000, *ApJ*, 542, 344
 Parker, N. D., Padman, R., & Scott, P. F. 1991, *MNRAS*, 252, 442
 Parker, N. D., Padman, R., Scott, P. F., & Hills, R. E. 1988, *MNRAS*, 234, 67P
 Patel, N. A., Goldsmith, P. F., Snell, R. L., Hezel, T., & Xie, T. 1995, *ApJ*, 447, 721
 Patel, N. A., Greenhill, L. J., Herrnstein, J., Zhang, Q., Moran, J. M., Ho, P. T. P., & Goldsmith, P. F. 2000, *ApJ*, 538, 268
 Persi, P., Palagi, F., & Felli, M. 1994, *A&A*, 291, 577
 Ray, T. P., Mixlow, T. W. B., Axon, D. J., Brown, A., Corcoran, D., Dyson, J., & Mundt, R. 1997, *Nature*, 385, 415
 Reid, M. J., & Moran, J. M. 1981, *ARA&A*, 19, 231
 Reipurth, B., Chini, R., Krugel, E., Kreysa, E., & Sievers, A. 1993, *A&A*, 273, 221
 Reipurth, B., & Olberg, M. 1991, *A&A*, 246, 535
 Reipurth, B., Rodríguez, L. F., & Chini, R. 1999, *AJ*, 118, 983
 Richer, J. S. 1990, *MNRAS*, 245, 24P
 Richer, J. S., Hills, R. E., & Padman, R. 1992, *MNRAS*, 254, 525
 Richer, J. S., Hills, R. E., Padman, R., & Russell, A. P. G. 1989, *MNRAS*, 241, 231
 Richer, J. S., Padman, R., Ward-Thompson, D., Hills, R. E., & Harris, A. I. 1993, *MNRAS*, 262, 839
 Rodriguez, L. F., Anglada, G., & Curiel, S. 1997, *ApJ*, 480, L125
 —. 1999, *ApJS*, 125, 427
 Rodriguez, L. F., Curiel, S., Ho, P. T. P., Torrelles, J. M., & Cantó, J. 1990, *ApJ*, 352, 645
 Rodriguez, L. F., Moran, J. M., Gottlieb, E. W., & Ho, P. T. P. 1980, *ApJ*, 235, 845
 Rodriguez, L. F., Myers, P. C., Cruz-Gonzalez, I., & Terebey, S. 1989, *ApJ*, 347, 461
 Rodríguez, L. F., & Reipurth, B. 1994, *A&A*, 281, 882
 —. 1996, *Rev. Mexicana Astron. Astrofís.*, 32, 27
 Rodríguez, L. F., et al. 1998, *Nature*, 395, 355
 —. 2000, *AJ*, 119, 882
 —. 2002, *A&A*, 389, 572
 Rogers, C. B., & Gottschalk, J. 1993, *AAS*, 183, 4904
 Saito, M., Kawabe, R., Kitamura, Y., & Sunada, K. 1996, *ApJ*, 473, 464
 —. 2001, *ApJ*, 547, 840
 Saito, M., Sunada, K., Kawabe, R., Kitamura, Y., & Hirano, N. 1999, *ApJ*, 518, 334
 Sandell, G., Aspin, C., Duncan, W. D., Russell, A. P. G., & Robson, E. I. 1991, *ApJ*, 376, L17
 Sandell, G., & Knee, L. B. G. 2001, *ApJ*, 546, L49
 Sandell, G., Knee, L. B. G., Aspin, C., Robson, E. I., & Russell, A. P. G. 1994, *A&A*, 285, L1
 Sanders, D. B., & Willner, S. P. 1985, *ApJ*, 293, L39
 Saraceno, P., André, P., Ceccarelli, C., Griffin, M., & Molinari, S. 1996a, *A&A*, 309, 827
 Saraceno, P., et al. 1996b, *A&A*, 315, L293
 Sargent, A. I. 1979, *ApJ*, 233, 163
 Sato, Y., & Fukui, Y. 1989, *ApJ*, 343, 773
 Schuster, K. F., Harris, A. I., Anderson, N., & Russell, A. P. G. 1993, *ApJ*, 412, L67
 Sekimoto, Y., Tatematsu, K., Umemoto, T., Koyama, K., Tsuboi, Y., Hirano, N., & Yamamoto, S. 1997, *ApJ*, 489, L63
 Snell, R. L., & Bally, J. 1986, *ApJ*, 303, 683
 Snell, R. L., Dickman, R. L., & Huang, Y.-L. 1990, *ApJ*, 352, 139
 Snell, R. L., Loren, R. B., & Plambeck, R. L. 1980, *ApJ*, 239, L17
 Stanke, Th., McCaughrean, M. J., & Zinnecker, H. 2000, *A&A*, 355, 639
 Strom, S. E., Vrba, F. J., & Strom, K. M. 1976, *AJ*, 81, 314
 Sugitani, K., Fukui, Y., Mizuni, A., & Ohashi, N. 1989, *ApJ*, 342, L87
 Tafalla, M., & Bachiller, R. 1995, *ApJ*, 443, L37
 Tafalla, M., Bachiller, R., & Martin-Pintado, J. 1993, *ApJ*, 403, 175
 Tafalla, M., Myers, P. C., Mardones, D., & Bachiller, R. 2000, *A&A*, 359, 967
 Tamura, M., Ohashi, N., Hirano, N., Itoh, Y., & Moriarty-Schieven, G. H. 1996, *AJ*, 112, 2076
 Tamura, M., Sato, S., Kaifu, N., Hough, J. H., & Suzuki, H. 1990, *ApJ*, 350, 728
 Terebey, S., Vogel, S. N., & Myers, P. C. 1989, *ApJ*, 340, 472
 —. 1992, *ApJ*, 390, 181
 Testi, L., & Sargent, A. I. 1998, *ApJ*, 508, L91
 Testi, L., Sargent, A. I., Olmi, L., & Onello, J. S. 2000, *ApJ*, 540, L53
 Tofani, G., Felli, M., Taylor, G. B., & Hunter, T. R. 1995, *A&AS*, 112, 299
 Torrelles, J. M., Gómez, J. F., Curiel, S., Ho, P. T. P., Eiroa, C., & Rodríguez, L. F. 1992, *ApJ*, 384, L59
 Torrelles, J. M., Gómez, J. F., Garay, G., Rodríguez, L. F., Curiel, S., Cohen, R. J., & Ho, P. T. P. 1998a, *ApJ*, 509, 262
 Torrelles, J. M., Gómez, J. F., Rodríguez, L. F., Curiel, S., Anglada, G., & Ho, P. T. P. 1998b, *ApJ*, 505, 756
 Torrelles, J. M., Gómez, J. F., Rodríguez, L. F., Curiel, S., Ho, P. T. P., & Garay, G. 1996, *ApJ*, 457, L107
 Torrelles, J. M., Ho, P. T. P., Moran, J. M., Rodríguez, L. F., & Cantó, J. 1986, *ApJ*, 307, 787
 Torrelles, J. M., Ho, P. T. P., Rodríguez, L. F., & Cantó, J. 1985, *ApJ*, 288, 595
 Torrelles, J. M., Rodríguez, L. F., Cantó, J., Carral, P., Marcaide, J., Moran, J. M., & Ho, P. T. P. 1983, *ApJ*, 274, 214
 Uchida, Y., & Shibata, K. 1985, *PASJ*, 37, 515
 Umemoto, T., Hirano, N., Kameya, O., Fukui, Y., Kuno, N., & Takakubo, K. 1991, *ApJ*, 377, 510
 Umemoto, T., Iwata, T., Fukui, Y., Mikami, H., Yamamoto, S., Kameya, O., & Hirano, N. 1992, *ApJ*, 392, L83
 Velusamy, T., & Langer, W. D. 1998, *Nature*, 392, 685
 Walker, C. K., Lada, C. J., Young, E. T., & Margulis, M. 1988, *ApJ*, 332, 335
 Ward-Thompson, D., Buckley, H. D., Greaves, J. S., Holland, W. S., & André, P. 1996, *MNRAS*, 281, L53
 White, G. J., Casali, M. M., & Eiroa, C. 1995, *A&A*, 298, 594
 Wiesemeyer, H., Güsten, R., Wink, J. E., & Yorke, H. W. 1997a, *A&A*, 320, 287
 Wiesemeyer, H., Güsten, R., & Wright, M. C. H. 1997b, in *IAU Symp. 182, Herbig-Haro Flows and the Birth of Low Mass Stars*, ed. B. Reipurth & C. Bertout (Dordrecht: Kluwer), 260
 —. 1999, in *The Universe as Seen by ISO* (ESA-SP 427; Noordwijk: ESA), 533
 Wilking, B. A., Blackwell, J. H., Mundy, L. G., & Howe, J. E. 1989, *ApJ*, 345, 257
 Wilking, B. A., & Claussen, M. J. 1987, *ApJ*, 320, L133
 Wilking, B. A., Claussen, M. J., Benson, P. J., Myers, P. C., Terebey, S., & Wootten, A. 1994, *ApJ*, 431, L119
 Williams, J. P., & Myers, P. C. 1999, *ApJ*, 511, 208
 Wilner, D. J., Ho, P. T. P., & Rodriguez, L. F. 1996, *ApJ*, 470, L117
 Wiseman, J., Wootten, A., Zinnecker, H., & McCaughrean, M. 2001, *ApJ*, 550, L87

- Wolf-Chase, G. A., Barsony, M., & O'Linger, J. 2000, AJ, 120, 1467
- Wolf-Chase, G. A., Barsony, M., Wootten, H. A., Ward-Thompson, D., Lowrance, P. J., Kastner, J. H., & McMullin, J. P. 1998, ApJ, 501, L193
- Wootten, A. 1989, ApJ, 337, 858
- _____. 1993, in *Astrophysical Masers*, ed. A. Clegg & G. Nedoluha (Berlin: Springer), 315
- Wootten, A., et al. 2002, in IAU Symp. 206, *Cosmic Masers: from Protostars to Black Holes*, ed. V. Migenes & E. Lüdke (San Francisco: ASP), in press
- Wouterloot, J. G. A., Henkel, C., & Walmsley, C. M. 1989, A&A, 215, 131
- Wouterloot, J. G. A., Walmsley, C. M., & Henkel, C. 1988, A&A, 203, 367
- Yang, J., Ohashi, N., & Fukui, Y. 1995, ApJ, 455, 175
- Yang, J., Umemoto, T., Iwata, T., & Fukui, Y. 1991, ApJ, 373, 137
- Young, E. T., Lada, C. J., & Wilking, B. A. 1986, ApJ, 304, L45
- Yu, K. C., Billawala, Y., Smith, M. D., Bally, J., & Butner, H. M. 2000, AJ, 120, 1974
- Yu, T., & Chernin, L. M. 1997, ApJ, 479, L63
- Zhang, C. Y., Laureijs, R. J., Wesselius, P. R., & Clark, F. O. 1988, A&A, 199, 170
- Zhang, Q., Ho, P. T. P., Wright, M. C. H., & Wilner, D. J. 1995, ApJ, 451, L71
- Zhang, Q., Wootten, A., & Ho, P. T. P. 1997, ApJ, 475, 713
- Zinnecker, H., Bastien, P., Arcoragi, J.-P., & Yorke, H. W. 1992, A&A, 265, 726
- Zinnecker, H., McCaughren, M. J., & Rayner, J. T. 1998, Nature, 394, 862

ERRATUM: “WATER MASER SURVEY TOWARD LOW-MASS YOUNG STELLAR OBJECTS
 IN THE NORTHERN SKY WITH THE NOBEYAMA 45 METER TELESCOPE
 AND THE VERY LARGE ARRAY” (ApJS, 144, 71 [2003])

RAY S. FURUYA¹

INAF, Osservatorio Astrofisico di Arcetri, Italy; rsf@subaru.naoj.org

YOSHIMI KITAMURA

Institute of Space and Astronautical Science, Kanagawa, Japan; kitamura@pub.isas.ac.jp

ALWYN WOOTTEN

National Radio Astronomy Observatory, Charlottesville, VA; awootten@nrao.edu

MARK J. CLAUSSEN

National Radio Astronomy Observatory, Socorro, NM; mclausse@nrao.edu

AND

RYOHEI KAWABE

National Astronomical Observatory, Tokyo, Japan; kawabe@nro.nao.ac.jp

In our original article, the equation (1) given for calculating the H₂O maser luminosity ($L_{\text{H}_2\text{O}}$) is incorrect. The correct version of this equation is

$$\begin{aligned} L_{\text{H}_2\text{O}} &= 4\pi d^2 \frac{2k}{\eta_a A_p} \frac{\nu}{c} \int T_A^* dv \\ &= 1.6 \times 10^{-9} L_\odot \left(\frac{d}{160 \text{ pc}} \right)^2 \left(\frac{\int T_A^* dv}{1 \text{ K km s}^{-1}} \right) \left(\frac{\eta_a}{0.65} \right)^{-1}. \end{aligned} \quad (1)$$

This correction requires that all the $L_{\text{H}_2\text{O}}$ values in Tables 2 and 4, as well as those in captions of Figures 43–46, should be multiplied by a factor of 1.0×10^3 .

In spite of this correction, we believe that our H₂O maser survey remains one of the most sensitive surveys.

In addition, we correct the following inconsistency between the tables and the main text. In § 4.3.16, the distance to GF 9-2 should be 200 pc and the LSR velocity of the masers to be 5.7 km s⁻¹. The distance listed in Table 4 and the LSR velocity in Table 2 are correct.

Finally, the coordinates of L1551-IRS 5 in Table 1 are incorrectly given in epoch J2000, instead of B1950. The correct B1950 coordinates are R.A. = 04^h28^m40^s24, decl. = 18°01'41".9.

Below are the figures and captions as they should have appeared.

¹ Current address: Subaru Telescope, National Astronomical Observatory of Japan, 650 North A'ohoku Place, Hilo, HI 96720.

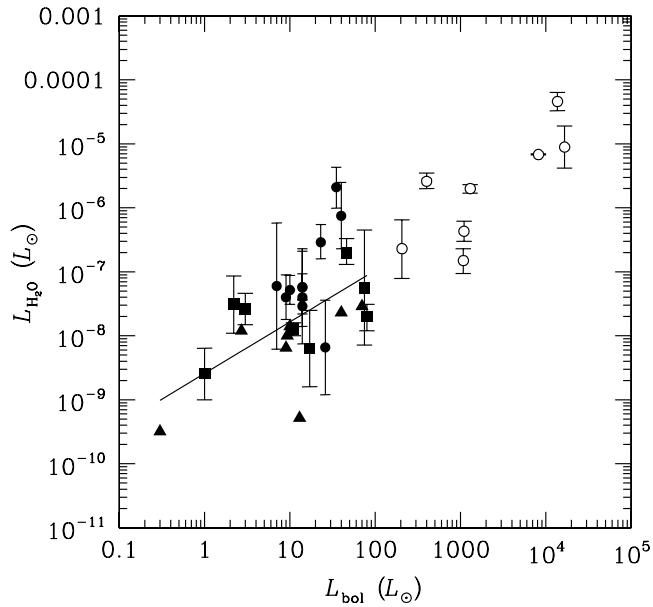


FIG. 43.—Observed isotropic H₂O maser luminosities ($L_{\text{H}_2\text{O}}$) vs. source bolometric luminosities (L_{bol}) for all the sources detected in the Nobeyama survey. Filled and open symbols present sources less and more luminous than $100 L_{\odot}$, respectively. The circles indicate the H₂O masers detected at all observing epochs. The squares indicate the H₂O masers that have not been detected at one or more epochs. The associated bars indicate the range of the luminosities for detected spectra in our observations. The triangles represent the maser luminosities for the sources that have been detected only once during the monitoring. The best-fit curve of $L_{\text{H}_2\text{O}} = 2.58 \times 10^{-9} (L_{\text{bol}})^{0.81}$ is shown by a line (correlation coefficient; $\rho = 0.28$).

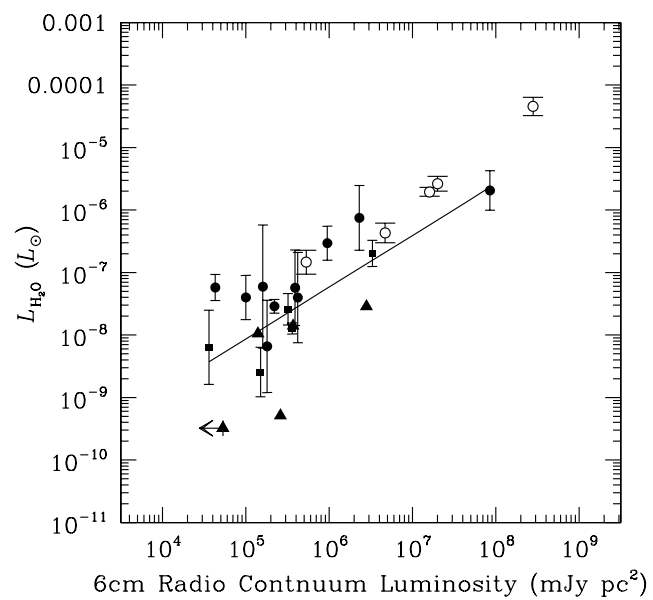


FIG. 44.—Plots of observed isotropic H₂O maser luminosities ($L_{\text{H}_2\text{O}}$) vs. 6 cm radio continuum luminosities ($4\pi d^2 S_{\text{6cm}}$). The symbols are same as in Fig. 43. The best-fit curve of $L_{\text{H}_2\text{O}} = 5.93 \times 10^{-13} (4\pi d^2 S_{\text{6cm}})^{0.83}$ is shown by a line ($\rho = -0.47$). A filled triangle with an upper limit is the source GF 9–2, which we did not use to fit the curve.

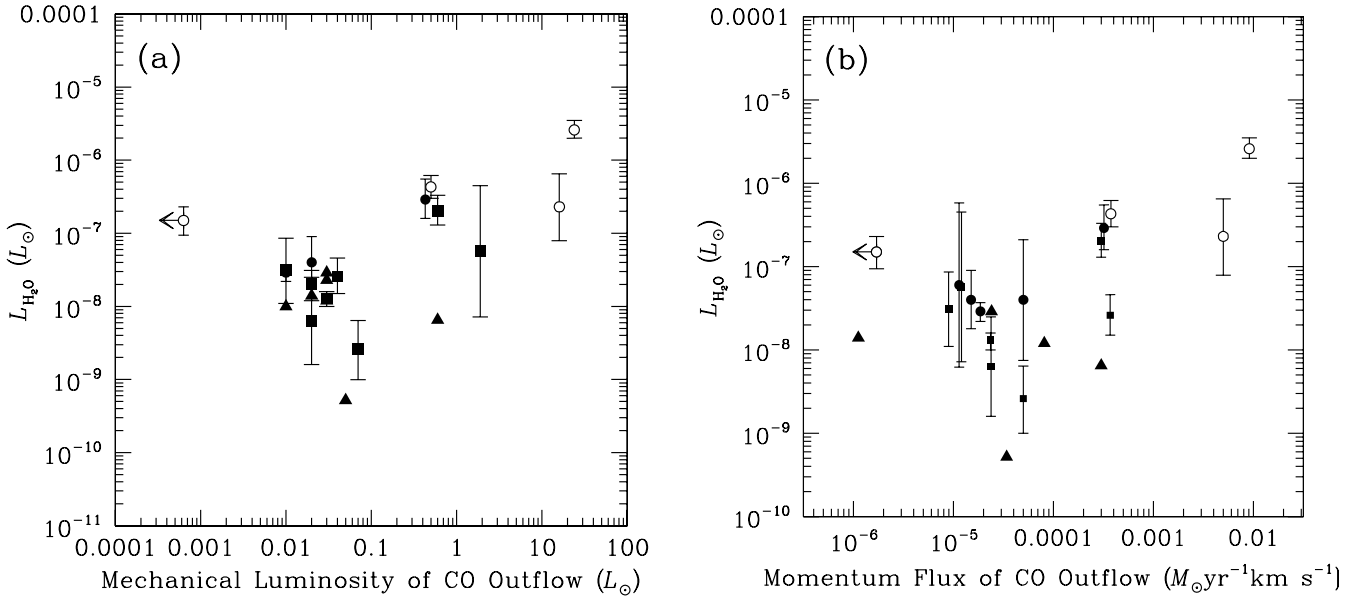


FIG. 45.—(a) Plots of observed isotropic H₂O maser luminosities ($L_{\text{H}_2\text{O}}$) vs. mechanical luminosity of CO outflows (L_{CO}). (b) Plots of observed isotropic H₂O maser luminosities ($L_{\text{H}_2\text{O}}$) vs. momentum flux of CO outflows (F_{CO}). The symbols are same as Fig. 43, and an open-circle with an upper limit is the source S106 FIR.

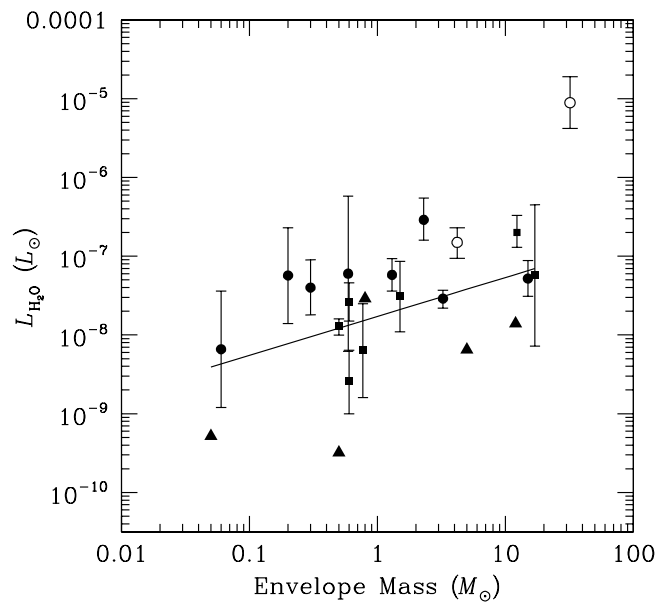


FIG. 46.—Plots of observed isotropic H₂O maser luminosities ($L_{\text{H}_2\text{O}}$) vs. circumstellar envelope mass (M_{env}). The symbols are same as Fig. 43. The best-fit curve of $L_{\text{H}_2\text{O}} = 1.72 \times 10^{-8} M_{\text{env}}^{0.49}$ is also shown by a line ($\rho = -0.53$).